

Stratospheric Processes and Their Role in Climate (SPARC)

A project of the World Climate Research Programme of WMO/ICSU

SPARC Intercomparison of Middle Atmosphere Climatologies

July 2002
Draft 2.1

Preface

This atlas presents detailed comparisons of several climatological wind and temperature data sets which cover the middle atmosphere (over altitudes ~10-80 km). A number of middle atmosphere climatologies have been developed in the research community based on a variety of meteorological analyses and satellite data sets. Here we present comparisons between these climatological data sets for a number of basic circulation statistics, such as zonal mean temperature, winds and eddy flux statistics. Special attention is focused on tropical winds and temperatures, where large differences exist among separate analyses. We also include comparisons between the global climatologies and historical rocketsonde wind and temperature measurements, and also with more recent lidar temperature data. These comparisons highlight differences and uncertainties in contemporary middle atmosphere data sets, and allow biases in particular analyses to be isolated. In addition, a brief atlas of zonal mean temperature and wind statistics is provided to highlight data availability and as a quick-look reference. This technical report is intended as a companion to the climatological data sets held in archive at the SPARC Data Center (<http://www.sparc.sunysb.edu>).

This report was produced by the SPARC Reference Climatology Group

William Randel (Chair)
Eric Fleming
Marvin Geller
Mel Gelman
Kevin Hamilton
David Karoly
Dave Ortland
Steve Pawson
Richard Swinbank
Petra Udelhofen

Contributors

Mark Baldwin
Marie-Lise Chanin
Philippe Keckhut
Dian Seidel
Adrian Simmons
Dong Wu

TABLE OF CONTENTS

Preface

1. Introduction
2. Climatological Data Sets for the Middle Atmosphere
 - A. Description of fundamental data and types of global analyses
 - B. Description of meteorological analyses and global data sets (acronyms described below)
 1. UKMO.....
 2. UKTOVS.....
 3. CPC.....
 4. NCEP.....
 5. ERA15.....
 6. ERA40.....
 7. FUB.....
 8. CIRA86.....
 9. UARS winds.....
 10. HALOE temperatures.....
 11. MLS temperatures.....
 - C. Rocketsonde wind and temperature data
 - D. Lidar temperature data
3. Data Intercomparisons
 - A. Temperature
 1. Zonal mean climatology
 - a. Comparisons with rocketsondes
 - b. Comparisons with lidars
 2. Interannual variability in extratropics
 3. Longitudinal structure
 4. Tropical seasonal cycle
 - a. Tropical rocketsondes
 - b. Semi-annual oscillation (SAO)
 5. Tropical interannual variability
 6. Temperatures for pre-1979 data

- B. Zonal mean zonal winds
 - 1. Zonal mean climatology
 - a. Comparisons with rocketsondes
 - 2. Interannual variability in extratropics
 - 3. Tropical seasonal cycle
 - a. Tropical rocketsondes
 - b. Semi-annual oscillation (SAO)
 - 4. Tropical interannual variability and the QBO

C. Zonal averaged heat and momentum fluxes

D. Summary: Biases and outstanding uncertainties

4. References

5. An Atlas of Middle Atmosphere Temperatures and Zonal Winds

1. Introduction

Climatological data sets for the middle atmosphere are useful for empirical studies of climate and variability, and also necessary for constraining the behavior of numerical models. The earliest comprehensive climatologies for the middle atmosphere were the 1964 and 1972 COSPAR reference atmospheres (CIRA), which were based largely on interpolation of single station balloon and rocket data. An updated version of CIRA in 1986 included early satellite observations of the stratosphere and mesosphere and has served as a community standard since that time. Around 1979, daily meteorological analyses with significant stratospheric coverage that included operational satellite temperature soundings began, and more recently (~ 1991) sophisticated model-based data assimilation schemes began to produce stratospheric analyses. These analyses (supplemented in the 1990's by extensive retrospective reanalyses) have served as the basis for some more recent middle atmosphere climatologies. Also, satellite observations from the Upper Atmosphere Research Satellite (launched in 1991 and continuing to operate in 2002) have provided additional climatological data sets for the middle atmosphere. Details of the circulation statistics derived from these various data sets will depend on several factors, including details of data inclusion and analysis techniques, and the respective time periods covered.

The objective of this work is to bring together several middle atmosphere climatological data sets which are in current use in the research community, and make direct comparisons of some basic measured and derived quantities. These data sets are based on a wide variety of analysis techniques, including manual analyses, objective analyses, and data assimilation systems. Our comparisons are used to identify biases in

particular data sets, and also to highlight regions where there is relatively large uncertainty for particular statistics (i.e., where large differences are found between several data sets).

The middle atmosphere climatologies considered here are primarily derived from global meteorological analyses and satellite data. Two independent data sets are also included for comparison, namely historical rocketsonde wind and temperature measurements (covering approximately 1965-1990), and lidar temperature data (covering the 1990's). Because the time and space sampling of the rocketsonde and lidar data are distinct from the global climatologies, direct comparisons require special attention, as discussed in Section 2C below.

An important aspect of numerical modeling for the middle atmosphere is to simulate not just the time mean structure, but also temporal (interannual) variability (e.g., Pawson et al., 2000). To that end we include here comparisons of both long-term means and interannual variance statistics. We also focus particular attention on the tropics, where there are relatively large differences among middle atmosphere climatological wind and temperature data sets (in particular, for variability related to the quasi-biennial oscillation (QBO) and semi-annual oscillation (SAO)). We furthermore present some comparisons between the few available sources of mesospheric winds and temperatures. Finally, we provide a brief atlas of middle atmosphere circulation statistics as a quick-look reference, and to highlight data availability.

All of the monthly mean data presented and compared here are available to the research community via the SPARC Data Center (<http://www.sparc.sunysb.edu>). This atlas is intended to be a companion to those on-line data.

2. Climatological data sets for the middle atmosphere

A. Description of fundamental data and types of global analyses

Two fundamental types of observations contribute to global (or hemispheric) stratospheric analyses. Radiosondes are balloon-borne instruments which provide vertical profiles of temperature, pressure and horizontal winds. These measurements cover the lowest 20-30 km of the atmosphere, with a nominal archive vertical resolution of ~ .2 km. The current radiosonde network is comprised of ~ 900-1000 stations which make measurements at least once daily, with the vast majority located over land masses of the Northern Hemisphere. Satellite-derived temperature profiles provide the other major source of stratospheric data. Operational meteorological polar orbiting satellites provide near-global temperature profile retrievals twice daily up to ~50 km altitude, but have the drawback of relatively low vertical resolution (> 10 km) in the stratosphere. A series of operational NOAA satellites has been in orbit since late 1978, containing a suite of instruments that are collectively called the TIROS Operational Vertical Sounder (TOVS) (Smith et al., 1979). An improved temperature sounder (called the Advanced TOVS, or ATOVS) is now replacing the older TOVS series, beginning with the NOAA-15 satellite launched in May 1998, NOAA-16 in September 2000, and NOAA-17 in June 2002. Temperature retrievals from TOVS and ATOVS data are a primary input to many of the global analyses here (including CPC, UKMO, UKTOVS, NCEP, ERA15 and ERA40 data sets).

Details of the various stratospheric analyses are described below, but the types of global or hemispheric analyses can be summarized as follows. The main objective is to depict the large-scale atmosphere behavior by some sort of interpolation between sparse

• observations, or by combining different types of measurements (i.e., radiosondes and satellites). The simplest analyses provide global fields based on hand-drawn analyses (FUB) or objective analysis gridding techniques (CPC and UKTOVS). More sophisticated analyses can be derived by the use of numerical forecast models to predict first-guess fields, and incorporate observations by optimal data assimilation (UKMO, NCEP, ERA15 and ERA40 data). A strength of the simple analyses is that they are most directly dependent on observations, but this can be a drawback in regions with less data availability. The data assimilation techniques have the advantage of incorporating knowledge of prior observations and dynamical balances, but have a down-side that details of the numerical model can influence the results. In fact most of the basic radiosonde and satellite-derived measurements are input to many of the separate analyses studied here, and the differences revealed in our comparisons highlight the sensitivity of the final statistics to details of the data usage and analysis techniques.

B. Description of data sets

This section presents short descriptions of the climatological data sets included in the comparisons. These are intended to be brief, and more details for each analysis can be found in the listed references. Table 1 provides a summary list of some relevant details for each analysis. For brevity, each data set is referred to throughout this work by the following short acronyms.

1. UKMO (UK Met Office Stratospheric Analyses)

Since October 1991 stratospheric analyses have been produced daily using a stratosphere-troposphere version of the Met Office's data assimilation system (Swinbank and O'Neill, 1994). These analyses were formerly referred to as UK Meteorological Office

(UKMO) stratospheric analyses, and we retain that name here. The stratosphere-troposphere data assimilation system is a development of the “Analysis Correction” data assimilation system (Lorenc et al., 1991), which was then in use for operational weather forecasting. In this system, observations are assimilated into a 42-level configuration of the UKMO Unified Model to produce a set of stratospheric analyses for 12 UTC every day. The analyses consist of temperatures, wind components and geopotential heights on a global grid, of resolution 2.5° latitude by 3.75° longitude. The analyses are output on the UARS standard pressure levels, with six equally spaced levels per decade of pressure (100, 68.1, 46.4, 31.6, 21.5, 14.7, 10,...hPa). The analyses span the range 1000-0.3 hPa (approximately 0-55 km).

The stratospheric analyses were originally produced as correlative data for the NASA UARS (Upper Atmosphere Research Satellite) project, starting from October 1991. The analyses have been used in a number of research studies of stratospheric dynamics, and to help interpret UARS constituent measurements. Since October 1995 the separate UARS assimilation system was discontinued, but stratospheric analyses continue to be produced using a similar data assimilation system, which is run as part of the Meteorological Office operational forecasting suite. Since November 2000 the Met Office stratospheric analyses have been produced using a new 3-D variational (3DVAR) data assimilation system (Lorenc et al., 2000). However, the majority of results presented here were derived from analyses produced before that change.

The stratosphere-troposphere data assimilation uses essentially the same set of meteorological observations that are used for operational weather forecasting. In the stratosphere the most important observation types are TOVS (and more recently ATOVS)

temperature profiles. Another important set of observations are radiosonde soundings of temperatures and winds, although most radiosondes only ascend as far as the lower stratosphere.

2. UKTOVS (Met Office Analyses of TOVS Data)

The Met Office also produced regular stratospheric analyses (not part of a model assimilation) from measurements made by NOAA polar orbiter satellites. The Met Office was formerly referred to as the UK Meteorological Office, and these analyses are frequently referred to in the community as UKTOVS (which we retain here). Monthly means from these analyses are available for the period January 1979-April 1997. The analysis method is described by Bailey et al. (1993), but a brief description is given below. Scaife et al. (2000) present climatological data and interannual variations diagnosed from the UKTOVS data.

The UKTOVS fields are derived from an independent analysis of TOVS radiance measurements. The daily TOVS data were used to derive geopotential thickness values, covering the layers 100-20, 100-10, 100-5, 100-2 and 100-1 hPa. The thicknesses were then mapped onto a 5 degree resolution global grid, and added to the operational analysis of 100 hPa height (obtained from Met Office operational global analyses) to produce height fields up to 1 hPa. In turn, temperatures and horizontal balanced winds are derived from the height fields. Winds at the equator are interpolated from low latitudes, and resultant tropical variations (e.g., the QBO) are rather weak (as shown below).

3. CPC (Climate Prediction Center)

Operational daily analyses of stratospheric geopotential height and temperature fields have been produced by the Climate Prediction Center (CPC) of the US National

Centers for Environmental Prediction (NCEP) since October 1978 (Gelman et al., 1986). NCEP was formerly called the National Meteorological Center (NMC), and these analyses have been referred to in the research community as “stratospheric NMC” analyses. Here they are termed CPC analyses (to differentiate from NCEP reanalyses). The CPC stratospheric analyses are based on a successive-correction objective analysis (Finger et al., 1965) for pressure levels 70, 50, 30, 10, 5, 2, 1 and 0.4 hPa, incorporating TOVS and ATOVS satellite data and radiosonde measurements (in the lower stratosphere of the NH). This analysis system has been nearly constant over time (October 1978-April 2001). The TOVS temperature profiles are provided as layer mean temperatures between standard pressure levels; geopotential thicknesses are calculated from these temperatures, and added to a base level 100 hPa geopotential field taken from operational NCEP tropospheric analyses. Stratospheric temperatures at standard levels are derived by interpolation between the TOVS layer mean temperatures. The fields are produced each day for a nominal time of 1200 UT, using 12 hours of TOVS data (0600-1800 UT). The NCEP operationally analyzed tropospheric fields over 1000-100 hPa are included, so that CPC analyses cover 1000-0.4 hPa. As a note, the CPC analyses were changed beginning in May 2001, with the data up to 10 hPa based on the NCEP operational analyses, and fields above 10 hPa based solely on ATOVS. However, comparisons here only include data prior to this change.

Satellite temperatures are the sole input to the CPC analyses over the SH and tropics, and over the entire globe for levels above 10 hPa. For levels 70-10 hPa in the NH, radiosonde data (for 1200 UT) are incorporated, using TOVS as a first guess field. TOVS temperatures have been provided by a series of operational NOAA satellites; these

instruments do not yield identical radiance measurements for a variety of reasons, and derived temperatures may change substantially when a new instrument is introduced (Nash and Forrester, 1986). Finger et al. (1993) have compared the CPC temperatures in the upper stratosphere (pressure levels 5, 2, 1 and 0.4 hPa) with co-located rocketsonde and lidar data, and find systematic biases of order $\pm 3-6$ K. Finger et al. (1993) provide a set of recommended corrections (dependent on time period and pressure level) to the CPC temperature analyses, which have been incorporated in the results here. However, in spite of these adjustments, the CPC analyses still probably retain artifacts of these satellite changes. One additional change of note is that before March 1984 NH fields were only archived over 20°N-pole; prior to this time CPC analyses over 0-20°N are interpolated values.

Horizontal winds are derived from the CPC geopotential data using the 'linear balance' technique (Randel, 1987). The calculations of longitudinally-varying wind fields become ill-behaved in the tropics, and eddy wind statistics are only reliable polewards of $\sim 20^\circ$ latitude. Tropical zonal mean winds are estimated using the second derivative of geopotential height at the equator (Fleming and Chandra, 1989). Extensive climatologies of the stratosphere have been derived from these CPC data by Hamilton (1982), Geller et al. (1983) and Randel (1992).

4. NCEP Reanalyses

The NCEP/National Center for Atmospheric Research (NCAR) reanalysis project uses a global numerical weather analysis/forecast system to perform data assimilation using historical observations, spanning the time period from 1957 to the present (Kalnay et al., 1996). For brevity, the NCEP/NCAR reanalyses are referred to as NCEP here. The model

used in the NCEP reanalysis has 28 vertical levels extending from the surface to ~40 km, and analyses of winds, temperatures and geopotential height are output on stratospheric pressure levels of 100, 50, 30, 20 and 10 hPa.

5. ERA15 (ECMWF 15-year Reanalysis)

The European Center for Medium Range Weather Forecasts (ECMWF) produced a global reanalysis for the period 1979-1993, based on data assimilation coupled with a numerical forecast model (Gibson et al., 1997). The forecast model used in that work spanned pressure levels 1000-10 hPa, with analyses output on stratospheric pressure levels of 100, 50, 30 and 10 hPa. An important detail is that the 10 hPa analysis level is at the top level of the model, and this has a detrimental impact on results at this level (as shown in the comparisons below).

6. ERA40 (ECMWF 40-year Reanalysis)

ECMWF is also producing an updated reanalysis, termed ERA40, covering the period 1957-2001. ERA40 will be a comprehensive set of global meteorological analyses, including the stratosphere up to 1 hPa, based on the use of variational data assimilation techniques. One important difference with the ERA15 reanalyses (in addition to the increased vertical domain) is that ERA40 will directly assimilate TOVS radiances, as opposed to retrieved temperature profiles. Production of the full ERA40 reanalyses is an ongoing activity at the time of writing of this atlas. However, we have obtained a subset of early production results for the time period 1992-1997, covering the parameters zonal mean temperature and zonal mean zonal winds (courtesy of Adrian Simmons of ECMWF), and these are included in our comparisons. The ERA40 analyses are available on 23 standard pressure levels spanning 1000-1 hPa.

7. FUB (Free University of Berlin Analyses)

The meteorological analyses from the Free University of Berlin (FUB) are northern hemispheric, gridded products at four levels: 100, 50, 30, and 10hPa. Monthly mean data at these levels are available since 1957 (geopotential height) and 1964 (temperature) on a 10-degree grid, with an increase in resolution to five degrees in the early 1970s (the precise date depends on the pressure level). Daily analyses are produced only at the three upper levels (i.e., not at 100hPa) and are provided only every second day in northern summer, when the flow evolves slowly. The analyses are performed by hand (subjective analysis) using station observations of geopotential height, wind, and temperature; thermal wind balance is used as a constraint on the analyses, so that even though wind is not analyzed, it plays an important part in the analysis procedure. Hydrostatic balance and the thermal wind are used as the analyses are built up from the 100-hPa tie-on level (for which data from FUB were used in the early years, but later operational products from the German Meteorological Agency were substituted), to build accurate analyses from the station data at the stratospheric levels. The resolution of the gridded data did increase in the early 1970s, as technological advances made the automated scanning of the hand-analyzed charts a practical reality.

The FUB data have been used in a large number of studies of the climatology of the middle atmosphere, including trends and the low-frequency variability (e.g., Labitzke and Nanjokat, 1983; Pawson et al., 1993). Daily data have been extensively exploited to understand the occurrence of very cold regions which are associated with polar stratospheric cloud formation and ozone loss (Pawson and Nanjokat, 1999). It should be stressed that these analyses do not include wind as a product; while their utility is restricted

by this, they are a valuable record of the stratosphere between about 1960 and 2000, analyzed in a consistent and uniform manner throughout this period.

8. CIRA86 Climatology

The COSPAR International Reference Atmosphere, 1986 (CIRA-86) of zonal mean temperature, geopotential height, and zonal wind has been described in detail in Barnett and Corney (1985a, 1985b) and Fleming et al. (1988, 1990). These reference climatologies are based on a variety of data sources, briefly summarized here.

Temperatures for 1000-50 hPa are taken from the climatology of Oort (1983) which is based primarily on data from the 1960s and early 1970s. Temperatures at 30 hPa over the NH are taken from analyses of the Free University of Berlin (FUB), and for the SH are taken from the radiosonde climatology of Knittel (1974). For 10-2.5 hPa, values are based on satellite data from the Nimbus 5 Selective Chopper Radiometer (SCR) averaged over 1973-1974. From 2.5-0.34 hPa (~40-56 km), the SCR data was merged with temperatures from the Nimbus 6 Pressure Modulator Radiometer (PMR) averaged over the period July 1975-June 1978. The PMR data were used exclusively for 0.34 hPa-0.01 hPa (~56-80 km), with temperatures from the mass spectrometer and incoherent scatter (MSIS-83) empirical model of the thermosphere (Hedin, 1983) used exclusively above 0.002 hPa (~90 km). All values were merged to obtain a smooth transition between the original data sets.

The zonal wind climatology in the troposphere is taken from Oort (1983), with winds in the middle atmosphere above 100 hPa based on gradient winds derived from the geopotential height climatology. At high latitudes, the zonal wind is derived by assuming that the relative angular velocity remains constant poleward of 70 S (70 N). At the equator where the standard gradient wind calculation fails, the zonal wind (above 100 hPa) is based

on the second derivative of geopotential height (Fleming and Chandra, 1989). The winds between the equator and 15 S (15 N) are computed by linear interpolation.

9. UARS Reference Atmosphere Winds

As part of the UARS Reference Atmosphere Project (URAP), Swinbank and Ortland (2000) compiled a wind data set using measurements from the UARS High Resolution Doppler Imager (HRDI; Hays et al., 1993), supplemented with data from the Met Office stratospheric analyses (UKMO). The data set comprises zonal-mean wind data from the earth's surface to the lower thermosphere every month for a period of about 8 years starting from the launch of UARS. The wind data set only includes the zonal (westerly) component of the wind and not the meridional (southerly) component. The wind data are stored on a pressure-latitude grid; the pressures are the UARS standard pressure levels, and the latitudes are equally spaced every 4° from 80°S to 80°N.

There were several periods when HRDI data were not available. The shorter data gaps in the stratospheric data were filled in using a time-smoothing procedure. In the mesosphere tidal variations in the wind field are much more important than in the stratosphere, so a different procedure was used that took into account the local time coverage of the observations (see Swinbank and Ortland, 2000). This reduced the impact of tidal variations on the final wind data set as much as possible.

Wind measurements from HRDI span most of the stratosphere and also extend from the middle mesosphere to the lower thermosphere. In order to obtain as full as possible coverage of the atmosphere, the HRDI measurements were combined with UKMO stratospheric analyses. Together, the two data sets cover the troposphere and stratosphere, but there is a gap between the uppermost reliable level of the UKMO data and the

lowermost reliable level of HRDI data in the mesosphere. So, the wind data in this region were supplemented with balanced winds calculated from the URAP temperatures (when available). Where there were insufficient HRDI data in a particular month, climatological data derived from HRDI data were used instead. In order to provide complete coverage in the data set, interpolated and extrapolated winds were used when no other data were available. The data set includes a quality flag to indicate where the wind values are based on direct measurements and when they are largely derived from climatological or interpolated data.

10. HALOE Temperatures

The Halogen Occultation Experiment (HALOE) instrument on UARS provides analyses of temperatures in the altitude range ~45-85 km (Russell et al., 1993; Hervig et al., 1996; Remsberg et al., 2002). HALOE uses a solar occultation measurement technique, providing 15 sunrise and 15 sunset measurements per day, with each sunrise or sunset group near the same latitude. The latitudinal sampling progresses in time, so that much of the latitude range ~ 60°N-S is sampled in one month; the measurements extend to polar regions during spring through late summer. The vertical resolution of these data are ~2 km, with sampling on UARS standard pressure levels (6 levels per decade of pressure). The results shown here are based on HALOE retrieval version 19.

The seasonal temperature analyses here use the combined sunrise plus sunset temperatures binned into monthly samples. The seasonal cycle is derived by a harmonic regression analysis of these monthly data over the period January 1992-December 1999, including annual and semi-annual harmonics at each height and latitude (spanning 60°N-S).

This regression provides a useful method of interpolating the irregular temporal sampling of HALOE.

11. MLS Temperatures

Middle atmosphere temperatures have also been obtained from the Microwave Limb Sounder (MLS) instrument on UARS (Fishbein et al., 1996). The data here are from an independent retrieval provided by Dong Wu (personal communication), covering the time period January 1992-December 1994. This retrieval is completely independent of other climatologies, using a single temperature profile (an annual mean) as the first guess and linearization point. The valid altitude range is 20-90 km, with large uncertainties at the two ends; the vertical sampling is the UARS standard pressure grid (six per decade of pressure). Compared to the MLS Version 5 (V5) retrieval, the data here have much better vertical resolution in the mesosphere, while it is about the same in the stratosphere. These data and further descriptions are available to the research community via an ftp site: [mls.jpl.nasa.gov/pub/outgoing/duu/temp](ftp://mls.jpl.nasa.gov/pub/outgoing/duu/temp).

The orbital characteristics of UARS allows MLS to obtain data from approximately 80°S-32°N or 32°S-80°N for alternating satellite yaw cycles (each approximately one month long). In order to handle these large data gaps in high latitudes, our analyses fit the seasonal cycle at each latitude and pressure level using harmonic regression analyses of monthly sampled data (including annual and semiannual harmonic terms in the analyses).

C. Rocketsonde wind and temperature data

Measurements from small meteorological rockets provide an important source of wind and temperature information for the middle atmosphere, in the 25 to 85 km altitude region. A program of rocketsonde measurements began in the United States in the late

1950s. During the 1960s the program expanded to about a dozen stations making regular measurements once to three times per week. Other locations made measurements for limited time periods and for special programs. The number of rocketsonde measurements peaked in the late 1970s, at about 1000 to 1500 yearly, including measurements from the former Soviet Union, Japan and several other countries. Most measurement locations were at middle latitudes of the northern hemisphere and tropical locations, but a few stations were located in polar and southern hemisphere mid latitude locations. The number of rocketsonde stations and frequency of observations decreased markedly in the 1980s, and by the 1990s fewer than a total of 100 rocketsonde measurements were made each year. Figure A.1 shows a summary of the number of rocketsonde observations for the 1960's, 1970's and 1980's a function of latitude.

The archived data collected from the 1950s to the 1990s from the rocketsonde network constitutes a valuable independent resource of in-situ, fine vertical scale, temperature and wind information, for climatology and research. Indeed, when rocketsonde measurements were first made, they constituted the only source of middle atmosphere information, providing an overall framework for understanding atmospheric temperature and wind structure and variability above radiosonde levels. Now, it is especially important to be able to compare climatological summaries of the rocketsonde data at their very few measurement locations with climatologies constructed using remotely sensed global satellite information.

There are two types of small meteorological rocketsonde systems, thermistor and sphere. By far, most measurements have been made using an instrumented thermistor package and parachute, ejected from the rocket at apogee and tracked during descent by a

ground radar. In situ measurements of thermistor temperature are transmitted to a ground station, so that a temperature versus altitude profile is obtained, with 1 km or finer vertical resolution, from apogee (up to 85 km for the USSR system and 70 km for the US system) to data cutoff (approx. 20 to 25 km). A pressure versus altitude profile is obtained with a support radiosonde observation, close in time and from a nearby location, that supplies the needed "tie on" pressure and height values. The horizontal wind versus altitude profile is obtained by ground radar tracking of the horizontal displacement of the descending parachute. Experimental studies for the US system have indicated temperature measurement precision (repeatability) of 1 to 3 C degrees and wind precision of 3 m/s. Corrections have been applied to measured temperatures to account for solar short wave radiative heating, long wave radiative cooling, and frictional heating of the thermistor. Corrections are less than 1 C below 40 km, up to 5 C at 55 km, a rising to several tens of degrees above 65 km. Wind corrections are large at the upper altitudes because of high fall velocity of the parachute, but are small below 50 km.

The number of sphere observations have been relatively small, from a few locations in middle northern latitudes and tropical locations. The sphere system consists of an inflatable mylar balloon, inflated at apogee, and tracked by high-precision ground radar as the inflated sphere descends. Atmospheric density from approximately 90 km down to 35 km is derived from the measured vertical profile of fall velocity of the sphere, assuming zero vertical atmospheric motion. Temperatures are derived from the density profile, using a "guess" temperature value at the top of the profile. The horizontal wind versus altitude profile is obtained by the ground radar tracking of the horizontal displacement of the descending inflated sphere. Studies have found average differences of 3 to 6 C degrees

between sphere and thermistor measurements. However, the analyses here make no distinction between these two types of measurements.

The rocketsonde wind and temperature climatologies shown here are based on simple monthly averages, derived by binning all of the available observations during 1970-1989. Due to data availability (Figure A.1), we focus the comparisons on the tropics and extratropical NH. The extratropical bins are centered at 30°, 60°, and 80° latitude, including measurements within $\pm 10^\circ$ of the central latitude. The tropical data are separated for measurements near 10°S (mostly from Ascension Is. at 8°S), and near 10°N (mostly from Kwajalein at 8°N). Based on this sampling, there are approximately 100-300 profile observations in each monthly bin, depending on latitude and altitude. Vertical sampling is made on the UARS pressure grid (six levels per decade of pressure). Figure A.2 shows an example of the data availability for rocketsonde zonal winds at 0.1 hPa for the latitude bin centered at 30°N.

Two important considerations apply to the comparisons of rocketsonde data with global analyses. First, the time periods covered by the data are different (1992-1997 for the analyses, and 1970-1989 for the rocketsondes). This is most important for temperatures in the upper stratosphere, and mesosphere, which have experienced strong cooling (larger than 2 K/decade) during the recent decades (Ramaswamy et al., 2001). A large part of the observed rocketsonde-analyses differences in these regions can be attributed to this cooling. Second, the monthly samples from analyses are based on zonal and monthly means of daily data, whereas the rocketsonde statistics are derived from infrequent samples at specific locations, taken over many years. Thus uncertainty levels for the rocketsonde means are significantly larger.

D. Lidar temperature data

Lidars provide measurements of the vertical temperature profile in the middle atmosphere, and a number of specific sites have made lidar temperature measurements for a decade or longer. The Rayleigh lidar technique uses the backscattering of a pulsed laser beam to derive the vertical profile of atmospheric density, from which the temperature profile is deduced (Hauchecorne and Chanin, 1980; Keckhut et al., 1993). This technique provides an absolute temperature measurement over altitudes ~30-75 km, which does not require adjustment or external calibration (derived temperatures above ~75 km can be influenced by first guess uncertainties and values below ~30 km by aerosols or details of the lidar measurements). The vertical resolution of the lidar data is approximately 3 km, and the profiles here are sampled on the UARS standard pressure grid.

For the climatological analyses here, we obtained a number of lidar temperature time series (for stations with relatively long records) from the Network for the Detection of Stratospheric Change (NDSC) web site: <http://www.ndsc.ws/>. The specific locations and available time records are listed in Table 2. The individual profiles are binned into monthly samples, focused on latitude bins centered at 20°N, 40°N and 80°N. We use all the lidar observations over 1990-1999, in order to most directly compare with the meteorological analyses over 1992-1997 (a slightly longer time record for the lidar data provides better monthly sampling). The total number of lidar observations and their latitudinal sampling is shown in Figure A.3. Our monthly and latitudinal sampling produces between ~20-80 measurements per bin for latitudes 20°N, and 80°N, and ~300 per month for the bin centered at 40°N. The associated monthly means and standard deviations are calculated identically to the rocketsonde analyses.

As a note, one important source of variability for lidar and all data sets in the upper stratosphere-mesosphere is that due to diurnal and semi-diurnal tides, which have large amplitudes above the stratopause. This variability is minimized for the lidar measurements by using temperature data taken at the same fixed time.

3. Data intercomparisons

In this section we make direct comparisons among the different data sets for global fields of temperature, zonal winds, and zonal averaged eddy fluxes of heat and momentum. The first requirement for such comparisons is to choose a time period which maximizes record length for overlap among most data sets. Here we choose the period January 1992-December 1997, which gives direct overlap of the UKMO, CPC, NCEP and ERA40 reanalysis, and FUB fields. The UKTOVS record is slightly shorter (to April 1997). The ERA15 reanalysis has a much shorter record during this 1992-1997 period (January 1992-December 1993). We include comparisons for these data by calculating differences only over this 1992-1993 record, rather than the full 6 years 1992-1997. We also include comparisons with the CIRA86 climatology, although it should be kept in mind that these data are derived from a very different time period (covering the 1960's-1970's). The FUB and NCEP reanalyses have data for the pre-satellite period (prior to 1979), and these are briefly compared separately in Section D below.

A. Temperature

1. Zonal mean climatology

A cross section of January average zonal mean temperature is shown in Figure 1 based on UKMO analyses. The overall latitude-height structure is similar in all data sets,

and comparisons are best made by considering differences with a single standard (UKMO in this case). Included in Figure 1 are January temperature differences from the UKMO for each climatology. The differences are typically $\pm 1-5^\circ$, with systematic vertical or latitudinal patterns depending on each data source. Differences which are consistent across several data sets suggest a systematic bias in the UKMO reference, whereas differing biases across many data sets suggest a fundamental uncertainty in estimates of that quantity. The patterns in Figure 1 show the overall character of temperature differences; and specifics are discussed below.

The latitudinal structure of 100 hPa temperature for each data source during January, April, July and October is shown in Figure 2, and differences with the UKMO analyses are shown in Figure 3. The overall latitudinal structure in Figure 2 is similar between the data sets, but there is substantial spread in the tropics and also the polar regions. The UKTOVS is a notable outlier (> 5 K warmer than all other data sets), and are not included in the differences in Figure 3. Aside from UKTOVS, the 100 hPa tropical temperatures fall into two groups, biased warmer (CPC, NCEP and CIRA86) or colder (FUB, ERA15 and ERA40) than UKMO. As discussed in more detail below, the latter group is probably more realistic, and the former data sets (plus UKMO) have a true warm tropical bias of $\sim 2-3$ K at 100 hPa. The CIRA86 data exhibit warm biases by up to ~ 5 K in the winter polar regions, and it is likely that at least a part of this may reflect true cooling in the lower stratosphere between the 1960's and 1990's (e.g., Ramaswamy, 2001). CPC data show a warm bias over Antarctica in April, July and October, apparently distinct from the other data sources. Manney et al. (1996) note warm biases (of order 3-5 K) for both CPC and UKMO data in the Arctic and Antarctic winters in comparisons to radiosondes,

suggesting problems in accurately capturing the coldest polar temperatures in these global analyses.

Figure 4 shows difference statistics for the 50 hPa level, for January, March, July and October. Here the differences have been calculated with respect to the UKMO analyses at 46.4 hPa (the closest level), resulting in slight cold differences in the tropics for most data sets. There is reasonable overall agreement between the different data sets over a broad range of latitudes, except for warm biases in CIRA86 (warm by ~ 2-3 K) and cold biases in UKTOVS (cold by up to 5 K). There is also a wide range of biases over Antarctica during spring (October), with differences of $\pm 2-4$ K, and no consensus between data sets.

The climatology of 10 hPa zonal mean temperature in January and July, and differences with UKMO, are shown in Figure 5. There is a wider range of differences at this level (typically $\pm 2-4$ K) than at 100 or 50 hPa, showing more uncertainty in the climatology. The CIRA86 and MLS data (in the tropics) are on the warm side of the ensemble, and the ERA15 10 hPa temperatures are biased cold in extratropics compared to all other data. Comparisons of temperatures at 1 hPa are shown in Figure 6. Here there are more substantial differences of order ~5 K between the different data sets. MLS data are relatively warm and UKMO relatively cold compared to the other analyses. The UKTOVS show a slightly different latitudinal structure than the other data sets at high winter latitudes in both hemispheres. This level near the stratopause presents special problems in analyses, because it is not captured accurately in TOVS thick layer radiance measurements, plus it is near the top of the UKMO forecast/assimilation model (at 0.3 hPa).

Statistics on mesospheric temperature at 0.1 hPa (~65 km) and 0.01 hPa (~80 km) are shown in Figure 7, comparing the few available data sets (HALOE, MLS and CIRA86). At 0.1 hPa the latitudinal structure is very similar, and the midlatitude minima are most pronounced in MLS and HALOE data. HALOE and MLS data are somewhat colder than the CIRA86 at 0.01 hPa, but absolute comparisons with CIRA86 are difficult in light of the ~20 year time difference between these measurements.

The climatological vertical profiles of temperature in January and July are shown in Figure 8, for statistics at 80°S, the equator, and 80°N. These plots show the extreme range of global temperature variations, and illustrate regions where there are relatively larger differences between data sets. One obvious region of uncertainty is in the upper stratosphere and near the stratopause, and a further region showing substantial differences (~5 K) is in the Antarctic polar stratosphere in July, near the temperature minimum over ~25-30 km. A similar level of uncertainty is found in the Antarctic lower stratosphere in October (see Figures 3-4). The seasonal variations of polar temperatures in the lower stratosphere (100 and 50 hPa) are compared among the different climatologies in Figures 9-10. In the NH there is excellent agreement (within 1 K) between UKMO, CPC and NCEP reanalyses; the FUB and UKTOVS have slightly larger differences, while CIRA86 is much warmer in winter (due at least in part to the temporal differences). In the SH the differences are somewhat larger; the CPC are warmer than UKMO by ~2-3 K throughout winter. The climatological minimum 50 hPa temperature over Antarctica varies from 184-188 K between the different data sets, and this highlights the problem of accurate temperature analyses in the intensely cold Antarctic stratosphere.

Figure 11 compares the temperature climatologies for January at 40°N, where optimal agreement might be expected in levels below ~25-30 km, due to maximum radiosonde coverage. Indeed, Figure 11 shows small differences over these altitudes ($\sim \pm 2$ K, aside from CIRA86) and the cluster of differences near -1 K suggest a small systematic bias in UKMO analyses. Above ~25 km the differences are larger ($\sim \pm 3-5$ K), showing the sensitivity to satellite data types and analyses. As at all other latitudes, relatively large differences are found near the stratopause, with the UKMO being systematically colder than most other analyses.

Variability at the midlatitude stratopause is explored further in Figure 12, showing the seasonal cycle of 1 hPa temperature at 40°N and 40°S from each analyses. These comparisons demonstrate that some biases can vary seasonally. In general, differences between analyses are somewhat larger during local winter. The UKTOVS have an accentuated annual cycle compared to the other analyses, with largest apparent cold biases during local winter. The MLS and CIRA86 data have a relatively warm stratopause throughout the year, while the UKMO, HALOE and ERA40 data are consistently on the cold side.

a. Comparisons with rocketsondes

As noted above, most of the extratropical rocketsonde data occur in latitude bins near 30°N, 60°N and 80°N, and we focus comparisons on these latitude regions. Figure 13 compares rocketsonde climatology profiles with analyses at 30°N for January and July statistics. The rocketsondes show good overall agreement in the stratosphere, and in locating the altitude of the stratopause. The rocketsonde temperatures in the mesosphere

(~50-70 km) are warmer than the analyses, especially in January, and this is probably a result of the differing respective time periods, as noted above.

The seasonal variation of temperatures near 30°N from rocketsondes and analyses are compared in Figure 14, for data at 10, 1 and 0.1 hPa. At 10 and 1 hPa the mean rocketsonde temperatures are slightly warmer than most analyses (except CIRA86 at both levels, UKTOVS at 10 hPa and MLS at 1 hPa), although there is substantial variability in the rocketsondes which overlaps the analyses. At 0.1 hPa the mean rocketsonde values are ~4-7 K warmer than MLS or HALOE data, and ~2-8 K warmer than CIRA86.

Similar comparisons for temperatures near 60°N are shown in Figure 15. Good agreement is seen at 10 hPa between rocketsondes and all analyses (except CIRA86, with a warm summer bias). At 1 hPa the rocketsondes are also in agreement with most analyses; the comparisons highlight cold biases for UKMO at the warm summer stratopause, and for the HALOE climatology in midwinter. At 0.1 hPa, rocketsondes are ~15-20 K warmer than CIRA86, MLS and HALOE, although each data set shows a similar semi-annual seasonal cycle.

(possibly related to the harmonic analysis of sparse HALOE observations near 60°N).

Comparisons at 80°N (Figure 16) show a similar overall character, with analyses agreeing reasonably well with rocketsondes at 10 and 1 hPa (except for cold rocketsonde biases at 1 hPa during winter). Systematic warm rocketsonde differences are observed at 0.1 hPa, but these differences are smaller than those observed at 60°N.

b. Comparisons with lidars

The lidar temperature measurements have the most data available in the latitude bands near 20°N and 40°N (Figure A.3). Figure 17 shows a comparison of seasonal temperature variations near 20°N between lidar (from Mauna Loa) and zonal mean

analyses at 10, 1 and 0.1 hPa. At 10 hPa the analyses form a relatively compact group, except for the warmer CIRA86 and UKTOVS data, and the lidar data are in excellent agreement with the larger group. At 1 hPa there is a wider spread (~5 K) between the analyses, with the lidar measurements generally toward the middle or lower range of analyses. At 0.1 hPa, there is overall reasonable agreement between the lidar and temperatures from CIRA86, MLS and HALOE data.

Similar comparisons for measurements near 40°N (lidars from Table Mountain, OHP, Hohenpeissenberg and Toronto) are shown in Figure 18. The overall patterns are very similar to 20°N (Figure 17), with excellent agreement at 10 hPa (again with CIRA86 and UKTOVS as warm outliers). The lidars fall in the mid-range of analyses at 1 hPa, and exhibit very good agreement at 0.1 hPa. We note that because of the substantial variability evident in the lidars at 1 hPa (even during local summer), they do not provide strong guidance in assessing uncertainties in the various analyses near the midlatitude stratopause. We note also that the overall good agreement between the lidars and satellite data at 0.1 hPa in Figures 17-18 is further evidence that the larger differences with rocketsondes in the mesosphere (Figures 13-16) are primarily due to the different time periods covered, given the knowledge of strong decadal-scale cooling near and above the stratopause (Ramaswamy et al., 2001).

Lidar data for the Arctic region are primarily available during winter, and a seasonal comparison is not possible. Figure 19 shows a profile comparison at 80°N for January, based on lidar data from Eureka, Ny Alesund and Thule. The lidars and analyses show good agreement up to the stratopause, and the lidars are slightly colder than the CIRA86 and MLS data in the polar mesosphere.

2. Interannual variability in extratropics

Time series of monthly, zonal mean temperatures are compared here in order to quantify how well year-to-year variability is captured in the various data sets. The focus here is on the extratropical stratosphere during winter and spring (times of maximum variability). Interannual variability in the tropics is discussed separately below.

Figure 20 shows comparisons for February temperatures in the Arctic polar region at 80°N for 1979-1999. Overall there is excellent agreement in detail at 100 hPa, and good correspondence between the different data sets at 10 and 1 hPa (aside from the approximately constant biases discussed above). Similar results are found for other months (not shown). Thus estimates of interannual variability in the Arctic are for practical purposes not dependent on data type. Figure 21 shows similar comparisons for the Antarctic (80°S) in October. Overall there is somewhat poorer agreement than for the analyses over the Arctic. At 100 hPa the CPC results show much less cooling during the 1990's than the other analyses. Note however that the 100 hPa CPC results are archived from operational NCEP tropospheric analyses, which are subject to continual analysis system improvements and changes; a similar plot at 50 hPa (where the stratospheric analyses are constant in time) does not highlight the CPC results as an outlier. Results at 10 hPa in Figure 21 show reasonable agreement, and the long records of CPC and UKTOVS data at 1 hPa have similar variability.

3. Longitudinal structure

Comparisons of the full 3-dimensional structures in the temperature climatologies show that differences are primarily a function of latitude, and accurately characterized by zonal means. However, zonal variations are evident in some difference fields, likely

related to data availability and analyses, and a few examples are shown here. Figure 22 shows the climatological January NH 10 hPa temperature from UKMO, together with difference fields for CPC and FUB data. The differences with CPC data are positive and linked to the cold polar vortex (i.e., the coldest temperatures are analyzed warmer in CPC results). Similar difference patterns tied to vortex structure are found in Southern Hemisphere spring statistics (not shown). In contrast, differences with FUB temperatures in Figure 22 are primarily negative and not as obviously tied to the vortex, but rather they are largest over the North American and European-Asian land masses (where the majority of radiosonde data are available).

4. Tropical seasonal cycle in temperature

The tropics present special problems for analysis of stratospheric temperatures and winds. The tropical tropopause temperature minimum has a sharp vertical structure that is not well resolved by satellite measurements, and it is also problematic for assimilation/forecast models with vertical resolution of ~1-2 km. Temperature anomalies associated with the quasibiennial oscillation (QBO) have relatively shallow vertical structures, which are also poorly resolved by nadir-viewing operational satellites. Thus it is not surprising to find a wide variance between climatological data sets in the tropics. Here we compare each data set for seasonal variation and interannual variability (the latter focusing on the QBO). The analyses here complement the tropical data comparisons shown in Pawson and Fiorino (1998a, b).

The seasonal variations of equatorial temperature at 100, 50 and 30 hPa derived from each climatological data set are shown in Figure 23. Included in these figures are estimates of monthly temperatures derived from radiosonde measurements at an ensemble

of approximately 30 near-equatorial stations (obtained from Dian Seidel, personal communication; the data set is described in Seidel et al., 2001). The amplitude of the seasonal cycle in temperature is reasonably well captured in most data sets at 100 hPa, but there are clear biases among the data sets. In particular, the ERA15, ERA40 and FUB data are the coldest and agree best with radiosondes, whereas UKMO, CPC, NCEP and CIRA86 data each have a consistent warm bias of ~2-3 K (and UKTOVS is almost 10 K too warm, and not shown in Figure 23). At 50 and 30 hPa the seasonal variations are smaller than at 100 hPa; most analyses at 30 hPa exhibit a December-March minimum which is less evident in the radiosondes. The CIRA86 and UKTOVS (not shown) data are warm outliers at 50 hPa with CPC, NCEP and ERA40 on the cold side compared to radiosondes. At 30 hPa, the NCEP and UKMO analyses are relatively cold.

Figure 24 shows similar statistics for temperature variations at 10, 1, 0.1 and 0.01 hPa, where at each level the dominant variation is a semi-annual oscillation (SAO). There is approximate agreement in the amplitude and phase of the SAO at 10 hPa across many data sets, but biases on the order of 5 K between the different analyses. Similar mean biases are seen at 1 hPa, along with larger differences in SAO amplitude and phase (quantified below). The 0.1 hPa temperatures show quite good agreement between CIRA86, MLS and HALOE, whereas at 0.01 hPa (~80 km) there are substantial differences in detail between these three data sets.

a. Tropical rocketsondes

Rocketsonde comparisons in the tropics are available near 10°N and 10°S; the temperature comparisons are similar at both latitudes, and we focus here on results near 10°N. Figure 25 shows the 10°N rocketsonde climatology and analysis temperatures at 10,

1 and 0.1 hPa. The SAO amplitude and phase evident in rocketsonde data at 10 and 1 hPa is reasonably consistent with the various analyses, although note that observations near 10°N do not capture the full SAO amplitude at the equator (as shown below in Figure 27). At 0.1 hPa the rocketsondes show a less coherent SAO than that inferred from the CIRA86, MLS and HALOE data, and furthermore the rocketsondes are approximately 10 K warmer.

b. Semi-annual oscillation (SAO)

Because the SAO dominates the seasonal variation in equatorial temperatures, it is useful to quantify the SAO amplitude and phase structures derived from the different data sets analyzed here. A more comprehensive review and climatology of the SAO (extending to 100 km) is provided in Garcia et al. (1997). The results here are based on simple harmonic analyses of the different data sets for the time periods available.

The vertical structure of the temperature SAO amplitude and phase are shown in Figure 27, including results from each data set. As well-known from previous analyses (e.g., Hirota, 1980), the temperature SAO has a double peaked structure in altitude, with maxima below the stratopause (~ 45 km) and mesopause (~ 70 km), and these maxima are approximately out of phase. The maximum near 45 km has an amplitude of ~4 K in MLS, HALOE, CIRA86 and ERA40 data sets, and substantially weaker amplitude in CPC, UKMO and UKTOVS data. For the maximum near 70 km the CIRA86, MLS and HALOE show a range of amplitudes of ~4-7 K. For further comparison of the upper level peak, Figure 27 shows results derived from Solar Mesosphere Explorer (SME) temperature data for 1982-1986 (taken from Garcia and Clancy, 1990). These SME results show similar amplitude and phases as the other data sets, but don't exhibit an absolute peak near 70 km.

Figure 27 compares the amplitude and phase structure of the temperature SAO as a function of latitude at 2hPa and 0.046 hPa (near the amplitude maxima seen in Fig. 26). The different data sets at 2 hPa show a clear separation in terms of SAO amplitude, with the ERA40, MLS, HALOE and CIRA86 data having amplitudes near 4 K, approximately twice as large as the CPC, UKMO and UKTOVS results. The rocketsonde results (near 8°N and 8°S) show amplitudes that agree better with values from the former (larger amplitude) group. Phases at 2 hPa are in good agreement between all data sets (maximum near April 1). Comparisons at 0.046 hPa show less agreement in amplitude between the few data sets. The HALOE and MLS data both show an equatorial maximum (5-7 K), which is not evident in CIRA86. Rocketsondes have weaker SAO amplitudes than the other data sets at this high altitude.

5. Tropical temperature interannual variability

Interannual anomalies in 100 and 70 hPa equatorial temperature for the period 1985-1999 are shown in Figure 28, with anomalies calculated as differences from the 1992-1997 mean seasonal cycles shown above. The size of the variations at 100 hPa ~~variations~~ are small ($\sim \pm 1-2$ K), and there are substantial differences among the different data sets regarding details of these small changes. At 70 hPa (where FUB and UKTOVS are not available) the interannual temperature changes are $\sim \pm 2-3$ K, larger than those at 100 hPa, and there is overall good agreement among the different data sets (with the latter half of the 1990's being relatively cold).

Interannual temperature changes at 50, 30 and 10 hPa are shown in Figure 29. Variability at these levels is dominated by the quasi-biennial oscillation (QBO), and while a QBO is evident in each data set, the amplitude varies considerably. For comparison, we

include in the 50 and 30 hPa plots in Figure 29 temperature anomalies derived from radiosonde measurements at Singapore (1°N). These comparisons suggest the QBO temperature anomalies are most accurately captured in FUB analyses, and underestimated in each of the other data sets to some degree. Negative temperature anomalies (easterly shear) are particularly poorly sampled. The interannual anomalies at 10 hPa show a clear QBO signal in the FUB analyses after 1991; the QBO is evident but much weaker in the other data sets. Prior to 1990 there are large differences among anomalies derived from the five available data sets (note the FUB 10 hPa temperatures are only available during winter months prior to 1992).

Interannual temperature anomalies at 1 hPa are shown in Figure 30, derived from UKMO, CPC and UKTOVS data. The only records extending prior to 1990 are the CPC and UKTOVS analyses, and these show differences of 2-3 K for the pre-1990 period (and hence substantial differences in decadal trends). A separate data set included in Figure 30 shows brightness temperature (radiance) anomalies for 1979-1998 derived from the series of Stratospheric Sounding Unit (SSU) measurements (which are part of the TOVS data that go into the CPC and UKTOVS analyses). The SSU data set in Figure 30 used overlap periods between the different satellite instruments to make adjustments, in an effort to produce a homogeneous long-term data set (see Ramaswamy et al., 2001). The SSU channel 27 data in Figure 30 are representative of a thick layer of the upper stratosphere, spanning approximately 34-52 km, with a peak near 44 km (between 1-2 hPa in pressure), and thus comparisons with the 1 hPa analyses are not exact. Nonetheless, the SSU time series suggests that interannual variations in the CPC temperatures at 1 hPa may have uncorrected biases which influence estimates of long term variability (such as decadal

trends or 11-year solar cycle changes); somewhat better overall agreement is seen between SSU and UKTOVS results. The UKMO analyses in Fig. 30 show cold anomalies after 1997, which are an erroneous result related to an ozone problem in the assimilation model during this time.

6. Temperatures for pre-1979 data

The FUB and NCEP reanalysis data sets have stratospheric temperatures (up to 10 hPa) for the pre-1979 period, i.e., prior to the availability of satellite data. The inclusion of satellite temperatures in the NCEP reanalysis has a significant impact on regions with relatively little radiosonde data (Mo et al., 1995). As an example, Figure 31a shows time series of 100 hPa equatorial temperature from the NCEP reanalysis, showing a clear discontinuity of approximately 3 K prior to and after 1979, coincident with the inclusion of satellite temperatures. The spatial structure of this temperature discontinuity in NCEP reanalyses is shown in Figure 31b, comparing 15-year averages before and after 1979. The largest differences are observed in the tropics and SH middle latitudes (regions of few radiosondes); altitudes near the tropopause are warmer with the inclusion of satellite data, while the region of 30-50 hPa is cooler. Corresponding stratospheric zonal wind discontinuities of $\pm 2-4$ m/s are found in the tropics and SH midlatitude and polar regions (not shown here). Extreme caution should be used in analyzing long-term variability of NCEP data in these regions.

Differences between NCEP and FUB temperature analyses over the NH are shown in Figure 32, comparing 5-year periods before (1974-1978) and after (1993-1997) the satellite changes in NCEP data (presumably the FUB data are more homogeneous). Significant differences between the two time periods are found in the tropics at 100 hPa,

where the NCEP reanalyses are colder than FUB for 1974-1978, but warmer for 1993-1997. The artificial warming in NCEP data between these periods is consistent with the results in Figure 31. Figure 32 also shows systematic differences in 30 hPa temperature over the entire hemisphere (NCEP warmer for the post-satellite period), but the differences are relatively small (~ 1 K). The comparisons in Figure 32 suggest temperatures in other regions are less sensitive to the satellite discontinuity.

B. Zonal mean zonal winds

1. Zonal mean climatology

The January zonal mean zonal wind climatology (for 1992-1997) from UKMO data is shown in Figure 33, together with differences from the other climatological data sets. In general there are relatively large differences in the tropics, related to the uncertainties in deriving balanced winds in low latitudes from temperature (height) data. Detailed comparison of tropical winds are discussed separately below. The difference patterns in NH extratropics show a consistent pattern of positive values near 60°N for each contemporaneous data set (CPC, UKTOVS, NCEP and ERA40), indicating a slightly weaker polar night jet in UKMO data. More complicated global patterns are seen in the CIRA86 differences. Figure 34 shows UKMO climatology and differences with CPC and ERA40 winds for July and October. In July there are relatively small differences (outside of the tropics), and the strength of the intense SH polar jet is similar in each analyses. During October the UKMO SH polar jet is somewhat stronger than the CPC and ERA40 jets. Note these October wind differences are consistent (via thermal wind) with the colder Antarctic polar vortex analyzed in UKMO data (see Figures 3-4).

Figure 35 compares January and July zonal wind climatologies from each data set at 100, 10 and 1 hPa. Outside of the tropics there is reasonable agreement between most analyses, with the CIRA86 climatology showing some biases in detailed structure. The westerly jets are strongest in UKTOVS data.

a. Comparison to rocketsondes

Rocketsondes provide direct measurements of zonal winds, and are unique for comparing to winds derived from analyses (given the caveat of differing time periods). Seasonal climatologies of zonal winds derived from rocketsondes are compared with the various analyses at 30°N and 60°N in Figure 36, for pressure levels 10, 1 and 0.1 hPa. At 30°N there is quite good agreement in the winds at all levels; note especially the strong subtropical mesospheric jet (at 0.1 hPa) in rocketsondes, CIRA86 and UARS data. At 60°N there are some systematic differences with rocketsondes during local winter (November-March) at 10 and 0.1 hPa, possibly related to real (decadal-scale) time changes. This effect is less evident at 1 hPa.

2. Interannual variability in extratropics

Interannual variability in zonal winds at 100, 10 and 1 hPa is compared in Figure 37 for the Arctic (60°N) in February and Antarctic (60°S) in October (these are periods of maximum variability). Year-to-year changes are nearly identical among the available data sets in the NH. Slightly larger differences are evident in the SH, although the main year-to-year changes are similar across the data sets. Thus overall there is good confidence in estimates of interannual wind variability in high latitudes.

3. Tropical seasonal cycle

Tropical stratospheric winds present particular problems, because there are few direct wind measurements on a daily basis above the lower stratosphere. Also, due to the smallness of the Coriolis parameter, determination of balance wind in the tropics requires a more accurate estimate of horizontal temperature gradients than at higher latitudes. Thus special attention is required in assessing the quality of tropical winds.

The seasonal variation of equatorial zonal winds at 100 and 50 hPa are shown in Figure 38. An annual cycle is evident at 100 and 50 hPa (maximum easterlies during July-September), and aside from the CIRA86 results there is overall ~~there is~~ agreement to within a few m/s between the different data sets. Similar statistics are compared for the 30, 10 and 1 hPa levels in Figure 39. There is approximate agreement among analyses at 30 and 10 hPa, aside from the CIRA86 (strong easterly biases). There is a pronounced SAO in a zonal wind at 1 hPa in Figure 39 which shows similar magnitudes and phases in each data set (discussed more below).

a. Tropical rocketsondes

Rocketsondes are particularly valuable for ground-truth measurements of tropical winds in the middle atmosphere, given the uncertainties in balance wind estimates discussed above. Extensive rocketsonde data are available near 10°N and 10°S, and because there is a substantially different seasonal cycle at these latitudes, we include comparisons for both 10°N and 10°S in Figure 40. The overall impression from Figure 40 is that there is remarkably good agreement between the rocketsonde climatologies and analyses at 10 and 1 hPa, with appropriate seasonal variations and cross-equatorial differences mirrored in all data sets. The rocketsondes at 10°S, 0.1 hPa also show

approximate agreement with the CIRA86 (and UARS) data sets; there are fewer rocketsondes available at 10°N, 0.1 hPa.

b. Semi-annual oscillation

The vertical and latitudinal amplitude and phase structure of the zonal wind SAO is shown in Figure 41, comparing each data set along with rocketsonde results at 8°N and 8°S. The vertical structure shows an amplitude maximum near the stratopause (~50 km), with reasonable agreement between various data sets. A second amplitude maximum near the stratopause (~80km) is suggested in UARS winds. The latitudinal structure at 1 hPa shows maximum SAO amplitude near 10-20°S for most data sets, which is distinct from the equatorially-centered SAO in temperature (Figure 27). The rocketsonde results near 8°N and 8°S suggest a latitudinal asymmetry consistent with analyses (i.e., larger zonal wind SAO in the SH subtropics). The rocketsonde SAO amplitudes are approximately 25% larger than most analyses, while the phases are in reasonable agreement.

4. Tropical interannual variability and the QBO

Figure 42 shows interannual anomalies in equatorial zonal wind at 50, 30 and 10 hPa during 1985-1999 derived from the various analyses. The QBO dominates variability in these time series, and included in Figure 42 are anomalies derived from Singapore radiosonde data, which are a standard reference for the QBO (e.g., Naujokat, 1986). The QBO signal is evident in each analysis, but the amplitude varies strongly between different data (and with altitude). In general the assimilated data sets (UKMO, NCEP, ERA15 and ERA40) have the largest amplitudes, and most closely approach the Singapore data, whereas the balance winds derived from CPC and UKTOVS are much too weak. The strength of the QBO in the different data sets is quantified in Figure 43, where the

equivalent “QBO amplitude” is plotted as a function of latitude (at 30 hPa) and height. The QBO amplitude is defined as $\sqrt{2}$ •rms deviation of deseasonalized anomalies during 1992-1997 (this is the equivalent amplitude of a harmonic oscillation, following Dunkerton and Delisi (1985)). For comparison, Figure 43 also includes the 30 hPa QBO amplitude derived from tropical radiosonde climatologies in Dunkerton and Delisi (1985), plus the equivalent result from Singapore radiosonde measurements over pressure levels 70-10 hPa (using data as in Figure 42). Overall the ERA40 data exhibit the largest QBO amplitude (in good agreement with the radiosonde climatology and Singapore data), with the ERA15, UKMO and NCEP reanalyses somewhat weaker, and CPC and UKTOVS (balance winds) as severe underestimates. The ERA40, ERA15, UKMO and NCEP data show approximately similar amplitudes between 70 and 30 hPa, whereas above 30 hPa there are much larger differences, and only the ERA40 approaches the Singapore amplitudes over 20-10 hPa. Above 10 hPa there is a factor of two difference between the ERA40 and UKMO results, but no radiosonde data for direct comparison.

Figure 44 shows wind anomalies at 1 hPa from UKMO, CPC and UKTOVS data. As with temperatures (Figure 30), there is some approximate agreement after 1990, but larger differences between CPC and UKTOVS for the earlier period. The UKTOVS time series suggest a QBO signal of 1 hPa in the early record which is seen in all three data sets after 1990 (and which is evident at 1 hPa in rocketsonde data, e.g., Gray et al., 2001).

C. Zonal averaged heat and momentum fluxes

The zonally averaged fluxes of heat ($\overline{v'T'}$) and momentum ($\overline{u'v'}$) are fundamentally important diagnostics of atmospheric wave behavior and large-scale transport. Their calculation is based on covariances of eddy winds and temperatures (in longitude), and

these fluxes provide sensitive diagnostics of planetary wave behavior and coupling with the mean flow (in both observations and models). Of primary importance is the poleward eddy heat flux ($\overline{vT'}$) in the extratropical lower stratosphere, which is proportional to the vertical wave activity flux from the troposphere into the stratosphere (e.g., Andrews et al., 1987). The fluxes considered here are calculated from daily data and then monthly averaged (i.e., they contain both stationary and transient components). Because daily data are involved in these calculations, we focus on comparisons among UKMO, CPC and NCEP reanalyses. The time period covered is 1992-1997 (a few ERA15 results are also shown for reference, but these are for the period 1988-1993 and are thus not directly comparable). Statistics are compared for NH winter-spring and SH spring seasons, when stratospheric planetary waves and fluxes are maximum.

January climatological heat fluxes at 100, 50 and 10 hPa are compared in Figure 45. Maximum values are observed approximately over 40-70°N, with similar latitudinal structures for each data set. The seasonal variations of $\overline{vT'}$ averaged over 40-70°N and 40-70°S at 100 hPa are shown in Figure 46. The magnitude of ($\overline{vT'}$) in the NH varies by ~ 10-20% between the analyses, with NCEP on the stronger side and CPC slightly weaker. These uncertainties are consistent with Newman and Nash (2000), who include comparisons with other data sets (for shorter periods). This 10-20% difference is thus the current level of uncertainty in this derived quantity over NH midlatitudes. Similar statistics for the SH in Figures 45-46 show the CPC data as an outlier with substantially smaller fluxes than the other analyses. Interannual variability of heat fluxes at 50 hPa are shown in Figure 47 for February in the NH and October in the SH (including results from ERA15

data). Reasonable agreement between analyses is seen in the NH (differences of ~15%), and the (weak) biased CPC estimates evident in the SH (although the year-to-year variations are captured to some degree in CPC data).

Climatological comparisons for momentum fluxes ($\overline{u'v'}$) are shown in Figure 48.

Reasonable agreement is found between the analyses at 100 hPa in both hemispheres (outside of the tropics). At higher levels there are larger differences. The NCEP reanalyses have particularly small ($\overline{u'v'}$) in the NH at 50 hPa, and the CPC analyses appear systematically small in the SH, similar to the heat fluxes in Figure 45.

D. Summary: Biases and outstanding uncertainties

Summary of largest biases

The following is a list of the largest apparent biases in each climatological data set, as derived from the foregoing intercomparisons. These are identified when individual data sets are 'outliers' from the group, for these particular features.

- UKMO
 - cold temperature biases (~5 K) near the stratopause (globally)
 - warm tropical tropopause temperature (1-2 K)
- UKTOVS
 - large temperature biases ($\sim \pm 3-5$ K) in low latitudes ($\sim 30^\circ\text{N-S}$) over much of the stratosphere (20-50 km)
 - winter polar night jets somewhat too strong
 - weak tropical wind variability (derived from balanced winds)
- CPC
 - warm temperature biases (~3K) in the Antarctic lower stratosphere during winter-spring
 - weak tropical wind variability (derived from balanced winds)
 - warm tropical tropopause temperatures (2-3 K)
 - weak eddy fluxes in SH
- NCEP
 - warm tropical tropopause (2-3 K)
 - satellite data discontinuity across 1978-1979
- ERA15
 - global cold biases (~3 K) at 30 and 10 hPa
- ERA40
 - cold temperature biases (up to 5 K) in the upper stratosphere
- CIRA86
 - warm biases of ~5-10 K over much of the stratosphere (20-50 km)

- relatively large easterly biases in tropical winds (derived from balanced winds)
- weak SAO's in mesospheric wind and temperature

MLS

- warm biases (~3-7 K) over much of the stratosphere (20-50 km)

Outstanding uncertainties and problem areas

The following aspects of the middle atmosphere climatologies show relatively large variability among each of the different data sets, suggesting a fundamental level of uncertainty or high sensitivity to the details of data analysis.

- 1) The tropical tropopause region is biased warm (compared to radiosonde data) in most analyses. The exceptions are the ERA15, ERA40 and FUB analyses, which are more strongly tied to radiosonde measurements. The warm biases in this region of sharp temperature gradients probably result from a combination of low vertical resolution in the analyses, plus the less than optimal use by most analyses of thick-layer satellite temperature measurements.
- 2) The temperature and 'sharpness' of the global stratopause shows large variability among different data sets. This is probably due to the relatively low vertical resolution of TOVS satellite measurements, and also the fact that the stratopause is near the upper boundary for several analyses (UKMO, CPC, UKTOVS).
- 3) Temperature variability in the tropics (associated with the QBO) is underestimated in all analyses (except FUB), compared to radiosonde measurements. The underestimates are particularly large for data that rely primarily on low resolution satellite data (CPC and UKTOVS).
- 4) QBO variations in zonal wind are underestimated to some degree in most analyses, as compared to Singapore radiosonde data. The best results are derived from assimilated data sets (ERA40, ERA15, UKMO and NCEP, in that order) and only ERA40 have realistic amplitudes above 30 hPa. The use of balance winds in the tropics (derived

from geopotential data alone) is problematic for the QBO, and produces large underestimates of variability in the CPC and UKTOVS data sets.

Acknowledgments

These climatological comparisons have resulted from work of the SPARC Reference Climatology Group, which has been ongoing since 1994. A majority of the work has centered around obtaining and archiving the numerous data sets in the SPARC Data Center. The Data Center was primarily organized by Dr. Petra Udelhofen, who unfortunately died during the final stages of preparation of this report. Petra was a valued friend and colleague of everyone involved with this work, and we dedicate it to her memory.

We wish to note special thanks to the NASA ACMAP Research Program, for support of the SPARC Data Center, and for supporting several individuals involved with the SPARC Climatology Group. We also acknowledge the careful work of Fei Wu at NCAR, who performed most of the statistical and graphical analyses included here. Marilena Stone (NCAR) expertly prepared the manuscript through many drafts. The National Center for Atmospheric Research is operated by the University Corporation for Atmospheric Research under sponsorship of the National Science Foundation. We also thank several reviewers (names) for comments and suggestions.

Figure Captions

Figure A.1. The availability of rocketsonde wind and temperature measurements as a function of latitude during the 1960's (top), 1970's (middle) and 1980's (bottom).

Figure A.2. Distribution of rocketsonde zonal wind measurements at 0.1 hPa (~65 km) for the latitude bin centered at 30°N. The crosses show each individual measurement during 1970-1989 binned into monthly samples, and the circles with error bars show the associated monthly means and ± 1 standard deviations which are used in comparisons with global analyses.

Figure A.3. The number and latitude distribution of lidar temperature measurements during the 1990's, which contribute to the lidar climatology.

Figure 1. Top panel shows meridional cross section of January average zonal mean temperature (K) derived from UKMO analyses. Each other panel shows a difference field for temperatures from other analyses (i.e., UKTOVS-UKMO, etc.). Contour interval for the difference fields is $\pm 1, 2, 3 \dots$ (zero contours omitted).

Figure 2. Latitudinal distribution of 100 hPa zonal mean temperature from different analyses, for January, April, July and October.

Figure 3. Latitudinal distribution of differences in 100 hPa zonal mean temperature between each analysis and UKMO (i.e., NCEP-UKMO, etc.). The (UKTOVS-UKMO) differences are relatively large in the tropics (~ 10K) and not included.

Figure 4. Latitudinal distribution of differences in 50 hPa zonal mean temperature between each analysis and UKMO (i.e., NCEP-UKMO, etc.).

Figure 5. Left panels show latitudinal distribution of 10 hPa zonal mean temperatures in January (top) and July (bottom). Right panels show the corresponding differences with UKMO analyses (i.e., CPC-UKMO, etc.).

Figure 6. Latitudinal distribution of 1 hPa zonal mean temperatures in January (left) and July (right).

Figure 7. Latitudinal distribution of zonal mean temperatures at 0.01 hPa (~80 km) (top) and 0.1 hPa (~65 km) (bottom), for January (left) and July (right).

Figure 8. Vertical profiles of zonal mean temperature for January (left) and July (right), for latitudes 80°N (top), the equator (middle) and 80°S (bottom).

Figure 9. Left panels show seasonal variation of 100 hPa zonal mean temperature at 80°N (top) and 80°S (bottom); note the respective time axes have been shifted by 6 months so that winter is in the middle of each plot. Right panels show the respective differences from UKMO analyses.

Figure 10. Seasonal variation of polar temperatures as in Figure 9, but for statistics at 50 hPa.

Figure 11. Left panel compares vertical profiles of zonal mean temperature at 40°N; right panel shows the respective differences from UKMO analyses.

Figure 12. Seasonal variation of 1 hPa zonal mean temperature at 40°N (left) and 40°S (right).

Figure 13. Comparison of rocketsonde temperature statistics at 30°N with zonal mean analyses, showing statistics for January (left) and July (right).

Figure 14. Comparison of the seasonal variation of rocketsonde temperatures near 30°N with zonal mean analyses, for pressure levels 0.1 hPa (top), 1 hPa (middle) and 10 hPa (bottom). Circles denote the rocketsonde means, and error bars the plus/minus one standard deviation.

Figure 15. Seasonal cycle comparison of temperatures near 60°N between rocketsondes and zonal mean analyses. Details are the same as Figure 14.

Figure 16. Seasonal cycle comparison of temperatures near 80°N between rocketsondes and zonal mean analyses. Details are the same as Figure 14.

Figure 17. Comparison of the seasonal variation of lidar temperatures near 20°N with zonal mean analyses.

Figure 18. Seasonal cycle comparison of temperatures near 40°N between lidars and zonal mean analyses.

Figure 19. Comparison of the vertical profile of temperature near 80°N in January between lidar measurements and zonal mean analyses.

Figure 20. Time series of February average zonal mean temperatures at 80°N from each available data set, comparing interannual variability statistics. Results are shown for 1 hPa (top), 10 hPa (middle) and 100 hPa (bottom).

Figure 21. Interannual variability of zonal mean temperatures in the Antarctic (80°S) during October, from each available data set.

Figure 22. Top panel shows climatological January average 10 hPa temperatures from UKMO analyses. Middle panel shows the differences with CPC analyses (CPC-UKMO), and lower panel differences with FUB (FUB-UKMO). Contour interval in the lower panels is 1 K.

Figure 23. Comparison of the seasonal variation in equatorial temperature from available analyses at 30 hPa (top), 50 hPa (middle) and 100 hPa (bottom). Because of relatively large biases, UKTOVS data are not included here. The circles show a climatology derived from near-equatorial radiosonde measurements.

Figure 24. Seasonal variation of equatorial temperature from different analyses, showing results for 0.01 hPa, 0.10 hPa, 1 hPa and 10 hPa.

Figure 25. Comparison of the seasonal cycle of temperatures near 10°N between rocketsondes and zonal mean analyses, at 0.1 hPa (top), 1 hPa (middle), and 10 hPa (bottom).

Figure 26. Comparison of the amplitude (left) and phase (right) of the semi-annual oscillation (SAO) in equatorial temperature derived from each temperature data set. Phase refers to month of the first maximum during the calendar year. The dots show the mesospheric results derived from SME satellite data, taken from Garcia and Clancy (1990).

Figure 27. Latitudinal structure of the amplitude (left) and phase (right) of the temperature SAO derived from each data set, for results at 0.046 hPa (~ 70 km) and 2 hPa (~ 44 km). The dots show the corresponding values derived from rocketsonde data near 8°S and 8°N.

Figure 28. Time series of interannual anomalies in zonal mean temperature at the equator derived from available analyses at 70 hPa (top) and 100 hPa (bottom). Anomalies are defined as differences from the 1992-1997 time average.

Figure 29. Time series of interannual anomalies in zonal mean temperature at the equator from various analyses, together with results from radiosonde measurements at Singapore (1°N). Statistics are shown for 10 hPa (top), 30 hPa (middle) and 50 hPa (bottom).

Figure 30. Interannual anomalies in zonal mean temperature at 1 hPa from available data sets (top), together with similar results derived from SSU satellite measurements (bottom). The SSU data represent temperatures over a ~ 15 km thick layer centered near 1-2 hPa.

Figure 31. Top panel shows time series of zonal mean equatorial temperature at 100 hPa from the NCEP reanalyses over 1957-2001. Heavy lines denote the time averages for 1960-1974 and 1985-1999. Note the jump in temperatures near 1979, associated with the introduction of satellite data into the reanalyses. Bottom panel shows a cross section of temperature differences between 15-year means before (1960-1974) and after (1985-1999) the satellite discontinuity. Contours are $\pm 0.5, 1.5, 2.5, \dots$ K, and shading shows statistically significant differences.

Figure 32. Differences between FUB and NCEP annual average zonal mean temperatures at 30, 50, and 100 hPa, comparing the pre-satellite (1974-1978) and post-satellite (1993-1997) time periods. Error bars show the ± 2 -sigma variability values associated 5-year means (just included on the 1993-1997 results for clarity).

Figure 33. Top left panel shows climatological January average zonal mean wind (m/s) from UKMO analyses. Other panels show the respective differences between each data set and UKMO (i.e., CPC-UKMO), with contours of $\pm 2, 4, 6, \dots$ m/s (zero contours omitted).

Figure 34. Top panels show climatological zonal mean zonal wind (m/s) from UKMO analyses in July (left) and October (right). Middle and lower panels show the respective differences in CPC and ERA40 reanalyses (i.e., ERA40-UKMO), with contours of $\pm 2, 4, 6 \dots$ m/s.

Figure 35. Latitudinal structure of zonal mean zonal wind from various analyses for January (left) and July (right), for statistics at 1 hPa (top), 10 hPa (middle) and 100 hPa (bottom).

Figure 36. Comparison of the seasonal variation of zonal winds measured by rocketsondes with zonal mean analyses at 30°N (left) and 60°N (right), for statistics at 0.1 hPa (top), 1 hPa (middle) and 10 hPa (bottom).

Figure 37. Interannual variation of zonal mean zonal winds during February at 60°N (left) and October at 60°S (right), for pressure levels 1 hPa (top), 10 hPa (middle) and 100 hPa (bottom).

Figure 38. Climatological seasonal cycle of zonal mean zonal winds at the equator from various analyses, for statistics at 50 hPa (top) and 100 hPa (bottom).

Figure 39. Climatological seasonal cycle of zonal mean zonal wind from various analyses at 1 hPa (top) 10 hPa (middle), and 30 hPa (bottom).

Figure 40. Comparison of the seasonal cycle of zonal winds derived from rocketsondes near 10°S (left) and 10°N (right) with zonal mean analyses. Statistics are shown for 0.1 hPa (top), 1 hPa (middle) and 10 hPa (bottom).

Figure 41. Top panels show the vertical profiles of the amplitude and phase of the zonal wind semi-annual oscillation (SAO) at the equator derived from each available data set. Lower panels show the respective latitudinal structures at 1 hPa, and the dots show results from rocketsonde data at 8°S and 8°N. The phase refers to the time of the first maximum during the calendar year.

Figure 42. Time series of interannual anomalies in equatorial zonal mean winds from various analyses at 10 hPa (top), 30 hPa (middle) and 50 hPa (bottom). Anomalies are calculated with respect to the 1992-1997 average. For comparison, these plots also show results derived from Singapore (1°N) radiosonde measurements, which are a standard reference for the zonal wind QBO.

Figure 43. (a) Latitudinal structure of the equivalent QBO amplitude at 30 hPa, defined as $\sqrt{2}$ times the rms anomaly values during 1992-1997 (see text). (b) Shows the vertical structure of QBO amplitude at the equator. For comparison, results of Dunkerton and Delisi (1985) are shown (dots), together with estimates from Singapore radiosondes (plus signs).

Figure 44. Time series of interannual anomalies in equatorial zonal mean wind at 1 hPa derived from various analyses.

Figure 45. Latitudinal structure of zonal mean eddy heat flux $\left(\overline{v'T'}\right)$ during January (left) and October (right), for statistics at 10 hPa (top), 50 hPa (middle) and 100 hPa (bottom).

Figure 46. Seasonal variation of zonal mean eddy heat flux $\left(\overline{v'T'}\right)$ at 100 hPa in the NH (40-70°N, right) and in the SH (40-70°S, left), derived from CPC, NCEP and UKMO analyses over 1992-1997.

Figure 47. Comparison of interannual variability of zonal mean eddy heat flux at 50 hPa from various analyses. Statistics are shown for the NH during February and March, and the SH during October.

Figure 48. Latitudinal structure of zonal mean eddy momentum flux $\left(\overline{u'v'}\right)$ during January (left) and October (right), for statistics at 10 hPa (top), 50 hPa (middle) and 100 hPa (bottom).

4. References

- Andrews, D. G., J. R. Holton and C. B. Leovy, Middle Atmosphere Dynamics. Academic Press, 1987.
- Bailey, M. J. A. O'Neill and V. D. Pope, Stratospheric analyses produced by the United Kingdom Meteorological Office, *J. Appl. Meteorol.*, 32, 1472-1483, 1993.
- Barnett, J. J. and M. Corney, Temperature data from satellites, "Middle Atmosphere Program, Handbook for MAP," Vol. 16, edited by K. Labitzke, J. J. Barnett and B. Edwards, 2-11, 1985a.
- Barnett, J. J. and M. Corney, Middle atmosphere reference model from satellite data, "Middle Atmosphere Program, Handbook for MAP," Vol. 16, edited by K. Labitzke, J. J. Barnett and B. Edwards, 47-85, 1985b.
- Dunkerton, T. J. and D. P. Delisi, Climatology of the equatorial lower stratosphere, *J. Atmos. Sci.*, 42, 376-396, 1985.
- Finger, F. G., H. M. Wolf and C. E. Anderson, A method for objective analysis of stratospheric constant pressure charts, *Mon. Wea. Rev.*, 93, 619-638, 1965.
- Finger, F. G., M. E. Gelman, J. D. Wild, M. L. Chanin, A. Hauchecorne and A. J. Miller, Evaluation of NMC upper stratospheric analyses using rocketsone and lidar data, *Bull. Amer. Meteor. Soc.*, 74, 789-799, 1993.
- Fishbein, E., et al., Validation of the UARS Microwave Limb Sounder temperature and pressure measurements, *J. Geophys. Res.*, 101, 9983-10,016, 1996.

- Fleming, E. L., S. Chandra, M. R. Schoeberl and J. J. Barnett, Monthly mean global climatology of temperature, wind, geopotential height, and pressure for 0-120 km, NASA Tech. Memo, NASA TM-100697, 85 pp., 1988.
- Fleming, E. L. and S. Chandra, Equatorial zonal wind in the middle atmosphere derived from geopotential height and temperature data, *J. Atmos. Sci.*, Vol. 46, 860-866, 1989.
- Fleming, E. L., S. Chandra, J. J. Barnett and M. Corney, Zonal mean temperature, pressure, zonal wind, and geopotential height as functions of latitude, *COSPAR International Reference Atmosphere: 1986, Part II: Middle Atmosphere Models, Adv. Space Res.*, 10, No. 12, 11-59, 1990.
- Garcia, R. R. and R. T. Clancy, Seasonal variation of equatorial mesospheric temperatures observed by SME, *J. Atmos. Sci.*, 47, 1666-1673, 1990.
- Garcia, R. R., T. J. Dunkerton, R. S. Lieberman and R. A. Vincent, Climatology of the semiannual oscillation of the tropical middle atmosphere, *J. Geophys. Res.*, 102, 26,019-26,032, 1997.
- Geller, M. A., M.-F. Wu and M. E. Gelman, Troposphere-stratosphere (surface-55 km) monthly winter general circulation statistics for the Northern Hemisphere-Four year averages, *J. Atmos. Sci.*, 40, 1334-1352, 1983.
- Gelman, M. E., A. J. Miller, K. W. Johnson and R. N. Nagatani, Detection of long term trends in global stratospheric temperature from NMC analyses derived from NOAA satellite data, *Adv. Sp. Res.*, 6, 17-26, 1986.
- Gibson, J. K., et al., ERA description, Reanalysis Project Rept. 1, Eur. Center for Medium-Range Weather Forecasts, Reading, England, 1997.

- Gray, L. J., S. Phipps, T. Dunkerton, M. Baldwin, E. Drysdale and M. Allen, A data study of the influence of the equatorial upper stratosphere on Northern Hemisphere stratospheric sudden warmings, *Q.J.R. Meteorol. Soc.*, 127, 1985-2004, 2001.
- Hamilton, K., Stratospheric Circulation Statistics. NCAR Technical Note NCAR/TN-191 STR, 174 pp., 1982.
- Hauchecorne, A. and M.-L. Chanin, Density and temperature profiles obtained by lidar between 35 and 70 km, *Geophys. Res. Lett.*, 7, 565-568, 1980.
- Hays, P. B., V. J. Arbreu, M. E. Dobbs, D. A. Gell, H. J. Grassl and W. R. Skinner, The high-resolution Doppler imager on the Upper Atmosphere Research Satellite, *J. Geophys. Res.*, 98, 10,713-10,723, 1993.
- Hedin, A. E., A revised thermospheric model based on mass spectrometer and incoherent scatter data: MSIS-83, *J. Geophys. Res.*, Vol. 88, 10, 170-10, 188, 1983.
- Hervig, M. E., et al., Validation of temperature measurements from the Halogen Occultation Experiment, *J. Geophys. Res.*, 101, 10,277-10,286, 1996.
- Hirota, I., Observational evidence of the semiannual oscillation in the middle atmosphere: A review, *Pine Appl. Geophys.*, 118, 217-238, 1980.
- Kalnay, E., et al., The NCAR/NCEP 40-year reanalysis project, *Bull. Am. Meteorol. Soc.*, 77, 437-471, 1996.
- Keckhut, P., A. Hauchecorne and M.-L. Chanin, A critical review of the data base acquired for the long term surveillance of the middle atmosphere by the French Rayleigh lidar, *J. Atmos. Ocean. Technol.*, 10, 850-867, 1995.
- Knittel, J., Ein Beitrag zur Klimatologie der Stratosphaere der Suedhalbkugel, *Meteorol. Abh. Met. Inst., Berlin*, A2, No. 1, 1974.

- Labitzke, K., and B. Naujokat, On the variability and trends of the temperature in the middle atmosphere, *Beitr. Phys. Atmos.* 56, 495-507, 1983.
- Lorenc, A. C., R. S. Bell and B. Macpherson, The meteorological office analysis correction data assimilation scheme, *Quart. J. R. Meteorol. Soc.*, 117, 59-89, 1991.
- Lorenc, et al., The Met Office global 3-dimensional variational data assimilation scheme, *Q.J.Roy. Meteorol. Soc.*, 126, 2992-3012, 2000.
- Manney, G. L. et al., Comparison of UK meteorological office and US NMC stratospheric analyses during northern and southern winter, *J. Geophys. Res.*, 101, 10,311-10,334, 1996.
- Mo, K., Y. Wang, R. Kistler, M. Kanamitsu and E. Kalnay, Impact of satellite data on the CDAS-reanalysis system, *Mon. Wea. Rev.*, 123, 124-139, 1995.
- Nash, J. and G. F. Forrester, Long-term monitoring of stratospheric temperature trends using radiance measurements obtained by the TIROS-N series of NOAA spacecraft, *Adv. Space Res.*, 6, 37-44, 1986.
- Naujokat, B., An update of the observed quasi-biennial oscillation of the stratospheric winds over the tropics, *J. Atmos. Sci.*, 43, 1873-1877, 1986.
- Newman, P. A. and E. R. Nash, Quantifying the wave driving of the stratosphere, *J. Geophys. Res.*, 105, 12,485-12,497, 2000.
- Oort, A. H., Global atmospheric circulation statistics, 1958-1983, NOAA Professional Paper 14, 1983.
- Pawson, S., and co-authors, Climatology of the Northern Hemisphere stratosphere derived from Berlin analyses. Part I. Monthly means, *Met. Abh. FU-Berlin, Neue Folge Serie A, Band 7, Heft 3*, 1993.

- Pawson, S., and co-authors, The GCM-reality intercomparison project for SPARC (GRIPS): Scientific issues and initial results. *Bull. Am. Meteorol. Soc.*, 81, 781-796, 2000.
- Pawson, S. and M. Fiorino, A comparison of reanalyses in the tropical stratosphere. Part 1: Thermal structure and the annual cycle, *Climate Dyn.*, 14, 631-644, 1998a.
- Pawson, S. and M. Fiorino, A comparison of reanalyses in the tropical stratosphere. Part 2. The quasi-biennial oscillation, *Climate Dyn.*, 14, 645-658, 1998b.
- Pawson, S., and B. Naujokat, The cold winters of the middle 1990's in the northern lower stratosphere, *J. Geophys. Res.*, 104, 14,209-14,222, 1999.
- Ramaswamy, V., M. L. Chanin, J. Angell, J. Barnett, D. Gaffen, M. Gelman, P. Keckhut, Y. Koshelkov, K. Labitzke, R. Lin, A. O'Neill, J. Nash, W. Randel, R. Rood, K. Shine, M. Shiotani and R. Swinbank, Stratospheric temperature trends: observations and model simulations, *Rev. Geophys.*, 39, 71-122, 2001.
- Randel, W. J., The evaluation of winds from geopotential height data in the stratosphere, *J. Atmos. Sci.*, 44, 3097-3120, 1987.
- Randel, W. J., Global Atmospheric Circulation Statistics, 1000-1 mb, NCAR Technical Note, NCAR/TN-366 STR, 256 pp., 1992.
- Remsberg, E. E., et al., The validation of HALOE temperature profiles in the mesosphere using Rayleigh backscatter lidar and inflatable falling sphere measurements, *J. Geophys. Res.*, submitted, 2002.
- Russell, J. M., et al., The Halogen Occultation Experiment, *J. Geophys. Res.*, 98, 10,777-10,979, 1993.

- Scaife, A. A., J. Austin, N. Butchart, S. Pawson, M. Keil, J. Nash and I. N. James, Seasonal and interannual variability of the stratosphere diagnosed from UKMO TOVS analyses, *Quart. J. R. Meteorol. Soc.*, 126, 2585-2604, 2000.
- Schmidlin, F. J, Rocket techniques used to measure the neutral atmosphere, *Middle Atmosphere Program Handbook for MAP Volume 19*, edited by Richard A. Goldberg, pp. 1-28 and references therein, March 1986.
- Seidel, D. J., R. J. Ross, J. K. Angell and G. Reid, Climatological characteristics of the tropical tropopause as revealed by radiosondes, *J. Geophys. Res.*, 106, 7857-7878, 2001.
- Smith, W. L., H. M. Woolf, C. M. Haydex, D. Q. Wark and L. W. McMillin, The TIROS-N operational vertical sounder, *Bull. Am. Meteorol. Soc.*, 60, 1177-1187, 1979.
- Swinbank, R. and A. O'Neill, A stratosphere-troposphere data assimilation system, *Monthly Weather Review*, 122, 686-702, 1994.
- Swinbank, R. and D. A. Ortland, Compilation of wind data for the UARS reference atmosphere project, *Adv. Space Res.*, submitted, 2000.
- World Meteorological Organization (WMO), Scientific assessment of ozone depletion: 1998. WMO Report No. 44, Geneva, 1999.

5. An atlas of middle atmosphere temperatures and zonal winds

This section presents a brief atlas of monthly mean temperatures and zonal winds (over 0-85 km), together with estimates of interannual variability in these quantities over 0-50 km. The zonal mean temperature climatology is derived using UKMO analyses over 1000-1 hPa, combined with the HALOE temperature climatology over pressures 1-0.0046 hPa (~ 85 km). The monthly HALOE climatology is available over 60°N-S, and mesospheric temperatures poleward of 60°N and 60°S are derived from the MLS climatology, with offsets at each pressure level used to match the HALOE data at 60°N and 60°S (i.e., the polar latitudinal gradients from MLS are used). The monthly zonal wind climatology (over ~ 0-85 km) is derived from the UARS wind analyses, based primarily on UKMO and UARS HRDI data (see Section 2.9). In order to provide smooth monthly estimates, we use a harmonic analysis of the available time series over 1992-1997.

Estimates of the interannual variability of the zonal mean temperatures and zonal winds are derived using UKMO analyses for the time period 1992-2000. The UKMO analyses have a shorter time record than the CPC or UKTOVS data sets, but provide improved estimates of tropical zonal winds. Interannual standard deviations are calculated from the standard formula

$$\sigma = \left[\frac{1}{N-1} \sum_{i=1}^N (x_i - \bar{x})^2 \right]^{1/2}$$

where \bar{x} represents the ensemble (climatological) mean, x_i is the monthly mean for each year, and N is the number of available years ($N = 9$ for 1992-2000).

As a note, the UKMO temperature analyses had some significant errors introduced after January 1998 at the uppermost levels (at and above 1 hPa), due to an ozone climatology problem in the assimilation model (as seen in Fig. 30). In order to avoid large effects on the interannual variability estimates, temperature variability at and above 1 hPa use statistics derived from the shorter record 1992-1997.

Climatological means and standard deviations are shown below, in the forms of: (1) latitude-height cross sections for each month, (2) latitude-time sections at a few selected pressure levels, and (3) height-time sections at a few latitudes. In the latitude-height and height-time sections we include heavy dashed lines indicating the location of the tropopause (taken from the NCEP/NCAR reanalyses), and the stratopause (defined by the local maximum in temperature near 50 km).

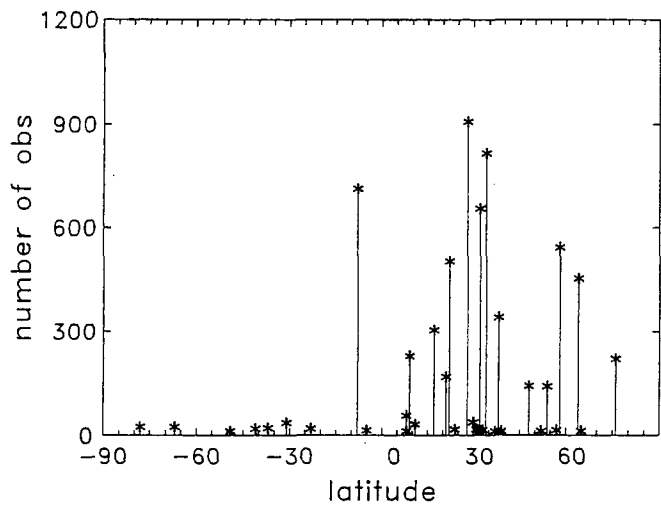
Table 1. Stratospheric climatological data sets

<u>Data Source</u>	<u>Type of Analysis</u>	<u>Analysis Quantities</u>	<u>Time Period Available</u>	<u>Vertical Coverage (in pressure)</u>
UKMO	assimilation	z,T,u,v,w	Nov. 1991-present	1000-0.3hPa
CPC	objective analysis (above 100 hPa)	z, T (balance winds)	Oct. 1978-present	1000-0.4 hPa
UKTOVS	objective analysis	z, T, (balance winds)	Jan. 1979-Apr 1997	100-1 hPa
NCEP reanalysis	assimilation	z,T,u,v,w	Jan. 1979-present	1000-10 hPa
ERA15 reanalysis	assimilation	z,T,u,v,w	Jan. 1979-Dec. 1993	1000-10 hPa
FUB	hand analysis	z,T		100-10 hPa
ERA40 reanalysis	assimilation	z,T,u,v,w	xxx?	1000-1 hPa
CIRA86 climatology	various	z,T,u	various (1960's-1970's)	1000-0.001 hPa
UARS winds	UKMO and HRDI data	u	Jan. 1992-Dec. 1998	1000-0.001 hPa
HALOE temps	harmonic analysis of seasonal cycle	T	Jan. 1992-Dec. 1997	2-0.01 hPa
MLS temps	harmonic analysis of seasonal cycle	T	Jan. 1992-Dec. 1994	32-0.01 hPa

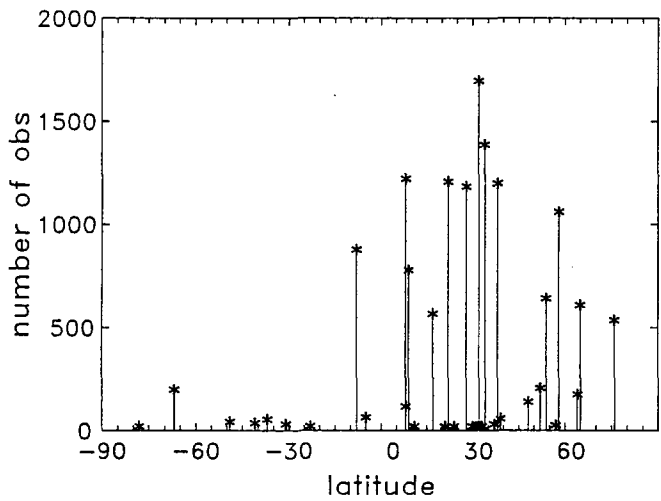
Table 2.
Lidar temperature data obtained from the NDSC web site: <http://www.ndsc.ws/>

<u>Location</u>	<u>available time period</u>
Eureka (80°N)	1993-1998
Ny Alesund (79°N)	1995-1998
Thule (77°N)	1993-1995
Hohenpeissenberg (48°N)	1987-1999
OHP (45°N)	1991-2000
Toronto (44°N)	1996-1997
Table Mountain (34°N)	1989-2001
Mauna Loa (20°N)	1993-2001

Rocketsondes 1hPa 1960-1969



Rocketsondes 1hPa 1970-1979



Rocketsondes 1hPa 1980-1989

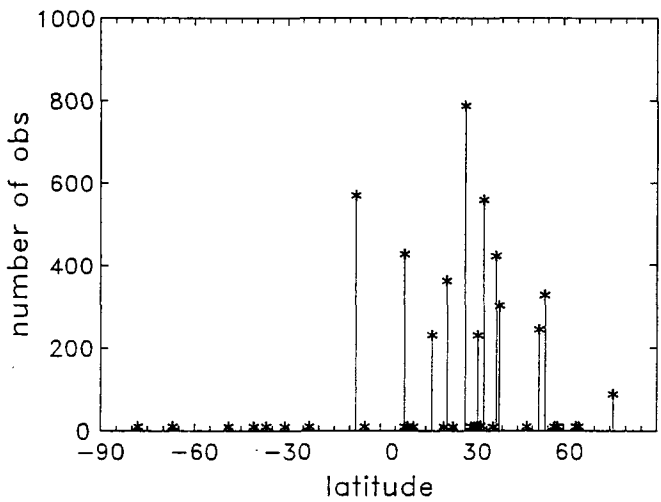


Figure A.1

Rocketsondes .1hPa 30N

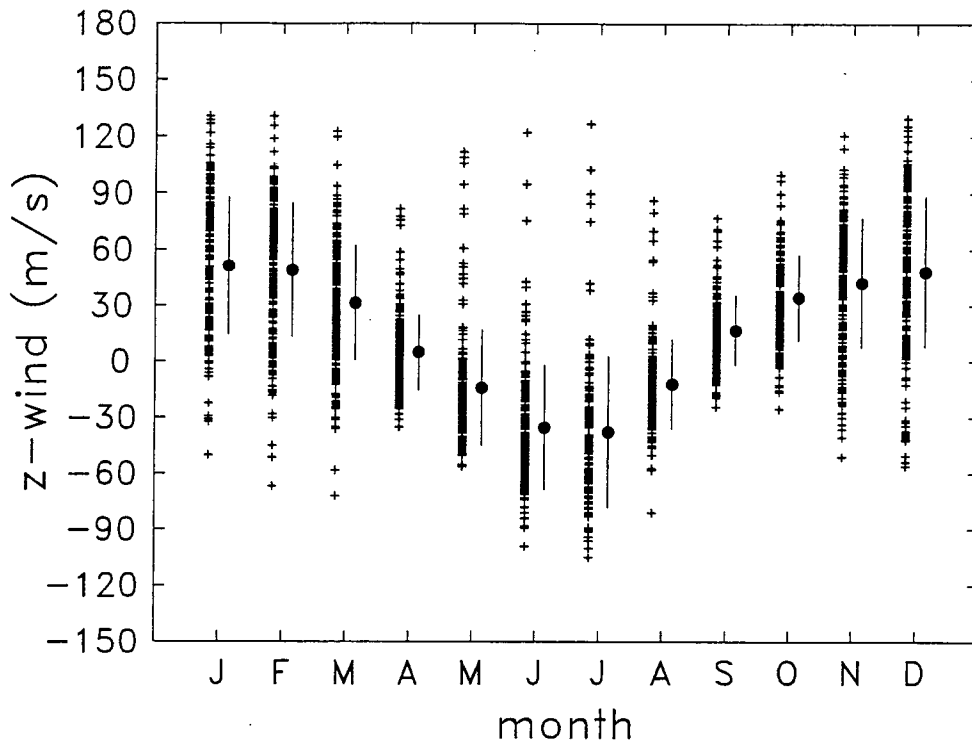


Figure A.2

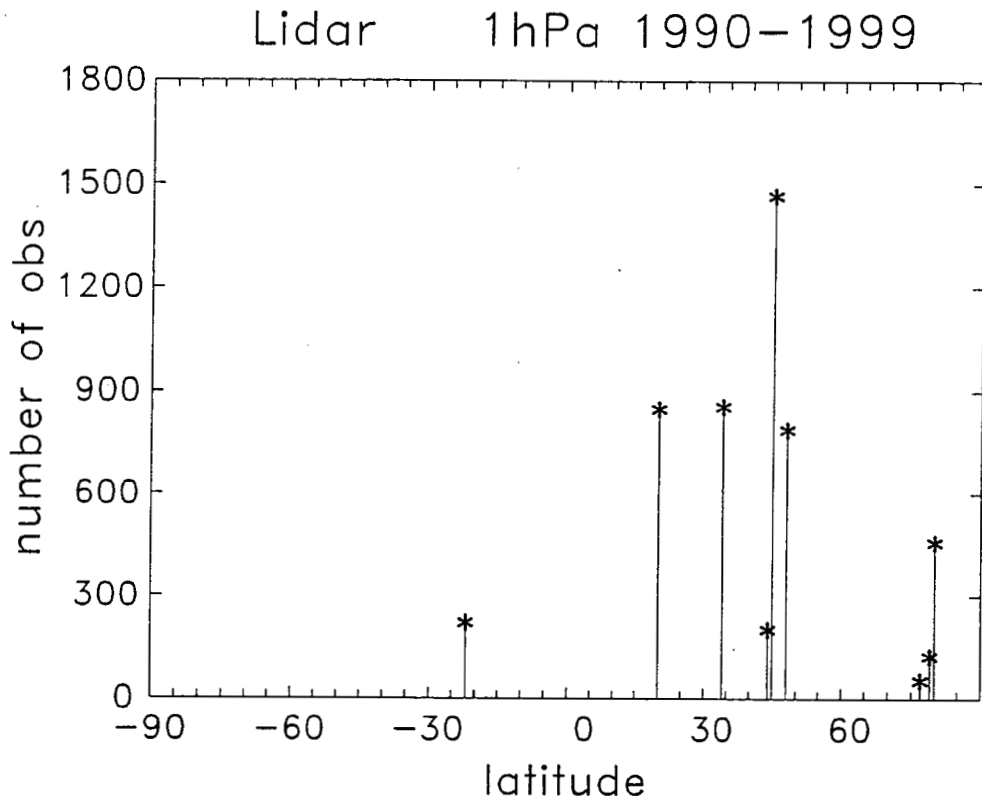
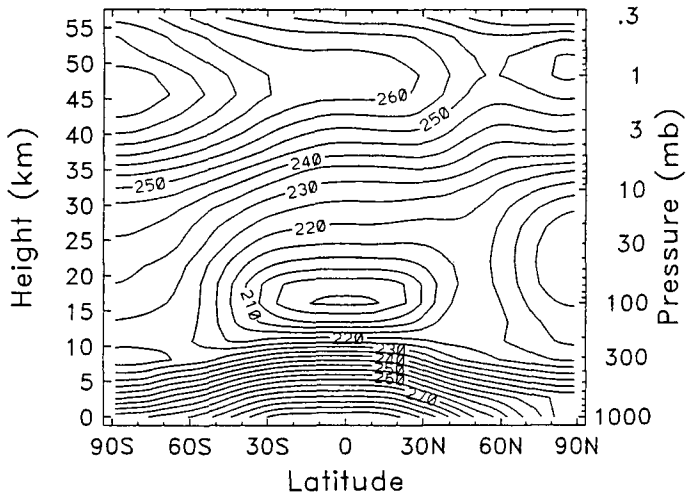
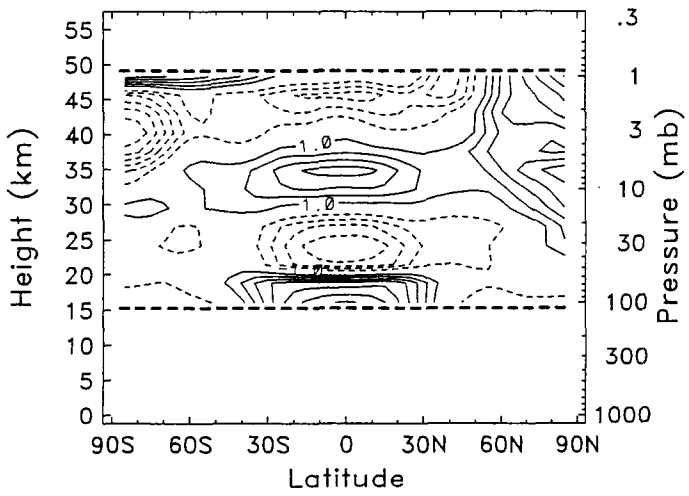


Figure 1.3

UKMO Jan Temp



UKTOVS Jan Temp diff



CPC Jan Janp diff

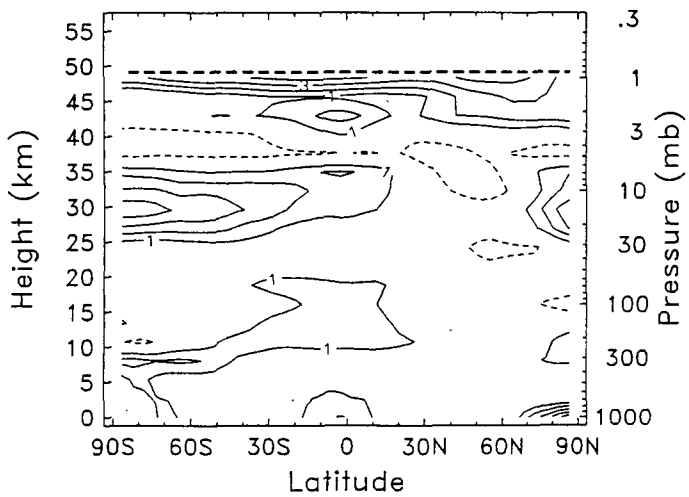
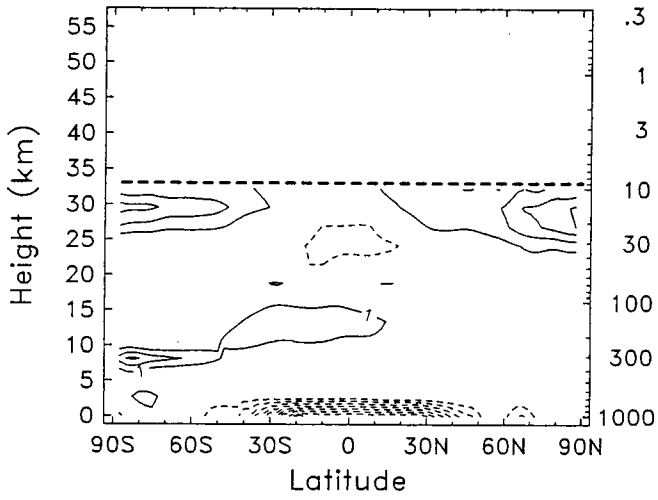
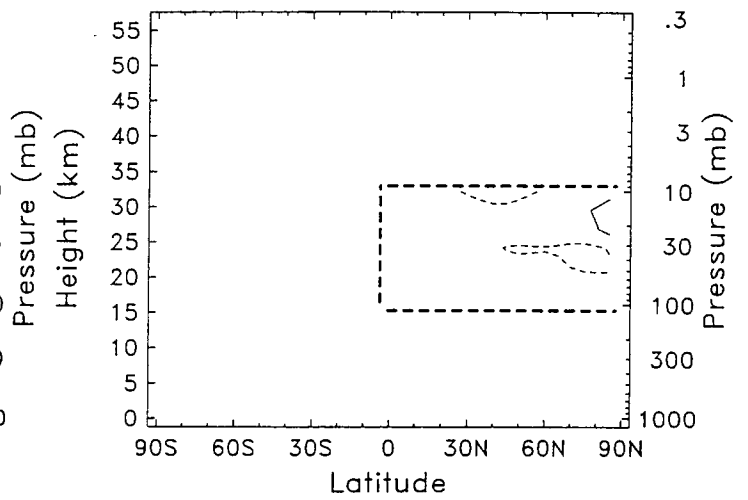


Fig. 1

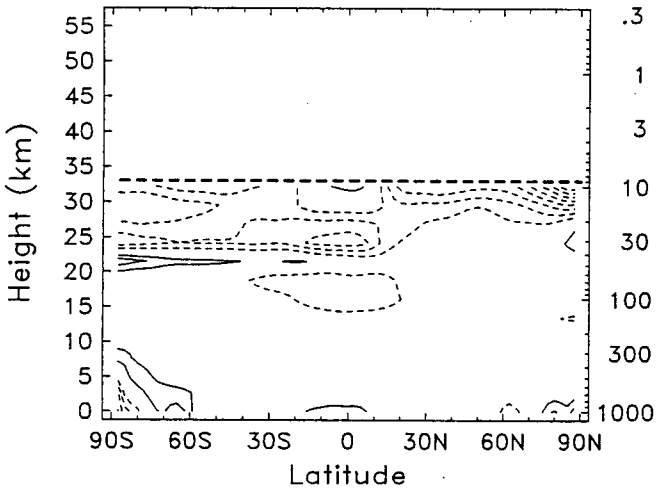
NCEP Jan Temp diff



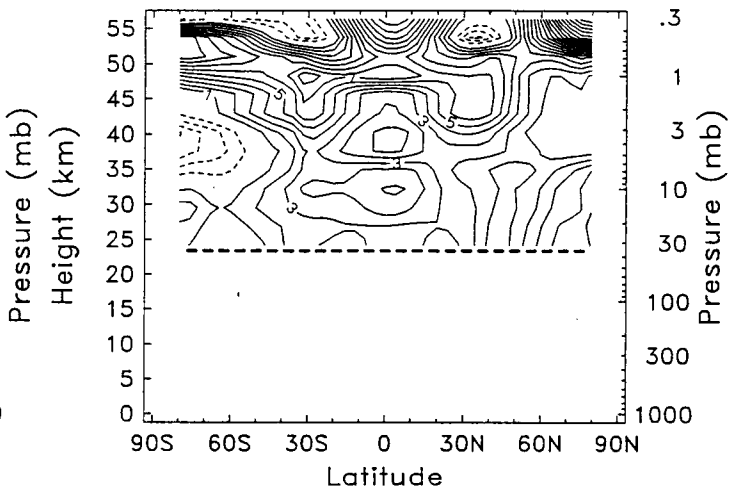
FUB Jan Temp diff



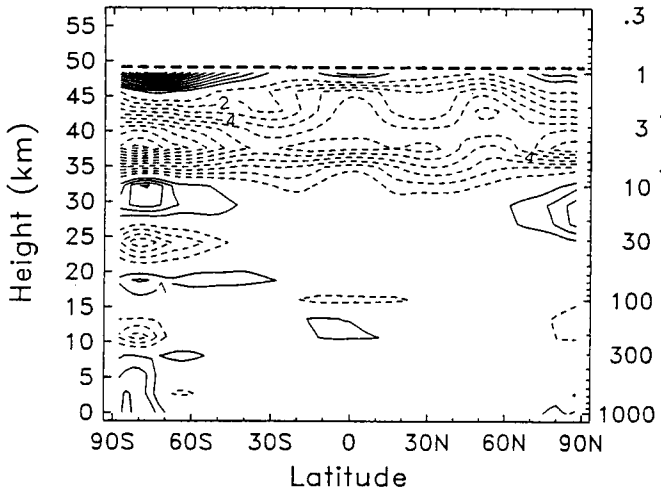
ERA15 Jan Temp diff



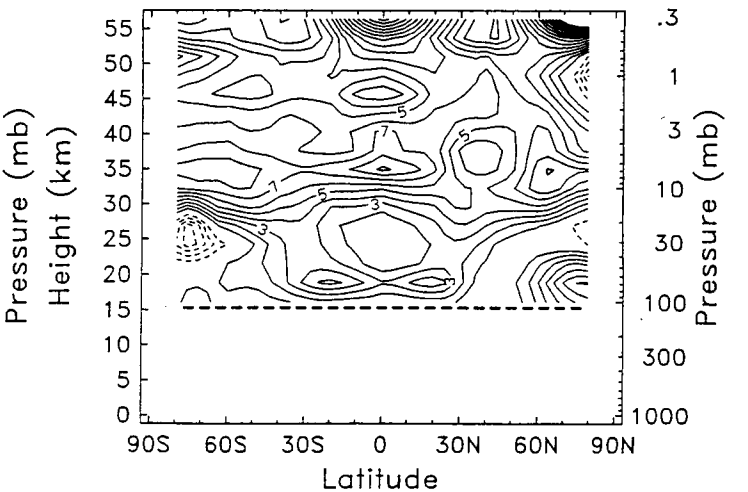
MLS Jan Temp diff



ERA40 Jan Temp diff



CIRA86 Jan Temp diff



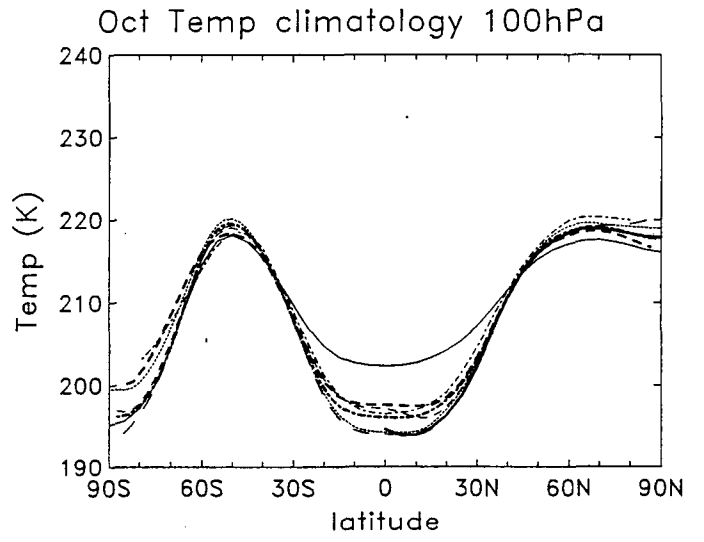
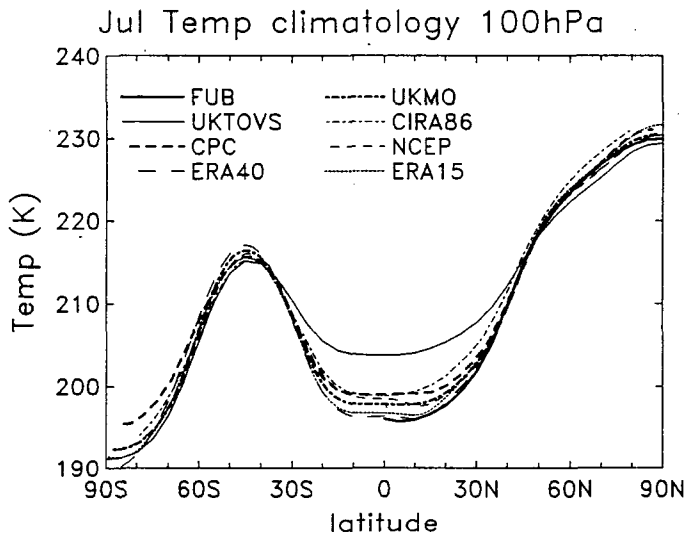
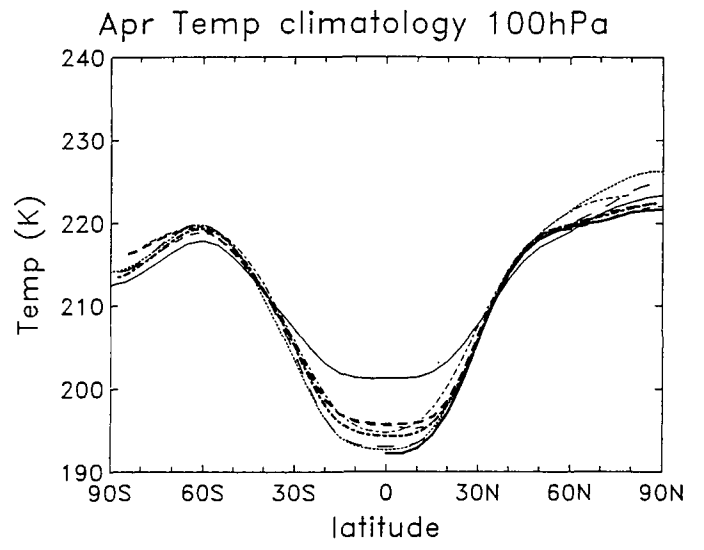
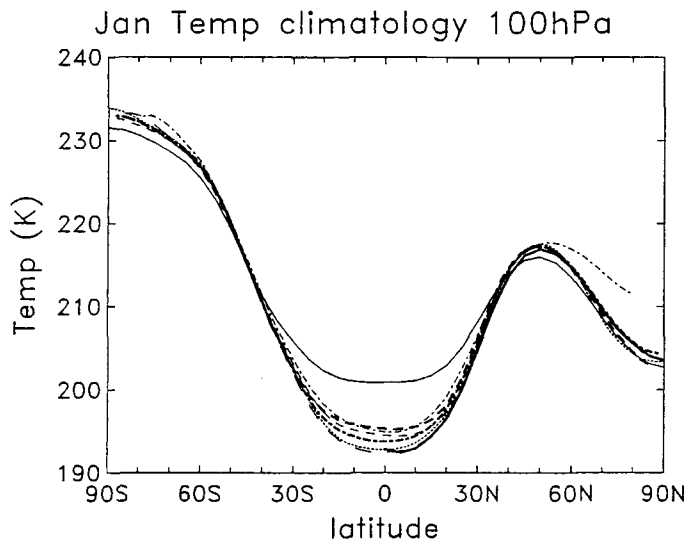


Fig. 2

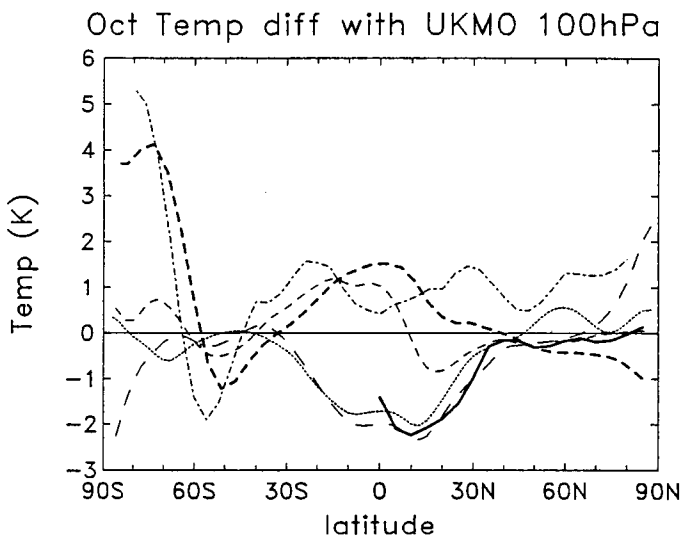
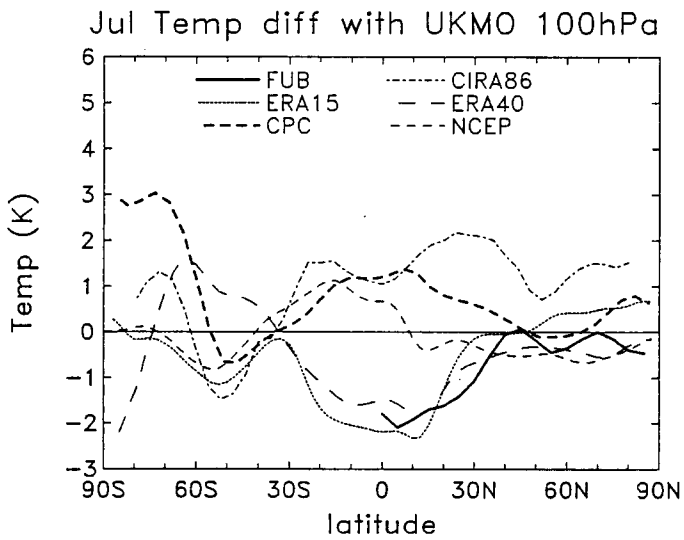
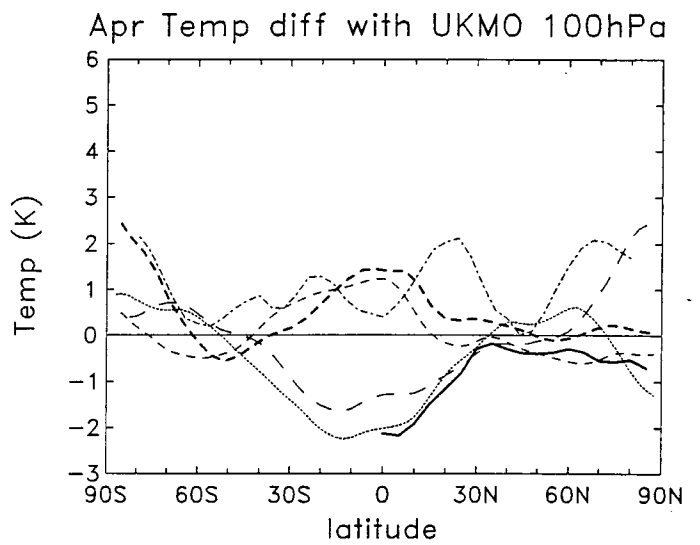
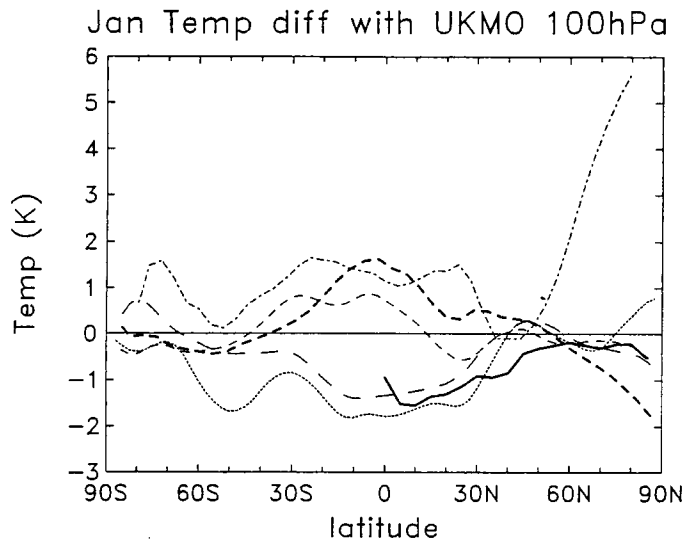


Fig. 3

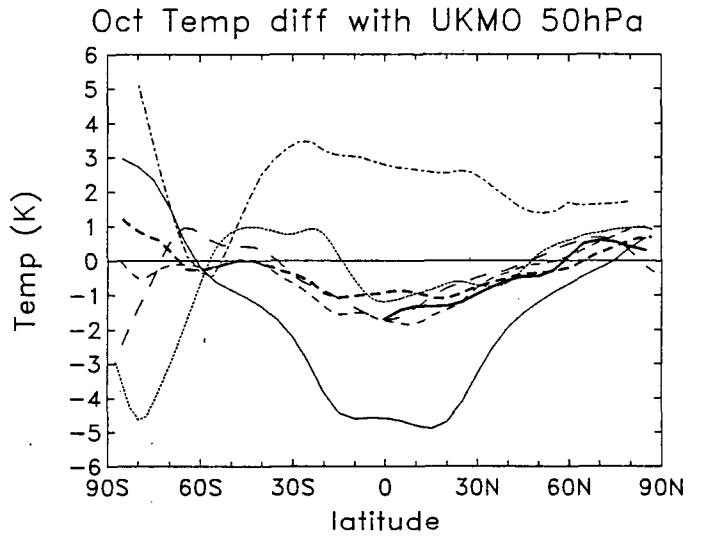
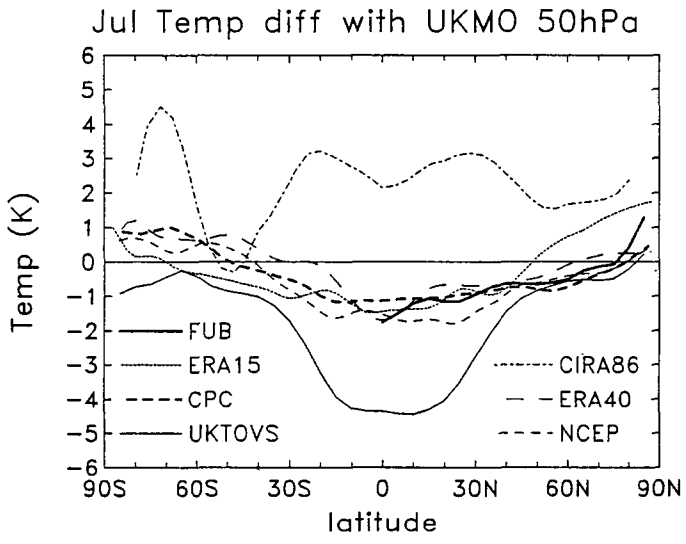
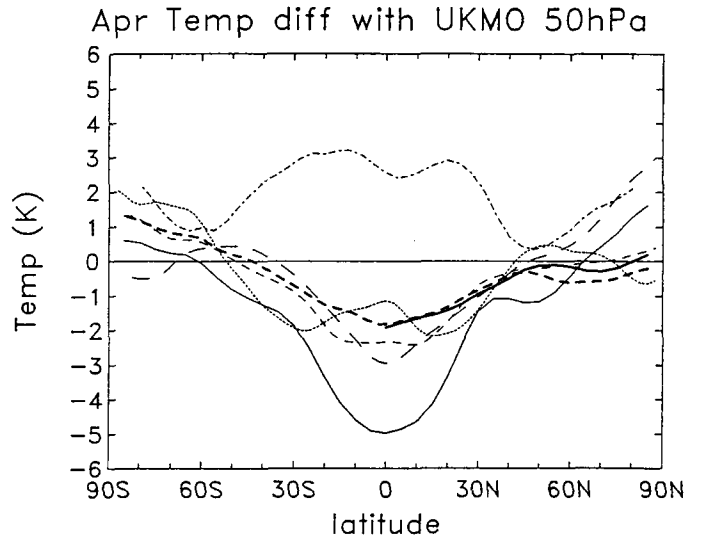
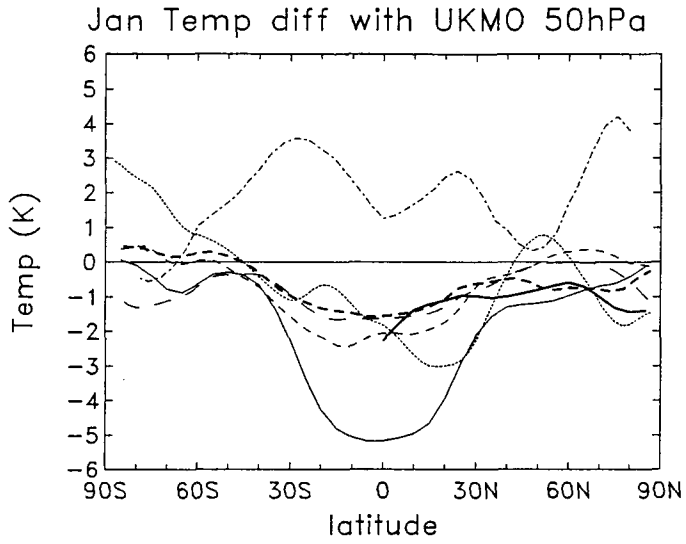


Fig. 4

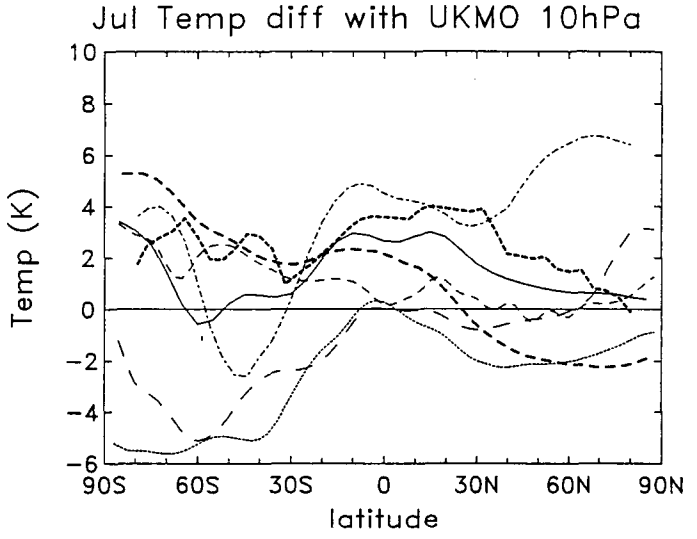
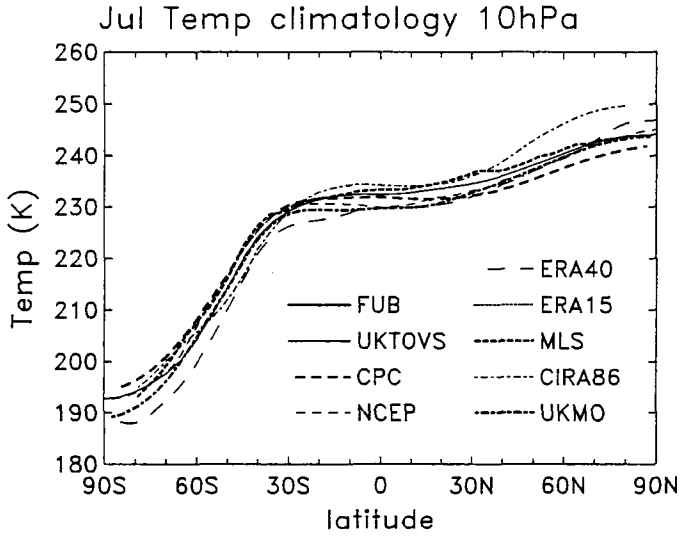
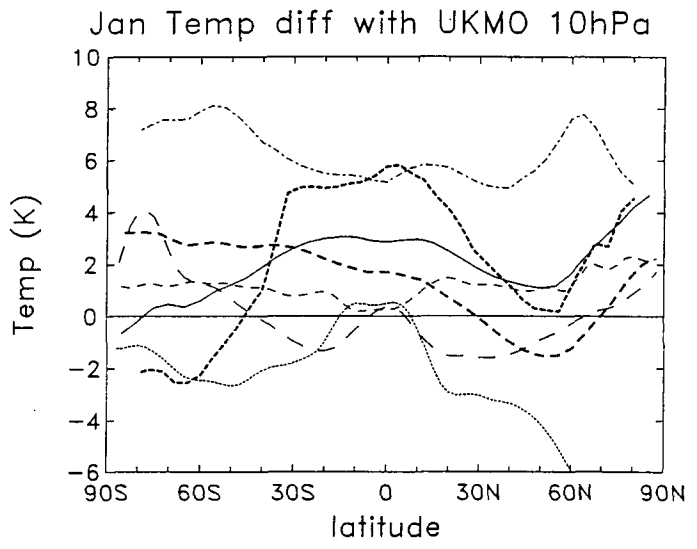
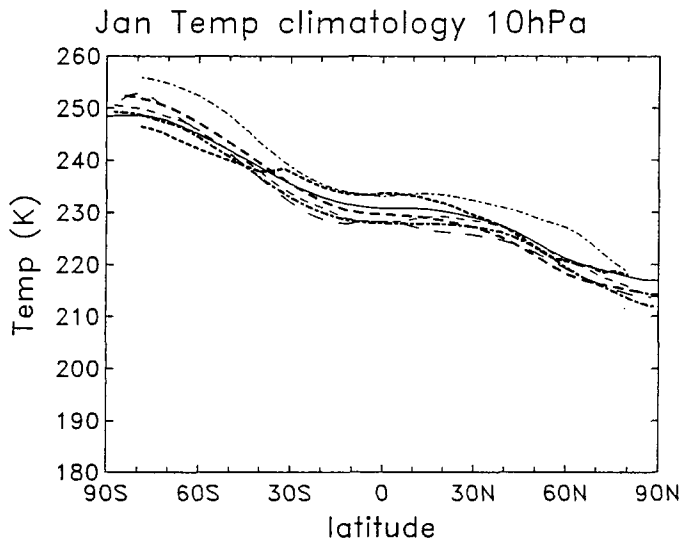


Fig. 5

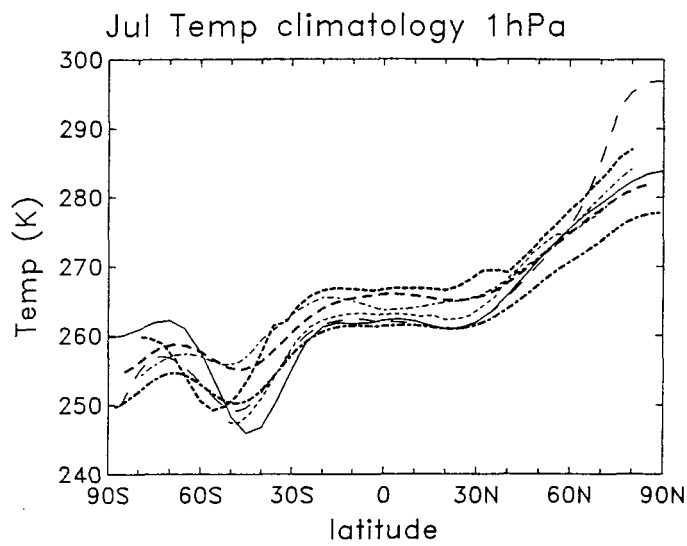
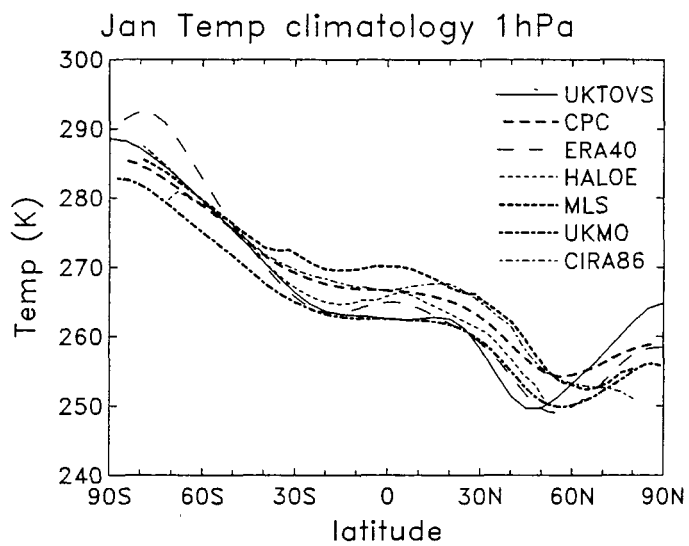


Fig. 6

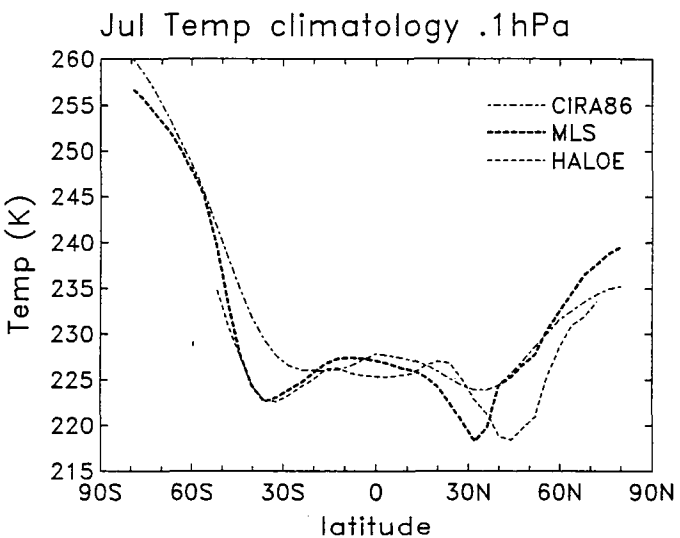
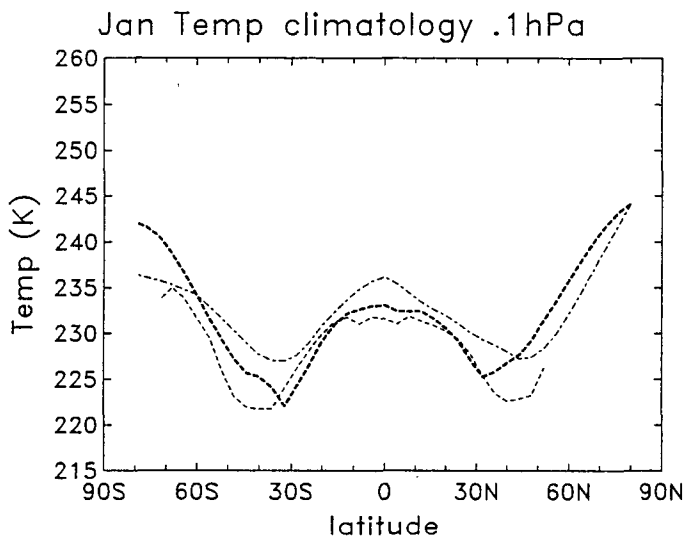
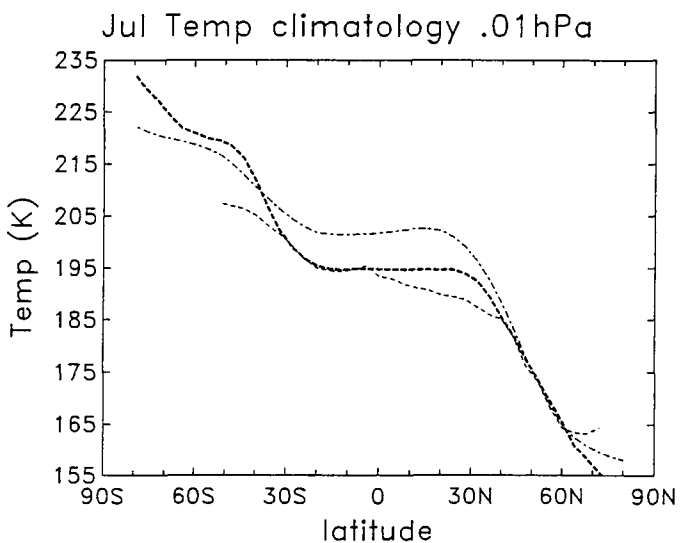
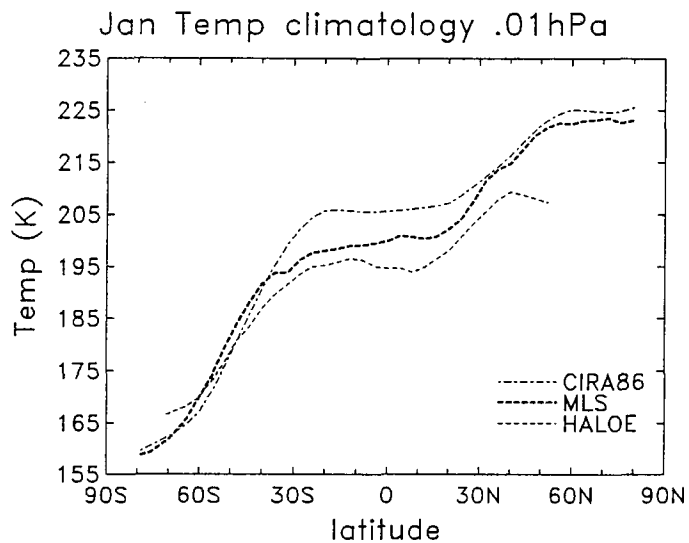


Fig. 7

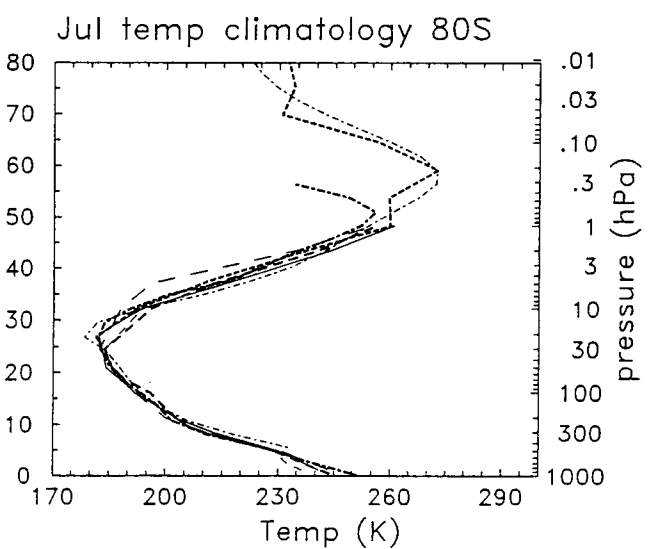
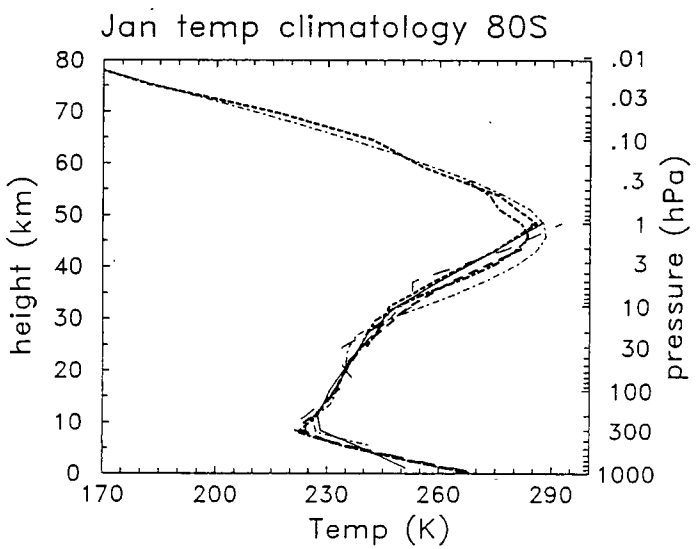
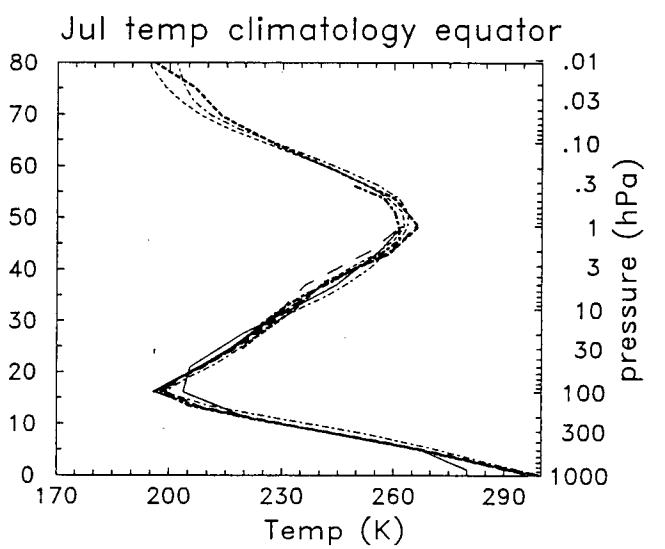
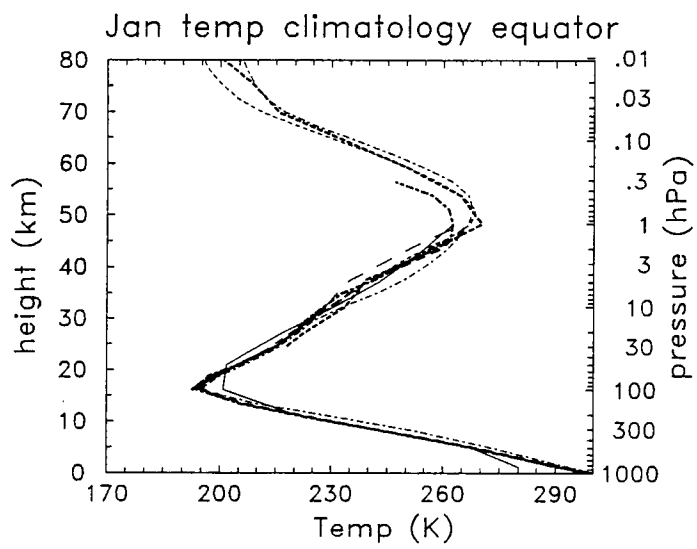
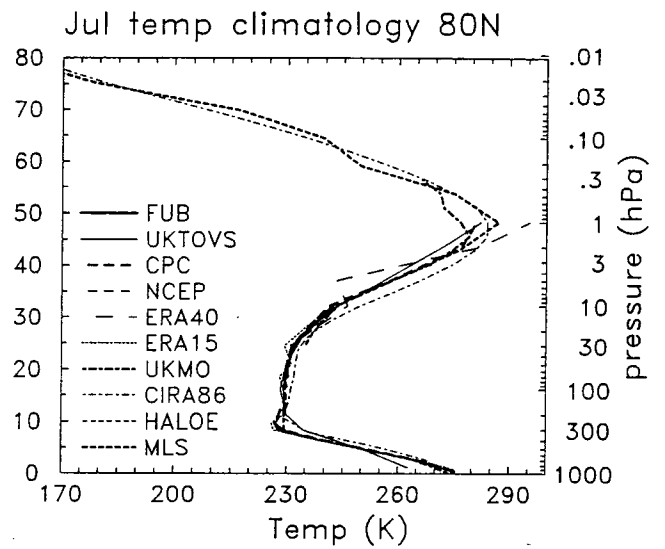
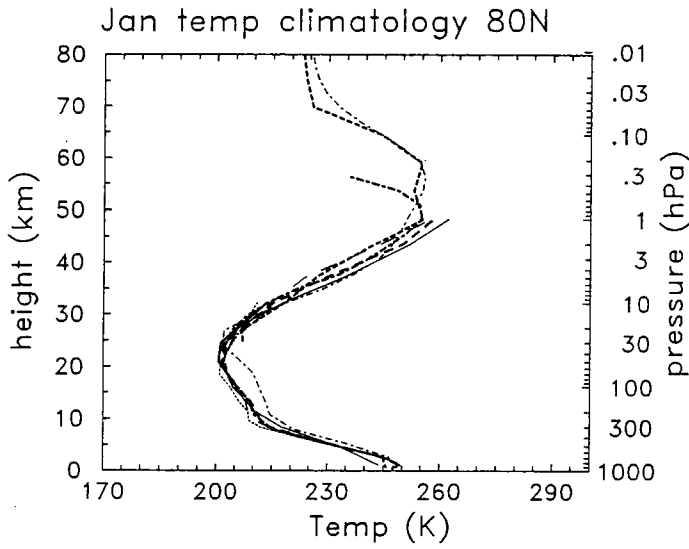


Fig 8

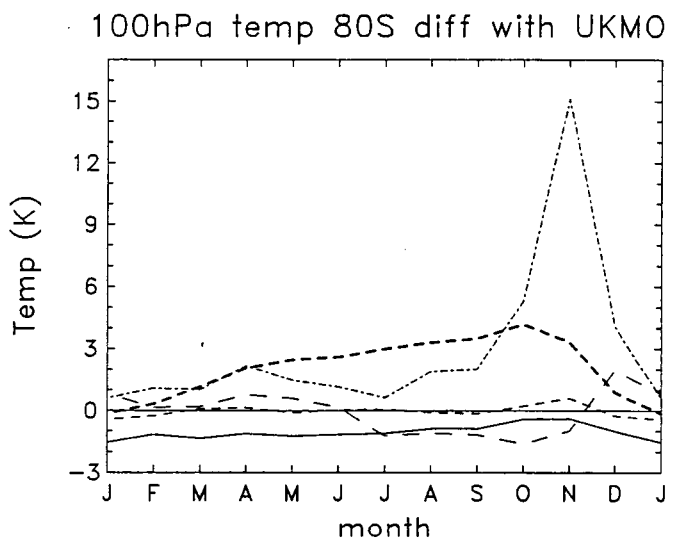
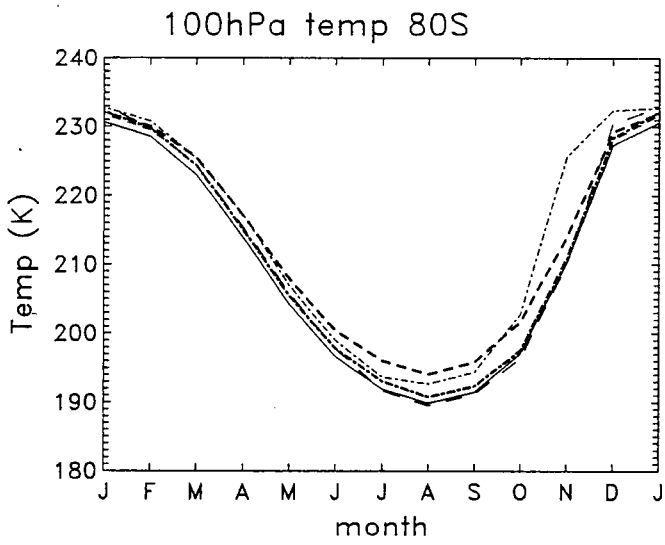
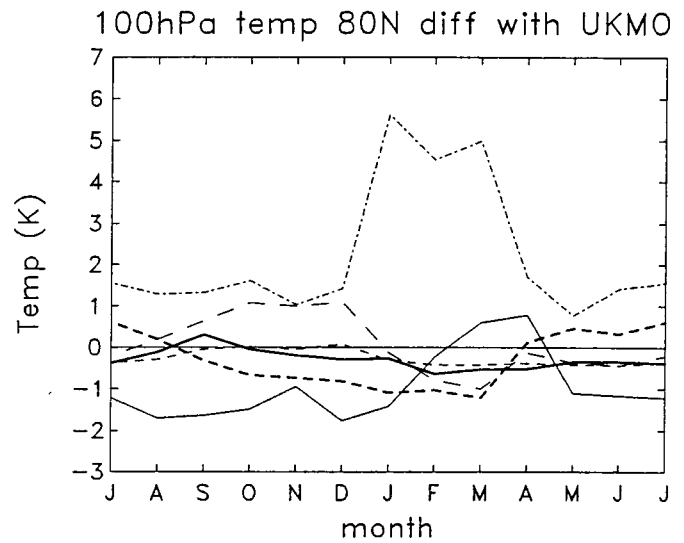
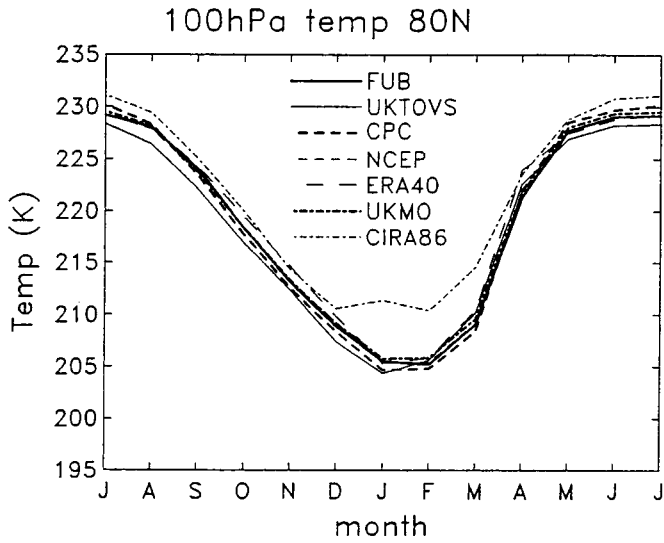


Fig. 9

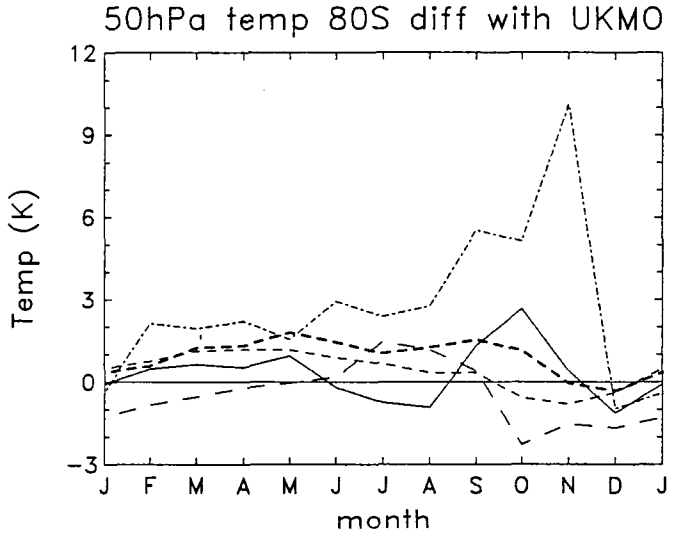
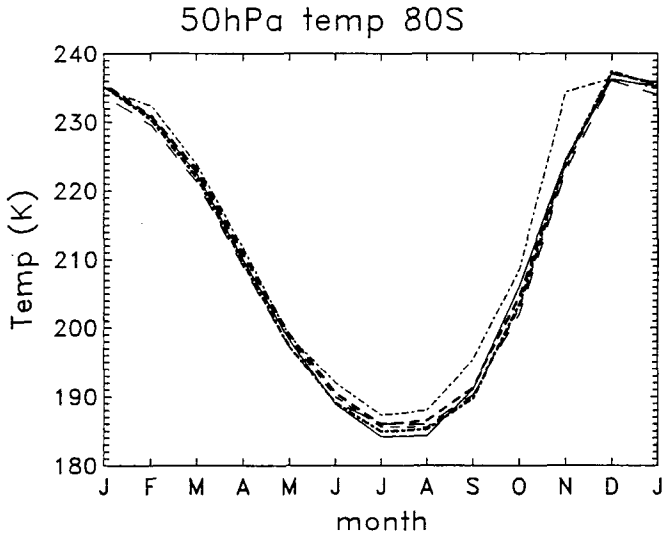
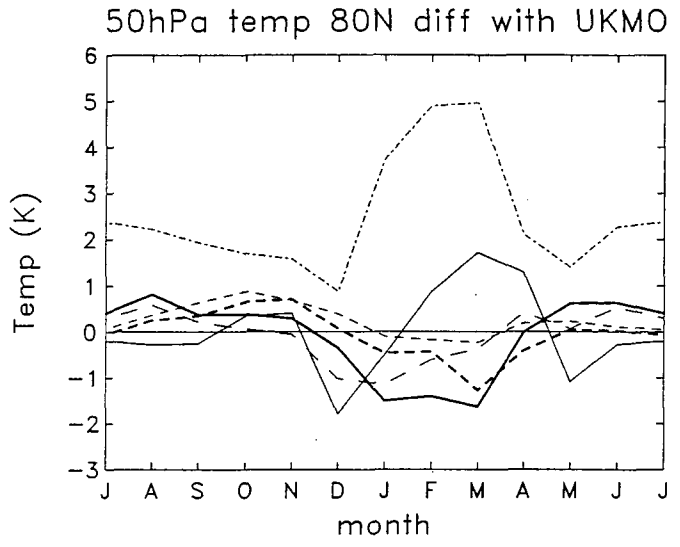
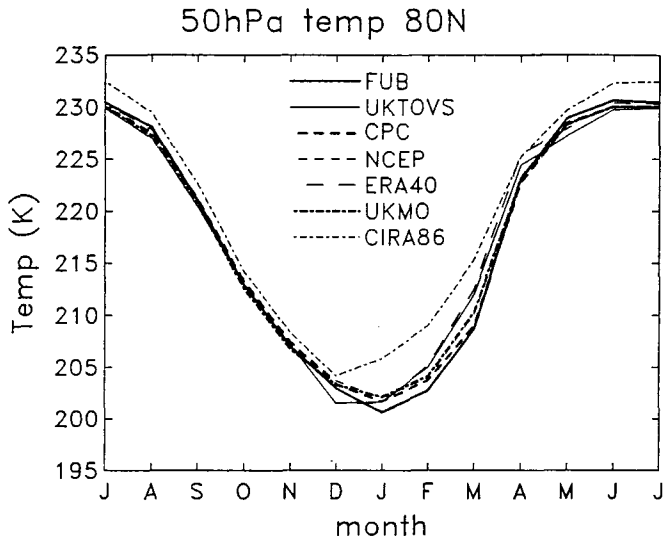


Fig. 10

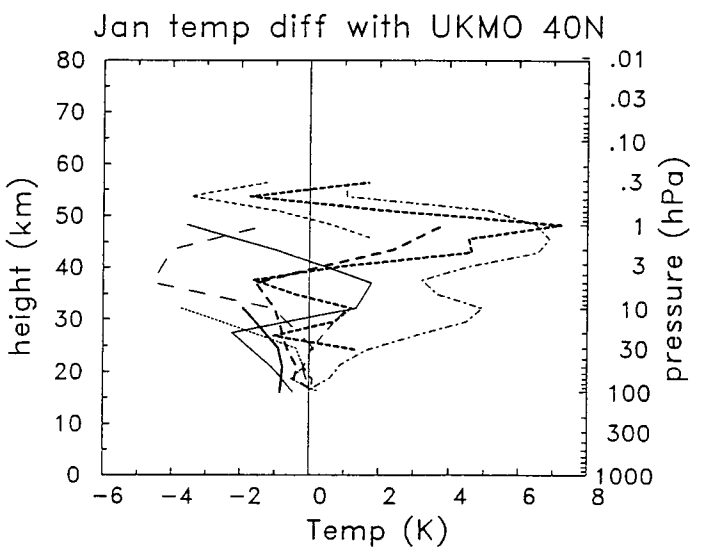
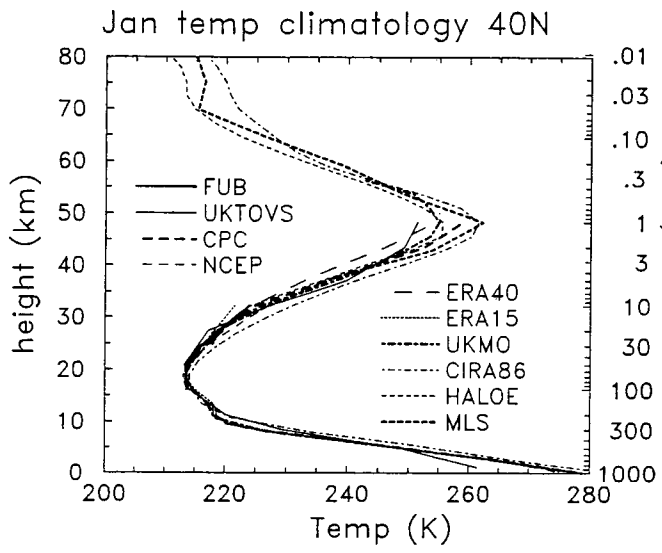


Fig. 11

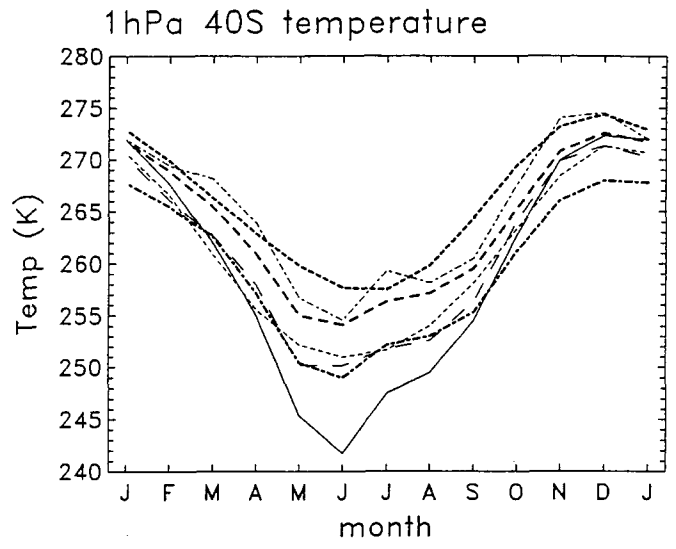
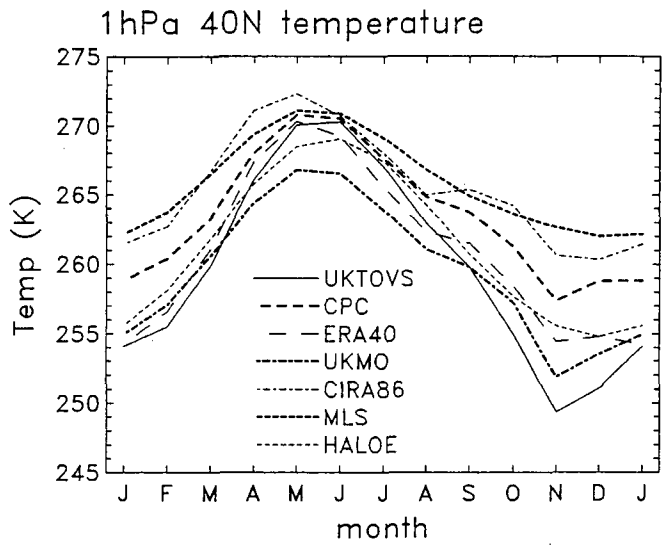


Fig. 12

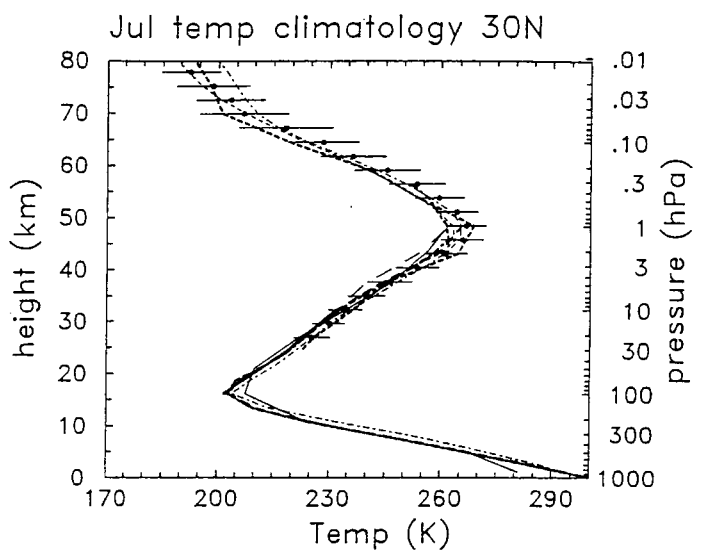
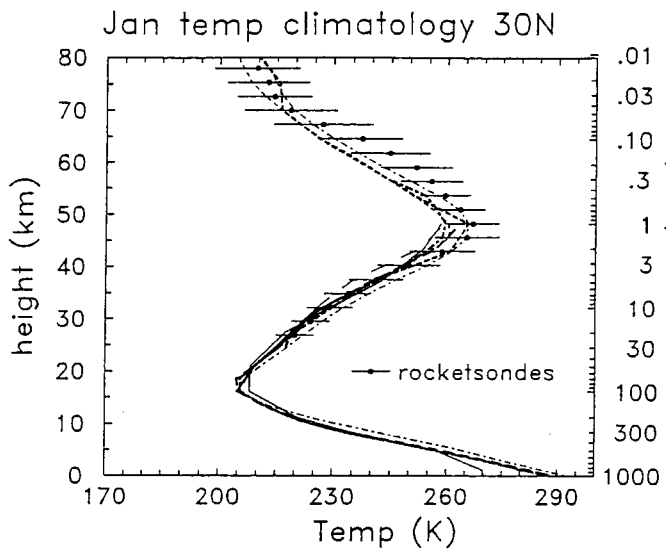


Fig. 13

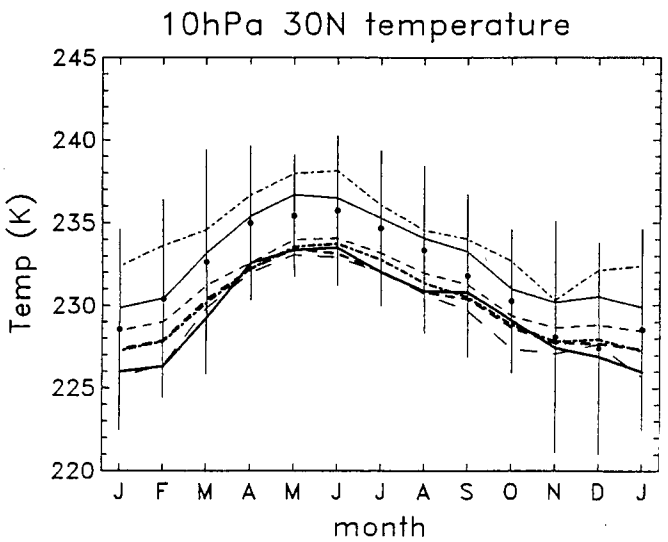
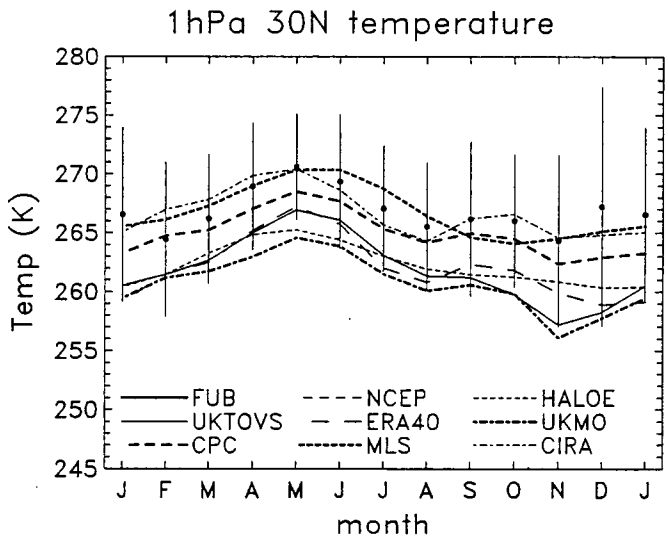
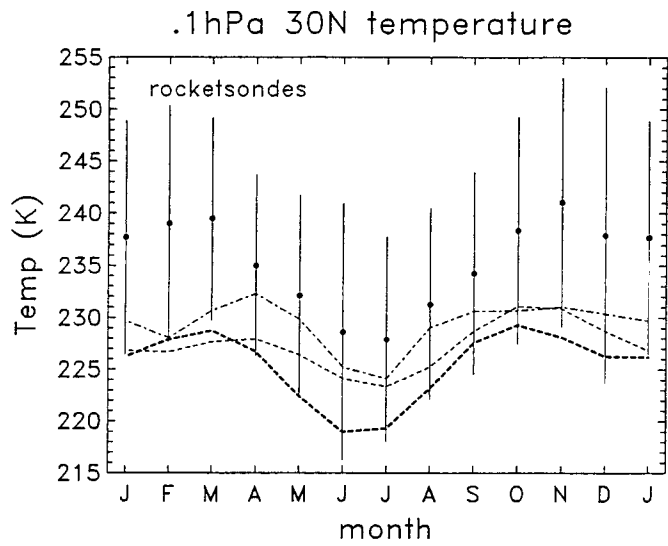
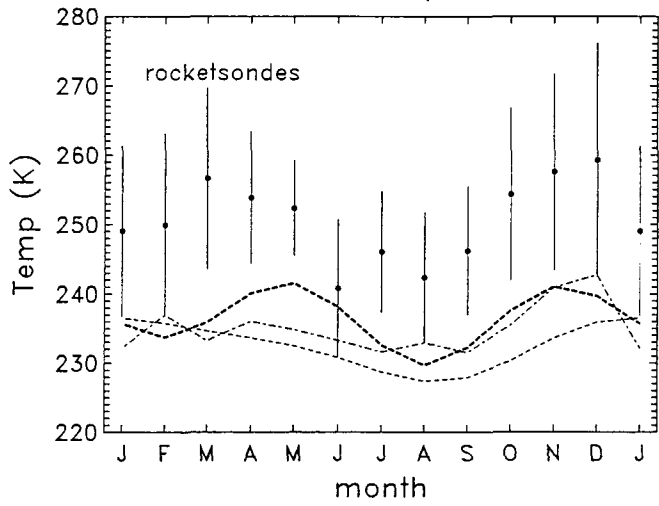
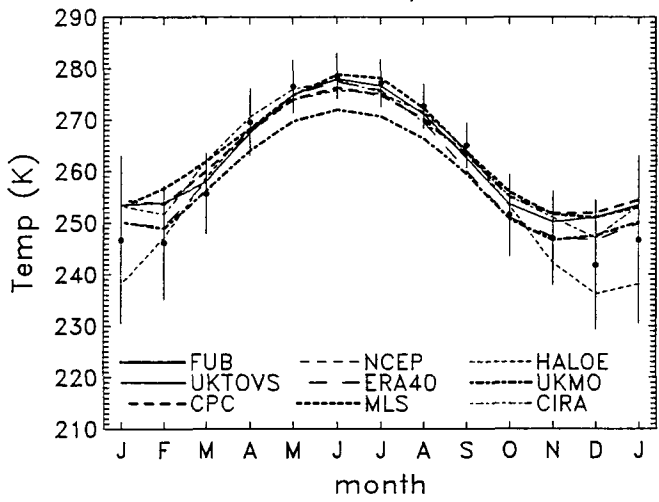


Fig. 14

.1hPa 60N temperature



1hPa 60N temperature



10hPa 60N temperature

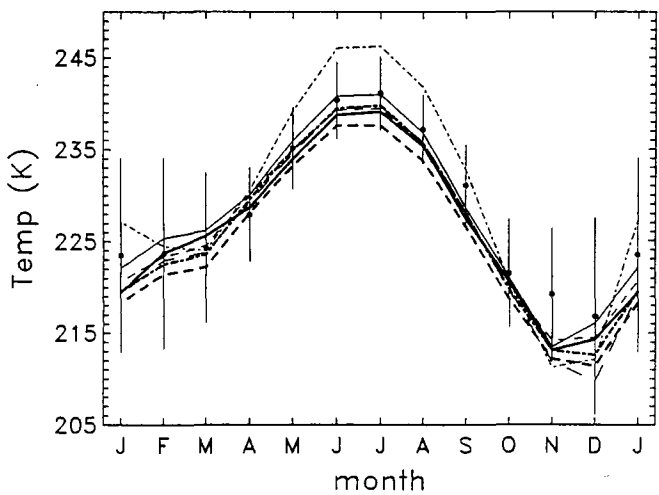


Fig. 15

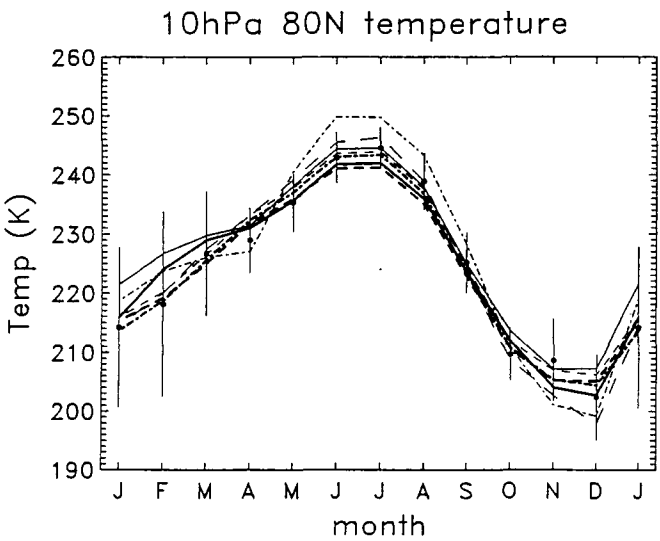
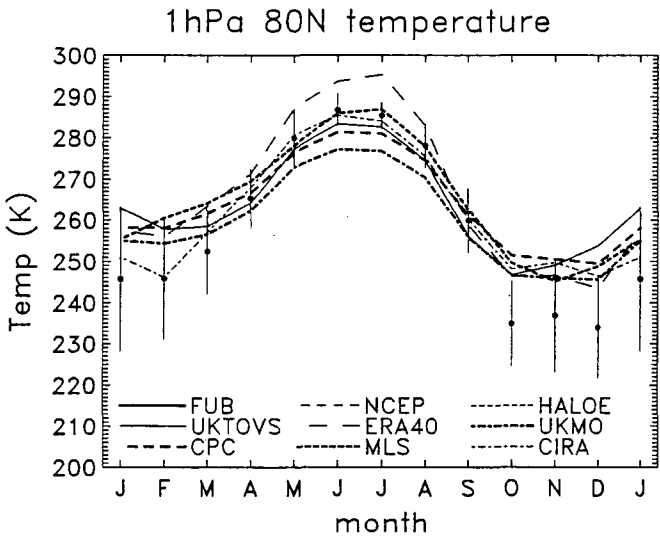
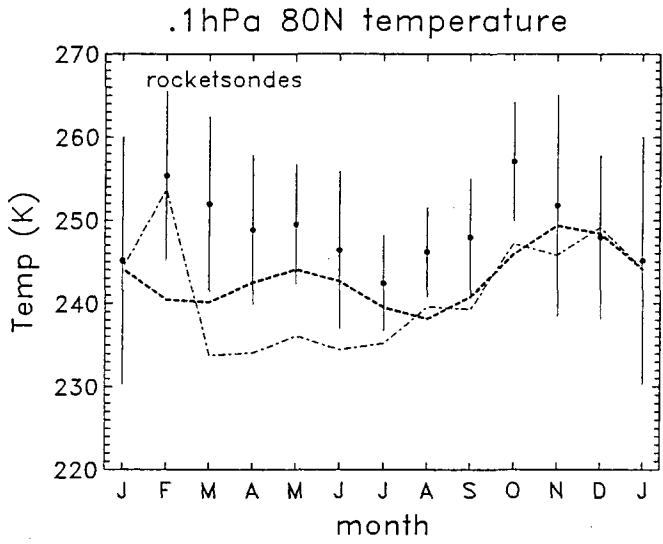
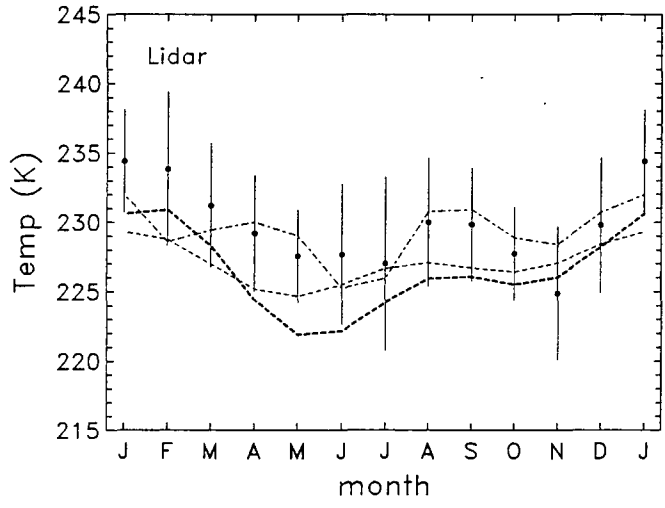
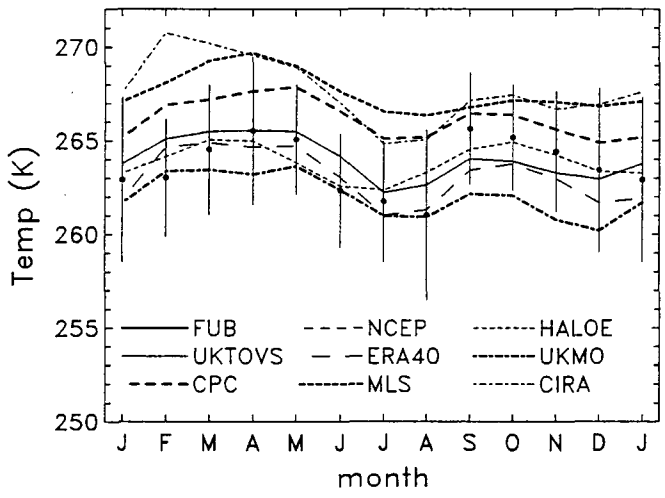


Fig. 16

.1hPa 20N temperature



1hPa 20N temperature



10hPa 20N temperature

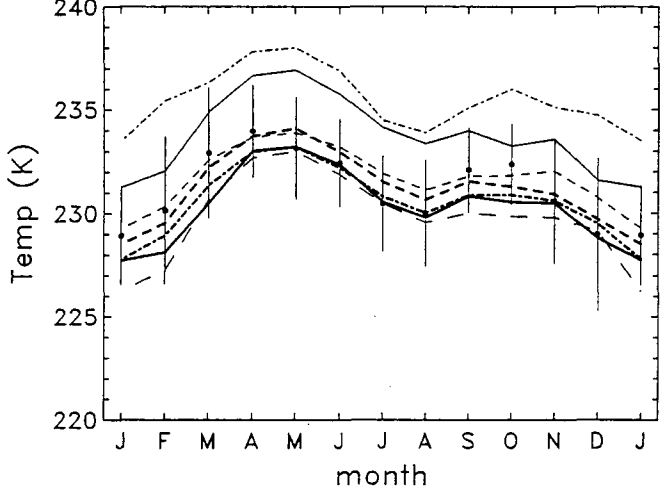
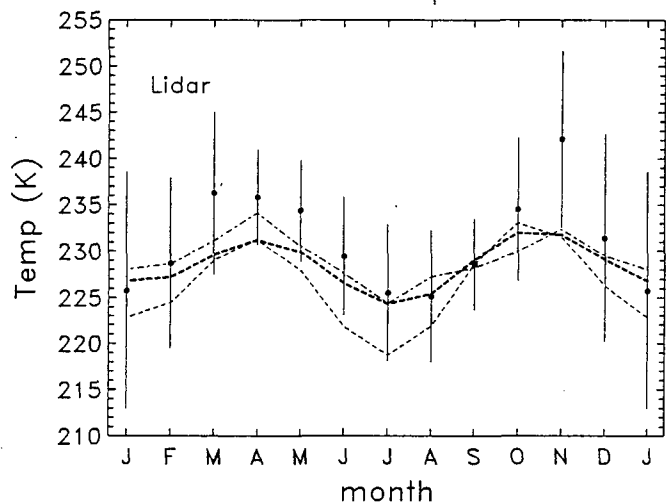


Fig. 17

.1hPa 40N temperature



1hPa 40N temperature

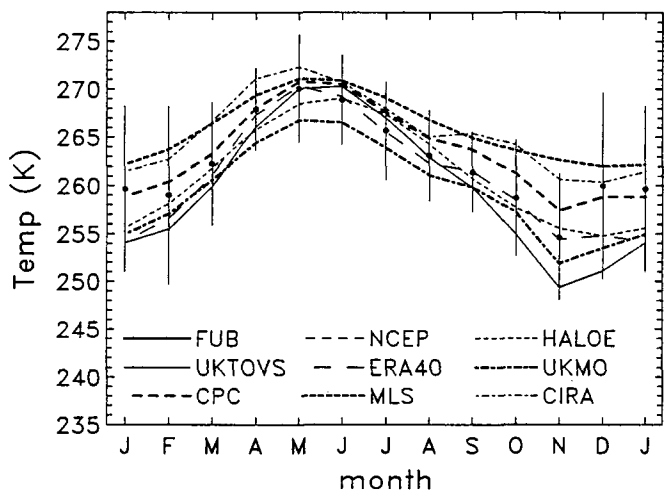
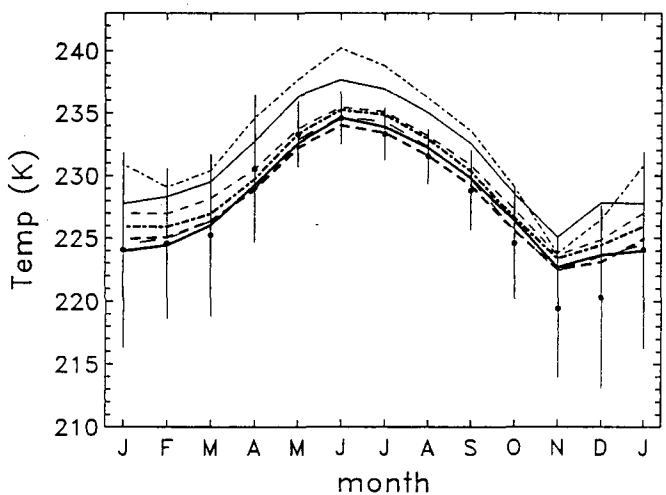


Fig. 18

10hPa 40N temperature



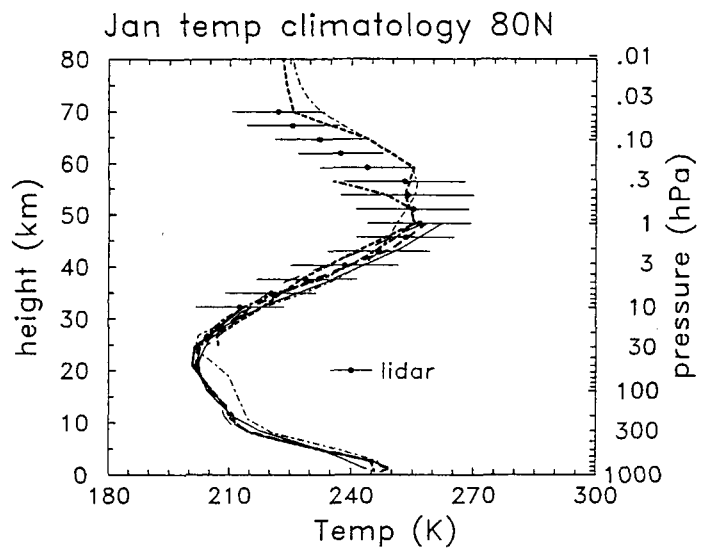


Fig. 19

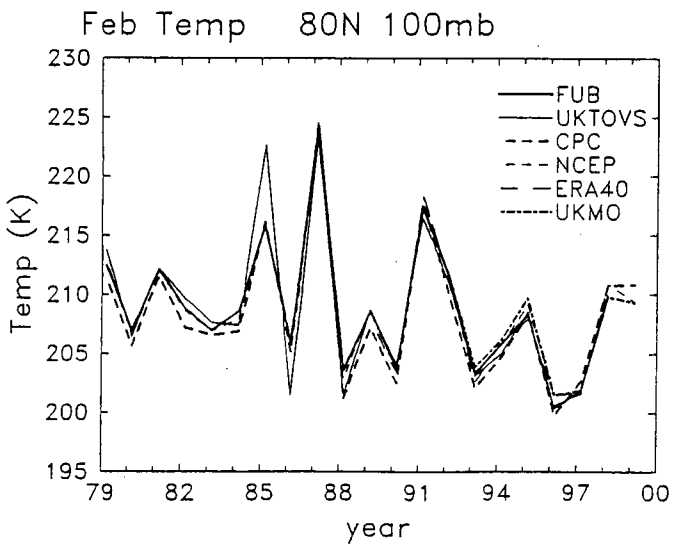
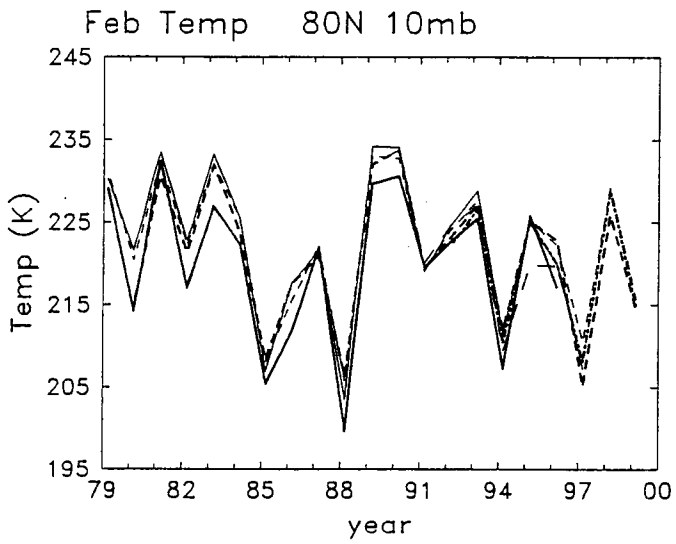
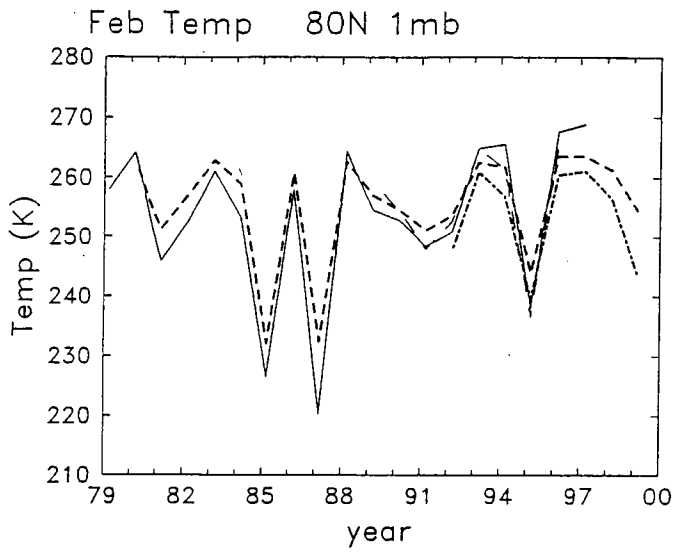


Fig. 20

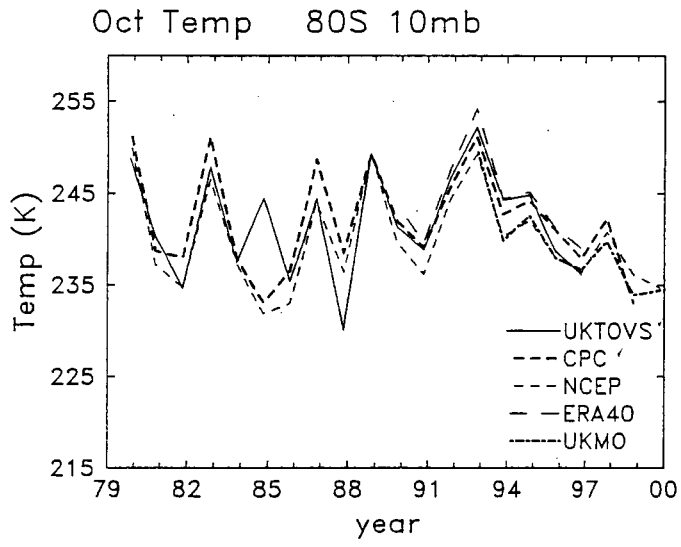
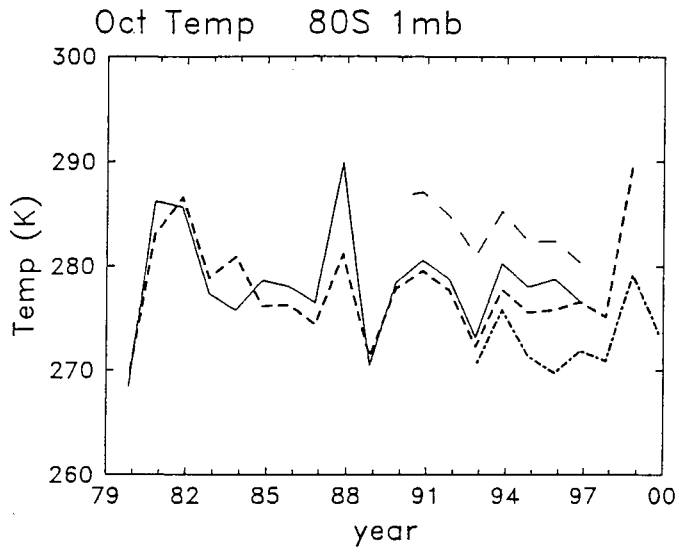
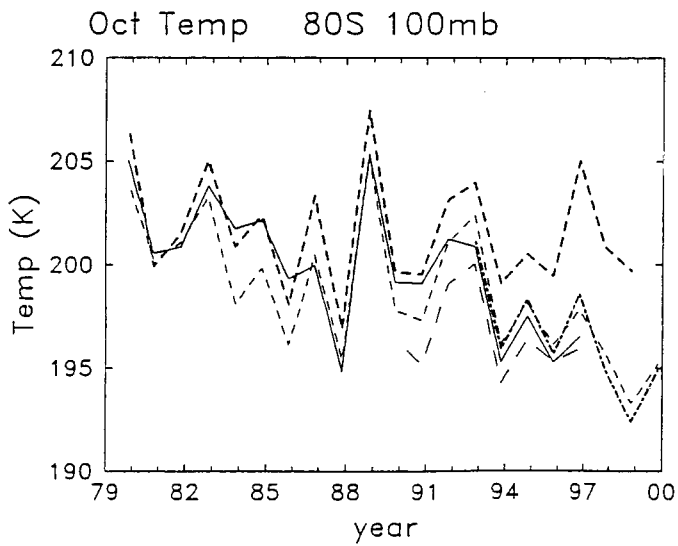
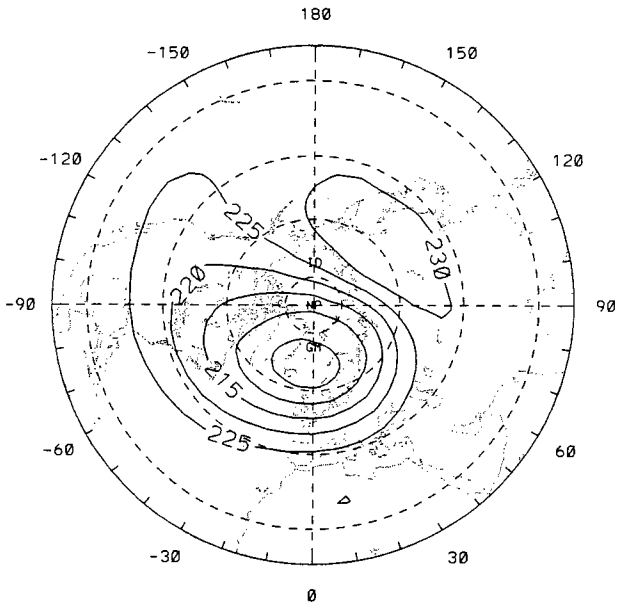


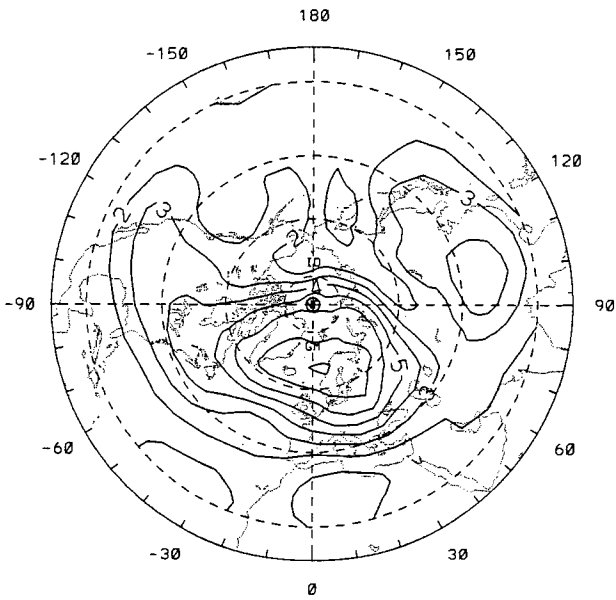
Fig. 21



NH Jan UKMO Temp 10hPa



NH Jan CPC-UKMO 10hPa



NH Jan FUB-UKMO 10hPa

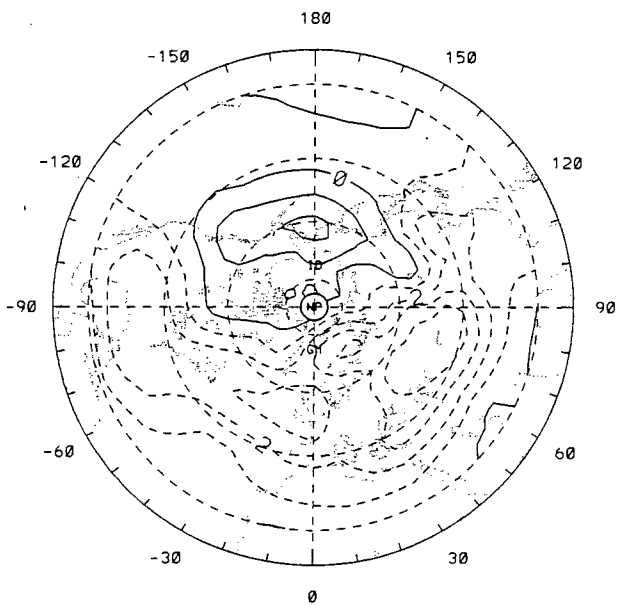
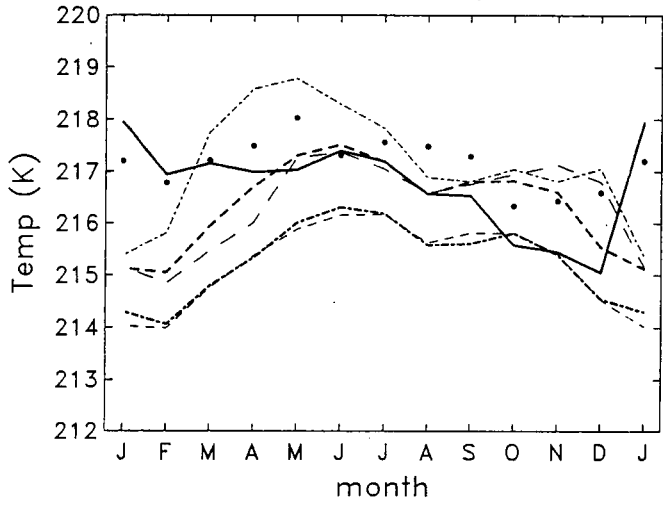
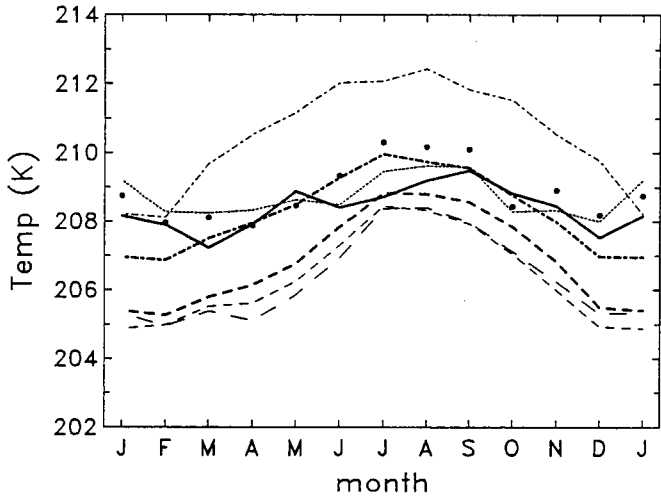


Fig. 22

30hPa equatorial temperature



50hPa equatorial temperature



100hPa equatorial temperature

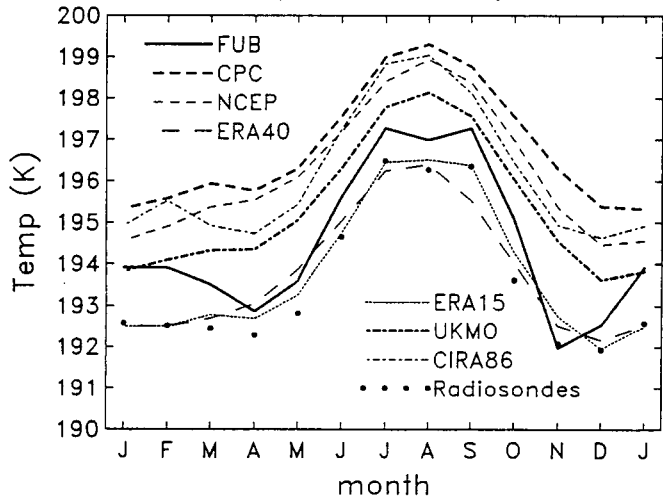


Fig-23

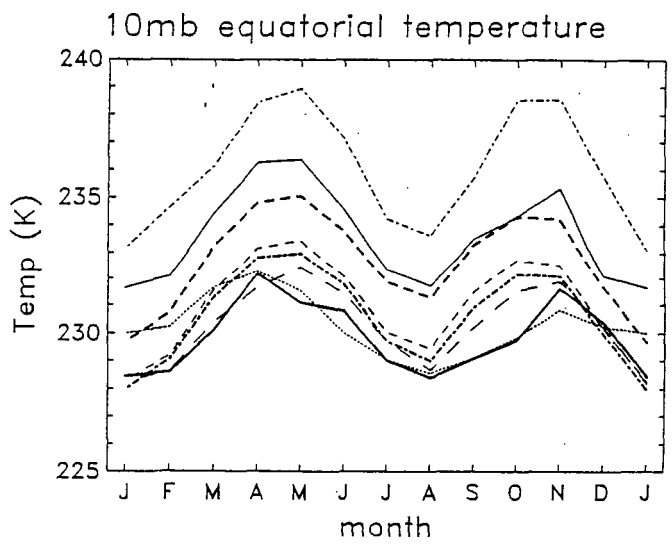
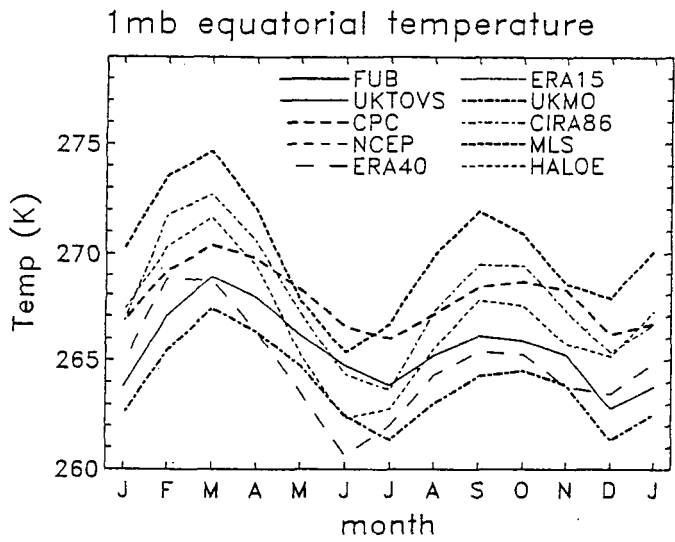
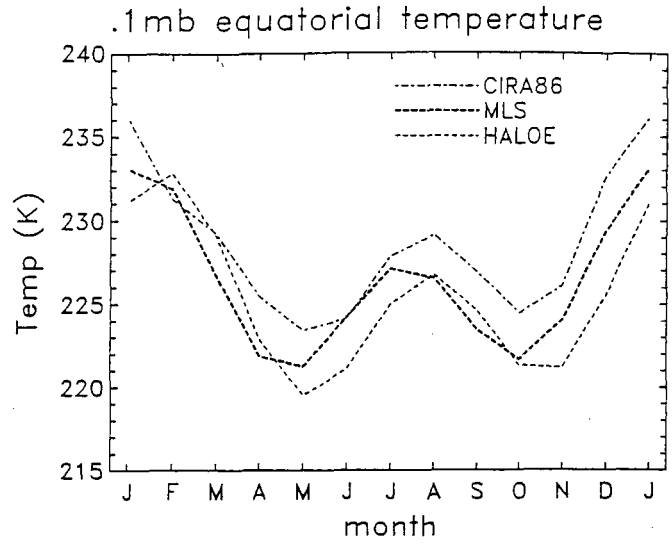
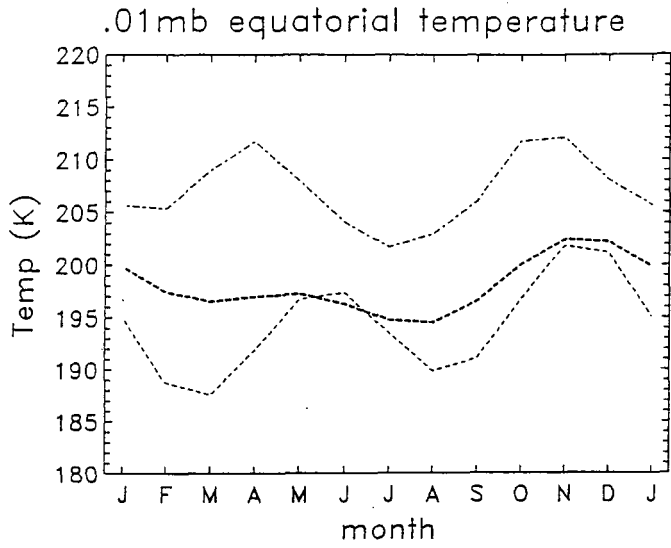
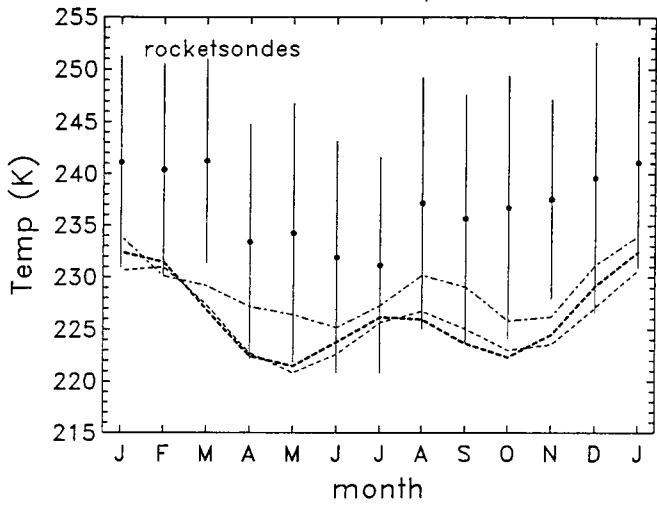
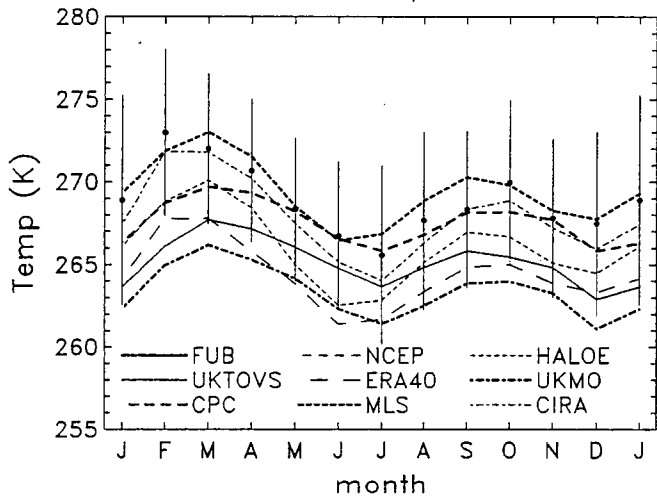


Fig. 24

.1hPa 10N temperature



1hPa 10N temperature



10hPa 10N temperature

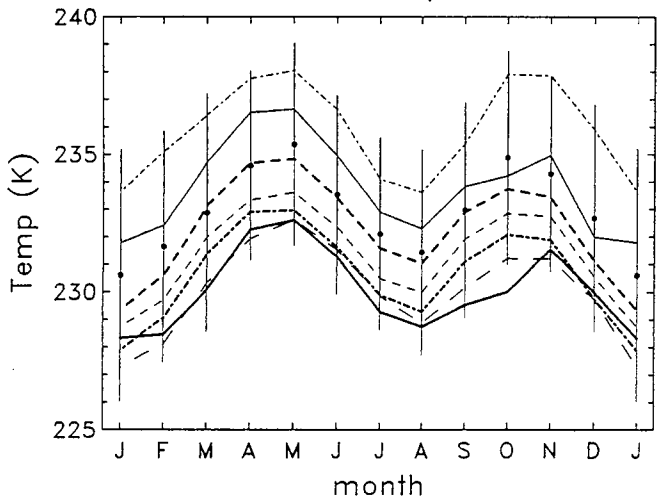


Fig. 25

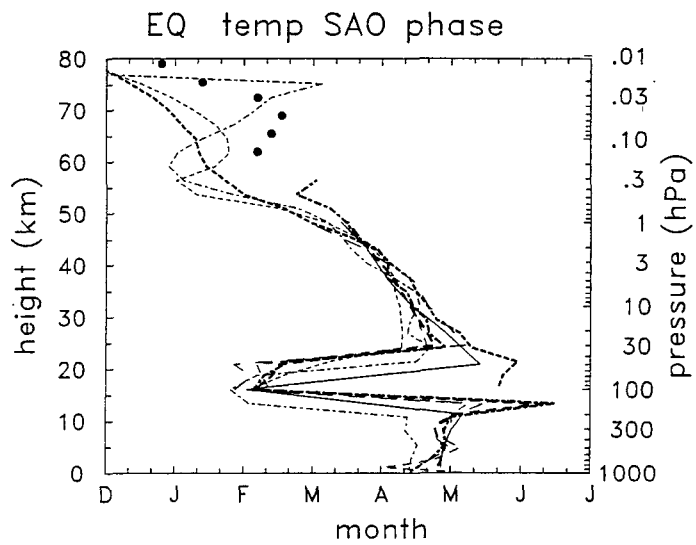
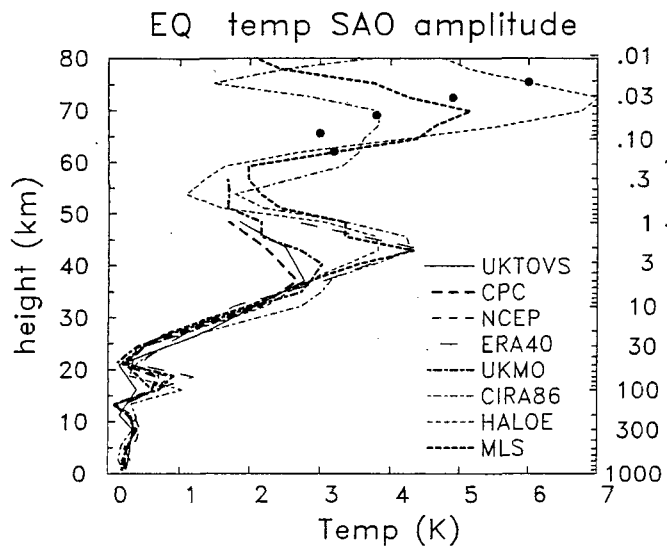


Fig. 26

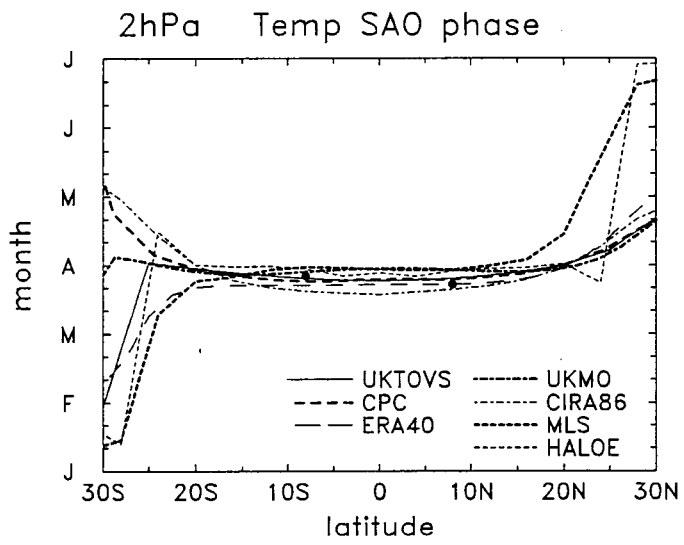
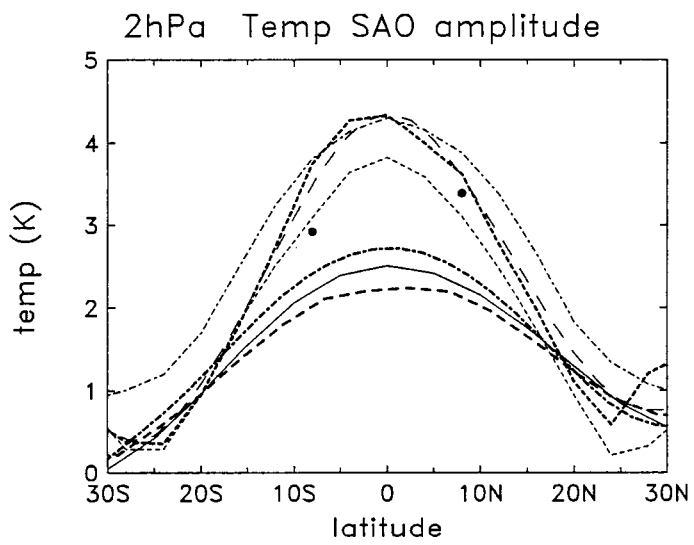
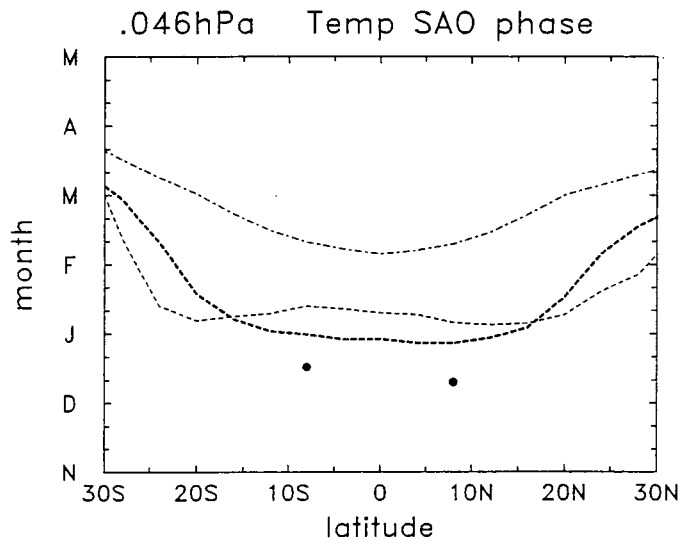
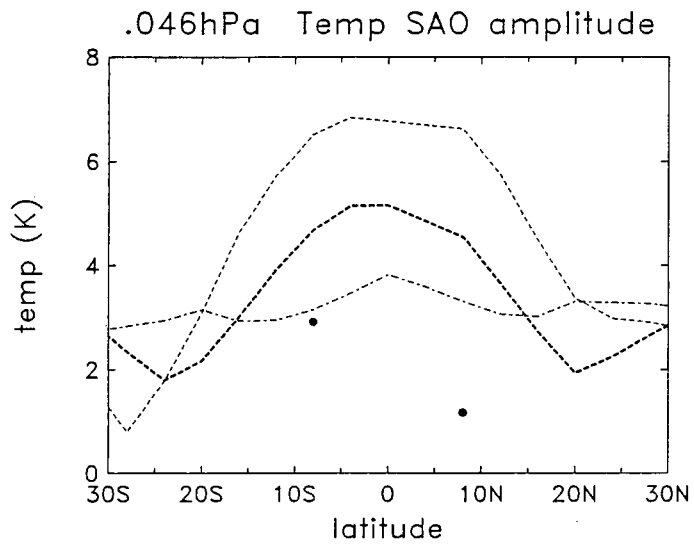
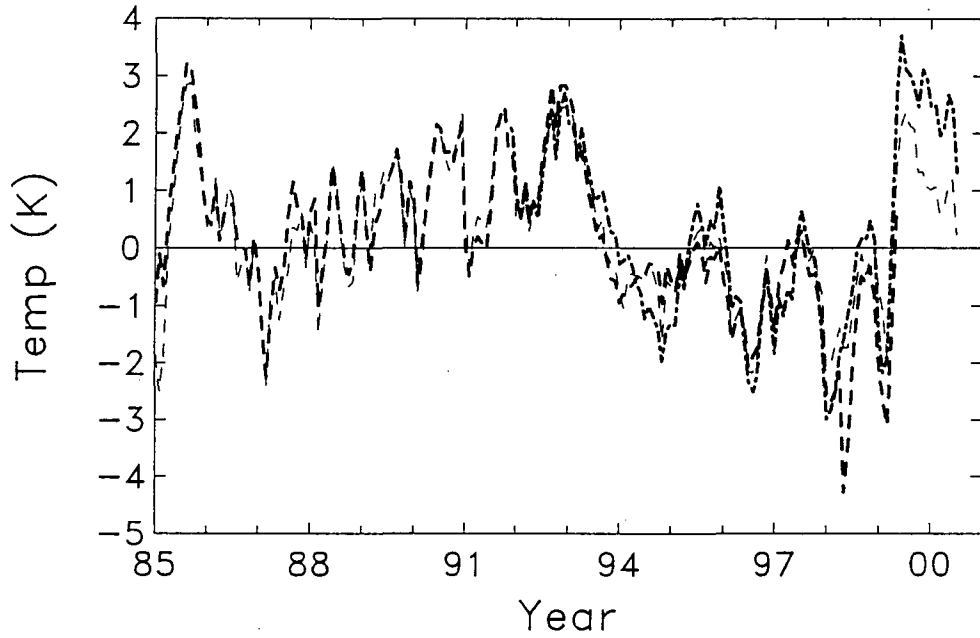


Fig. 27

70hPa temp anomalies equator



100hPa temp anomalies equator

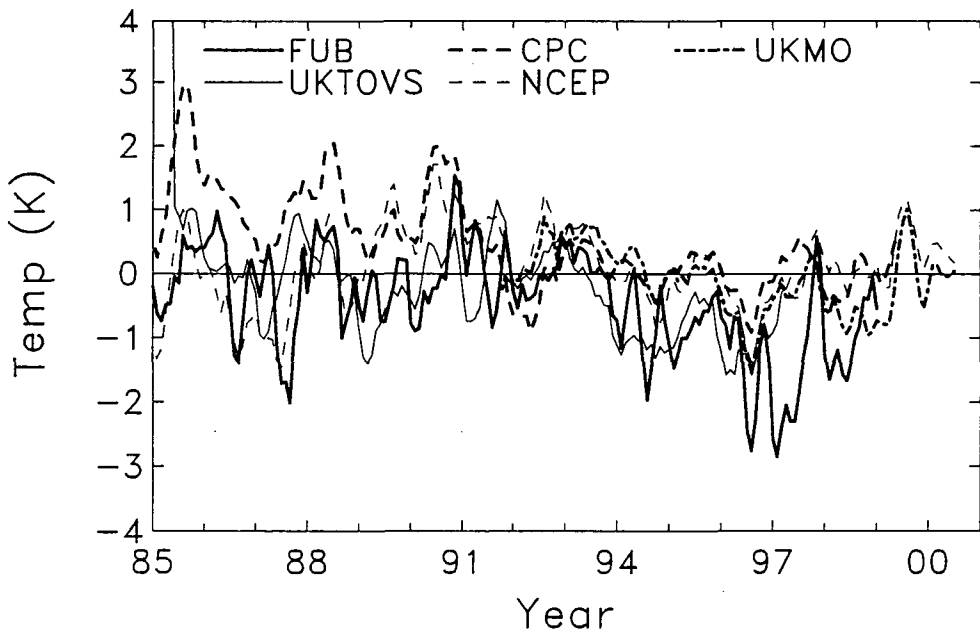
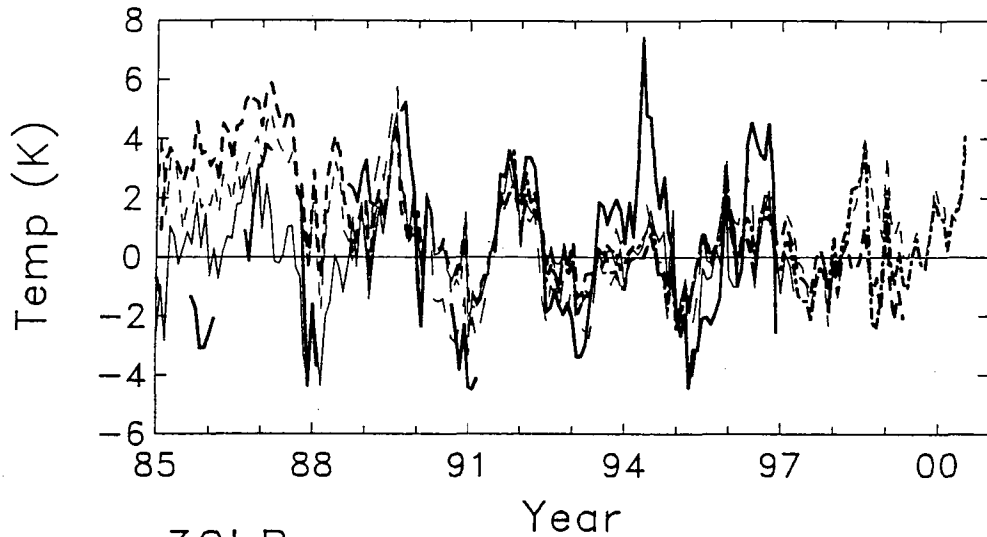
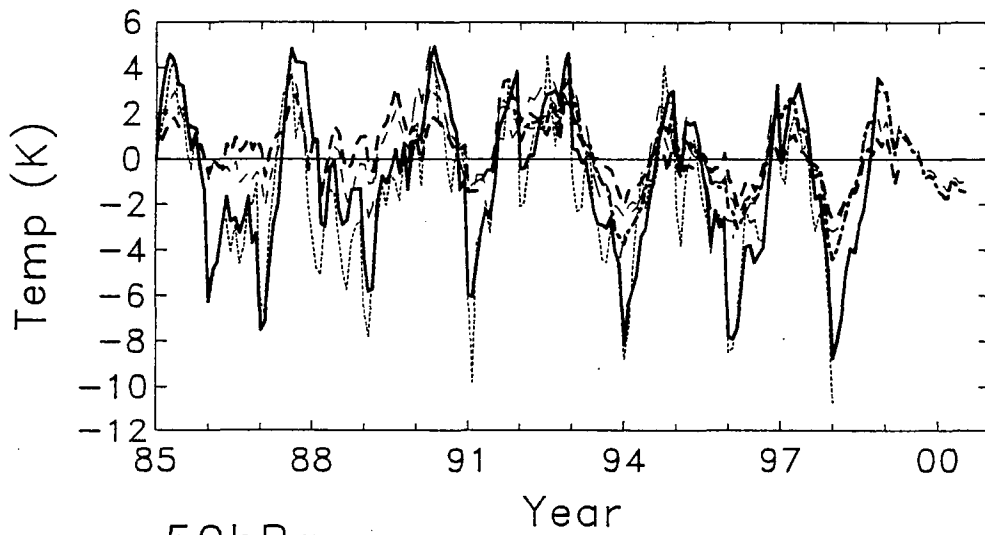


Fig. 28

10hPa temp anomalies equator



30hPa



50hPa

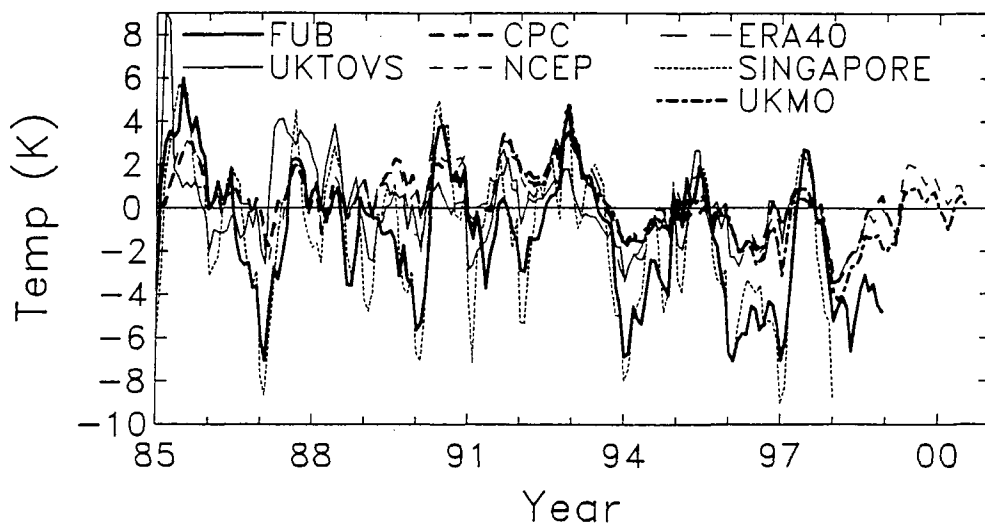


Fig. 29

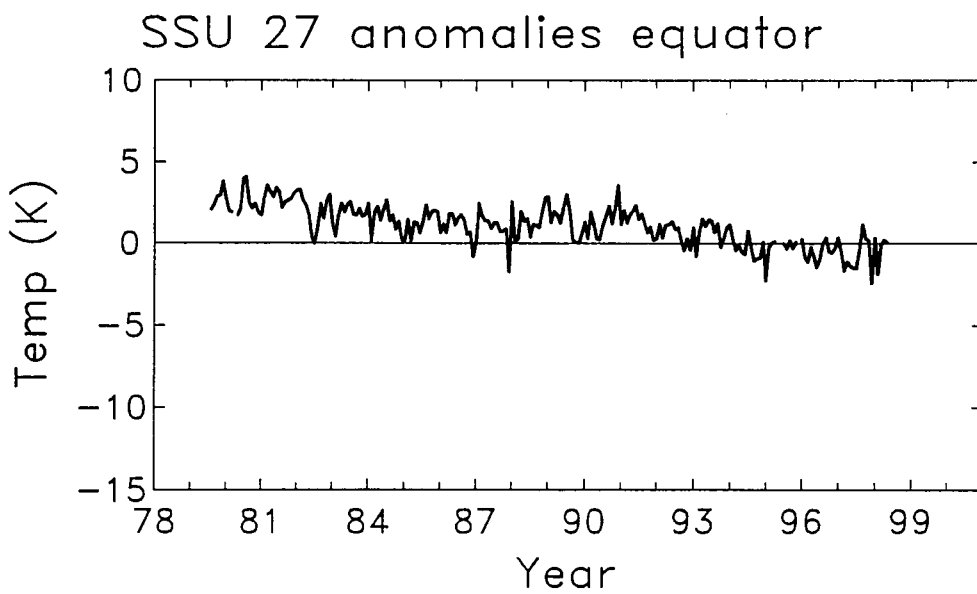
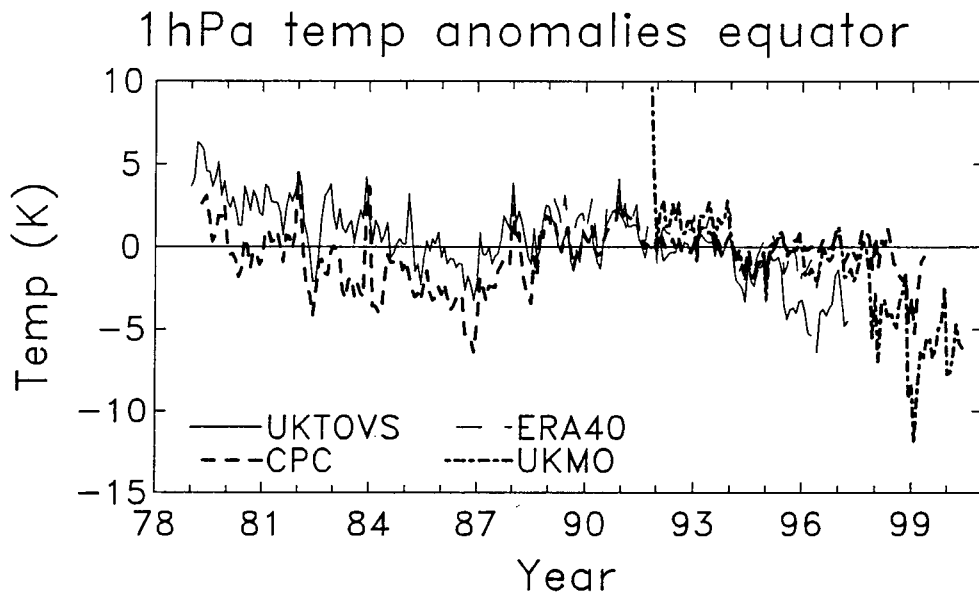


Fig-30

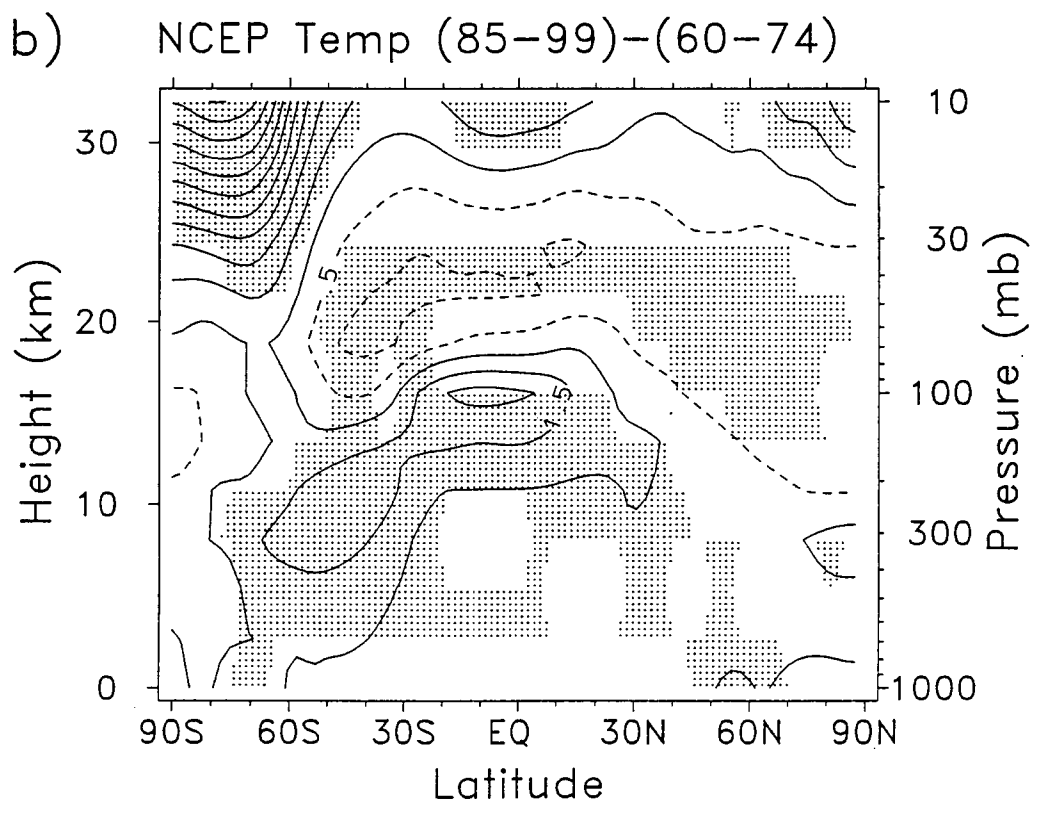
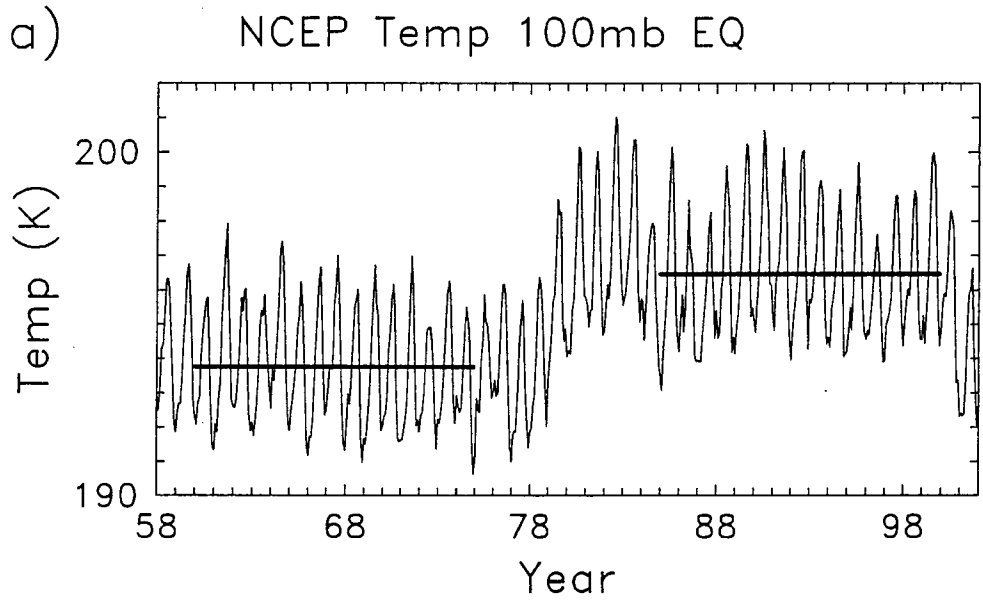


Fig. 31

FUB-NCEP zonal mean temp

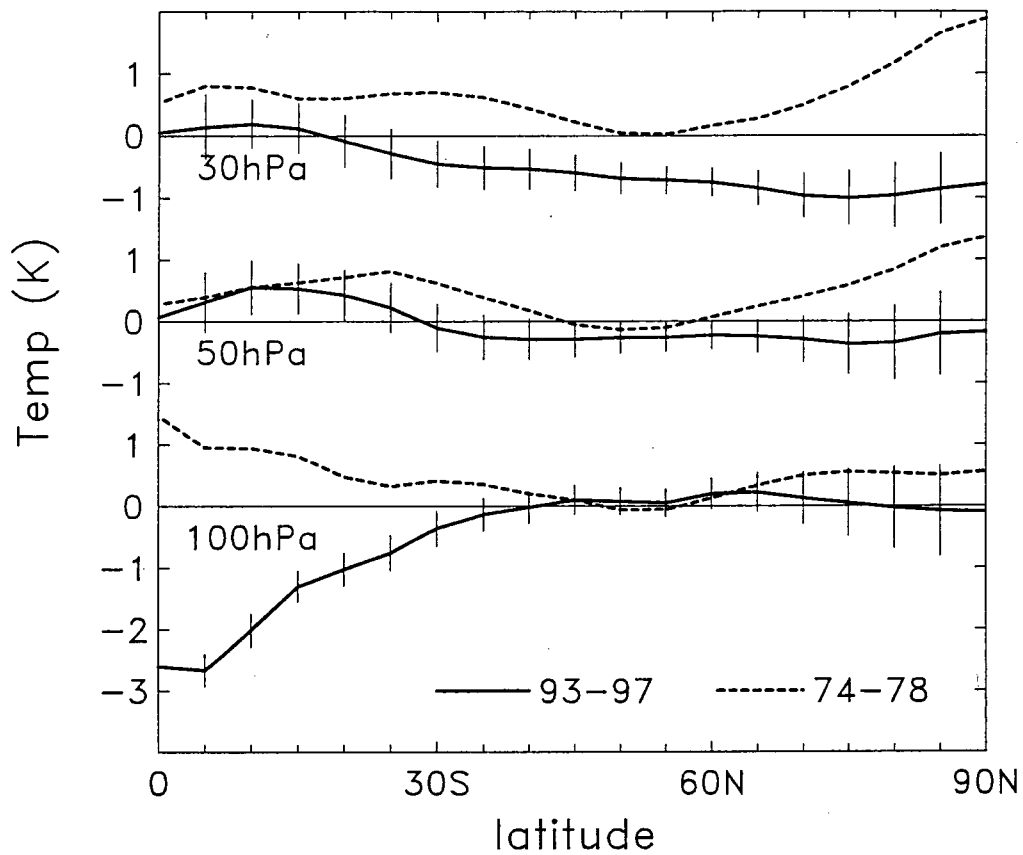
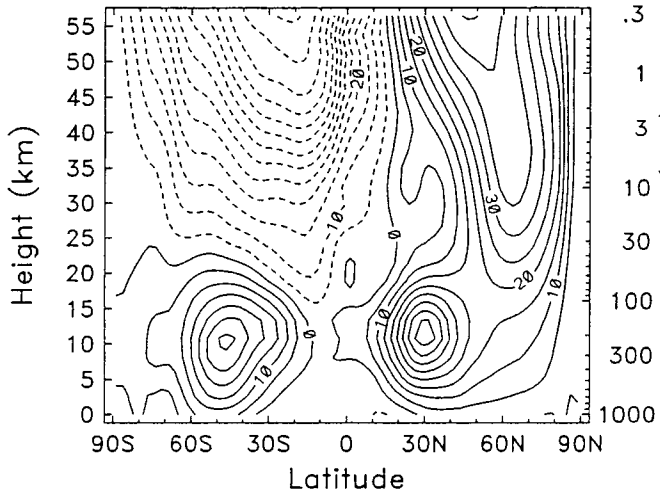
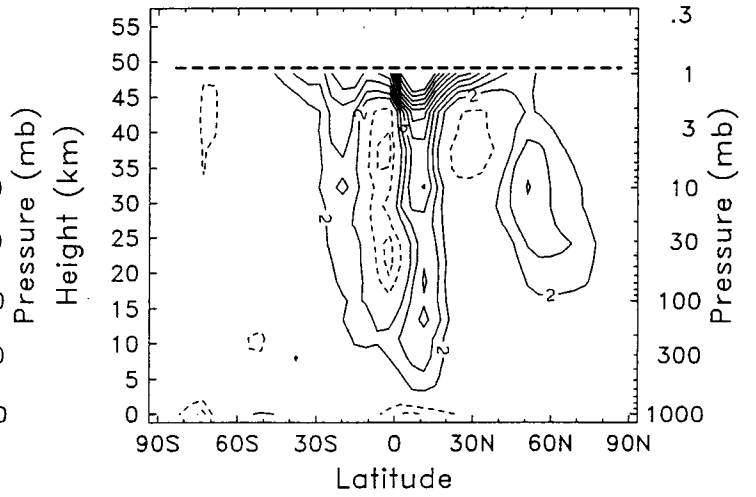


Fig. 32

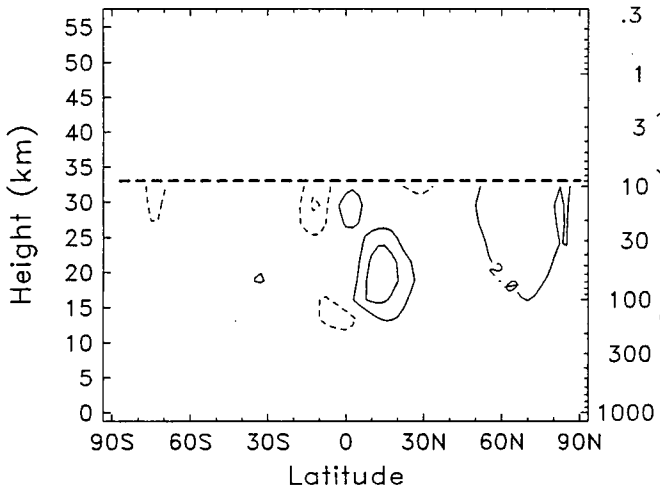
UKMO Jan z-wind



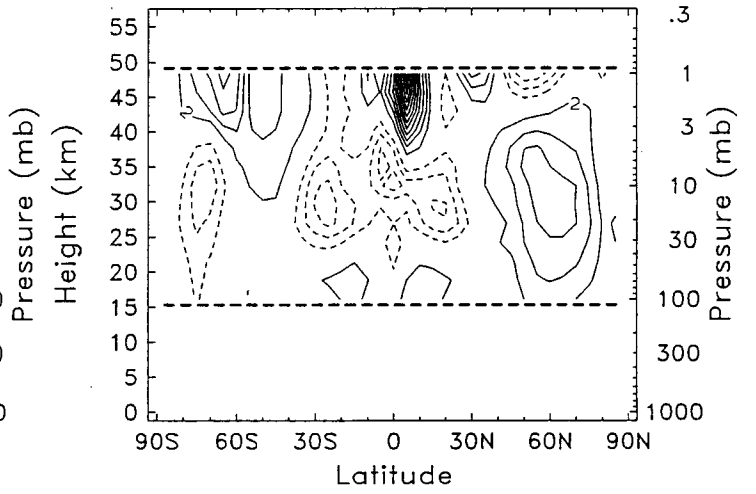
CPC Jan z-wind diff



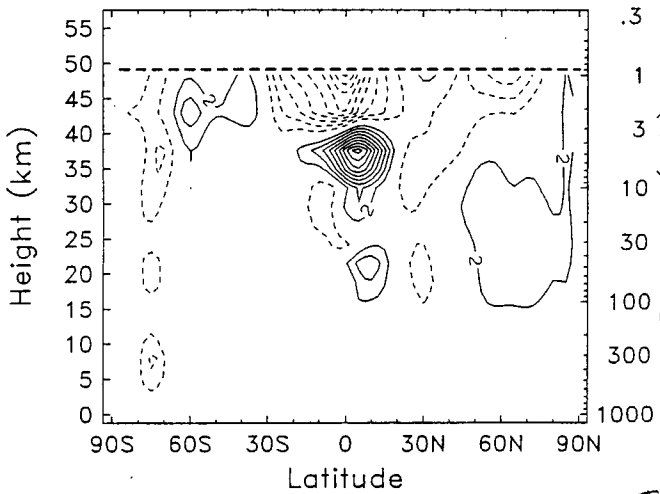
NCEP Jan z-wind diff



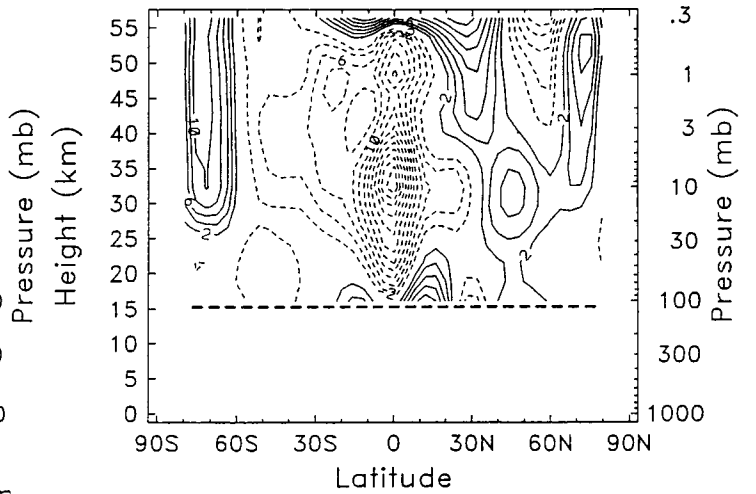
UKTOVS Jan z-wind diff



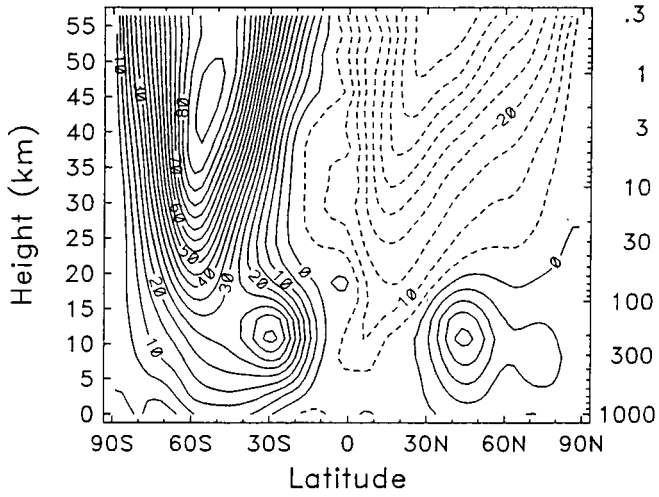
ERA40 Jan z-wind diff



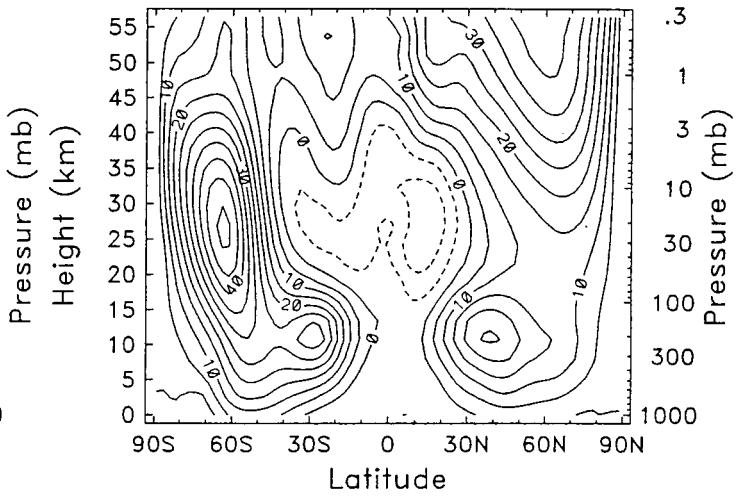
CIRA86 Jan z-wind diff



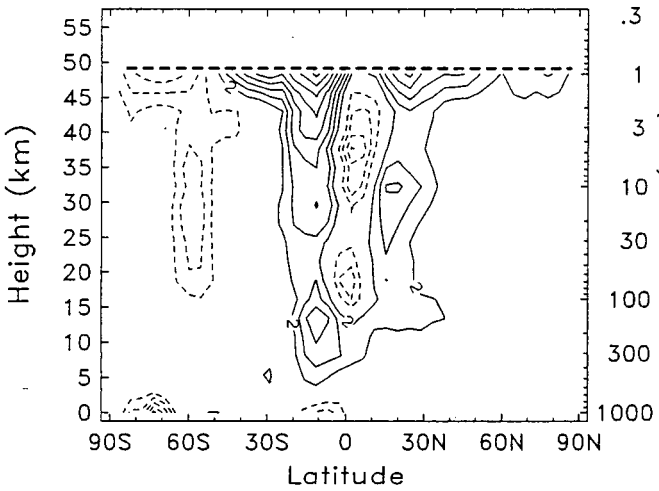
UKMO Jul z-wind



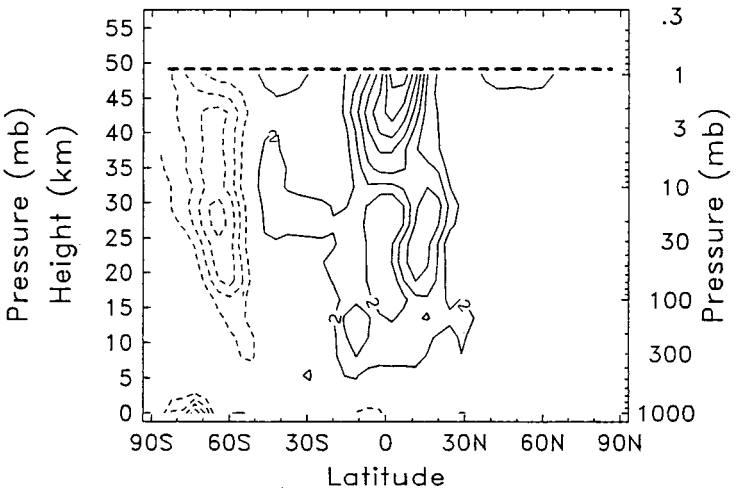
UKMO Oct z-wind



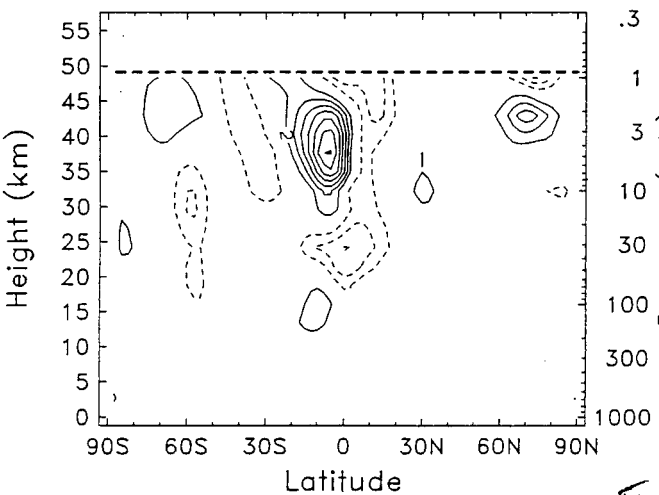
CPC Jul z-wind diff



CPC Oct z-wind diff



ERA40 Jul z-wind diff



ERA40 Oct z-wind diff

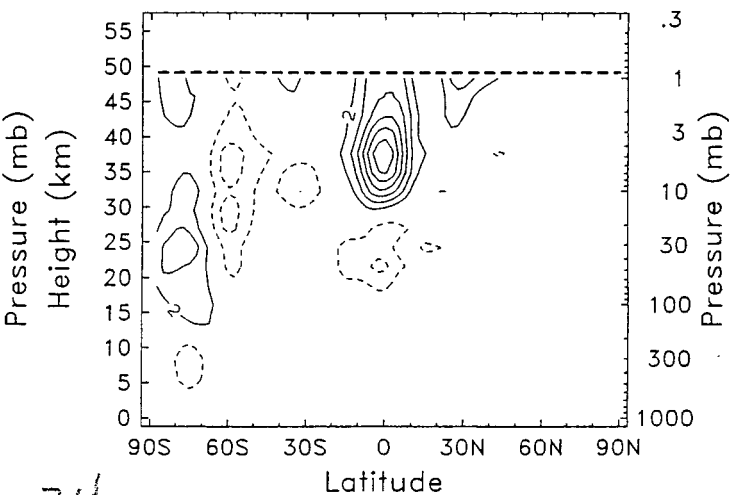


Fig-3c4

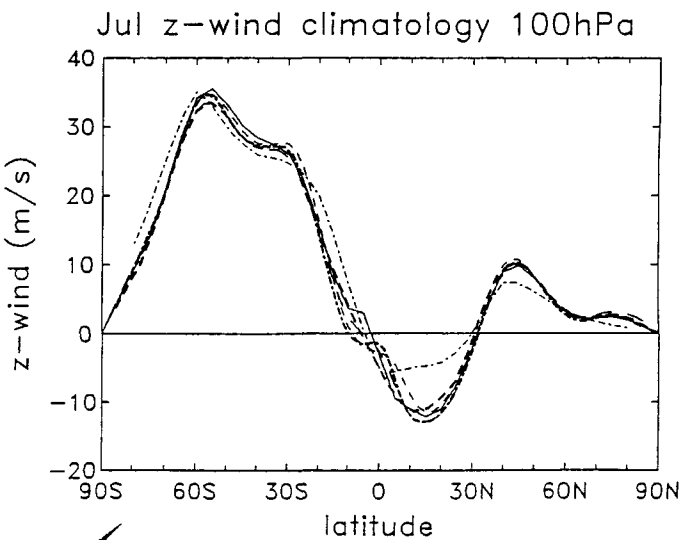
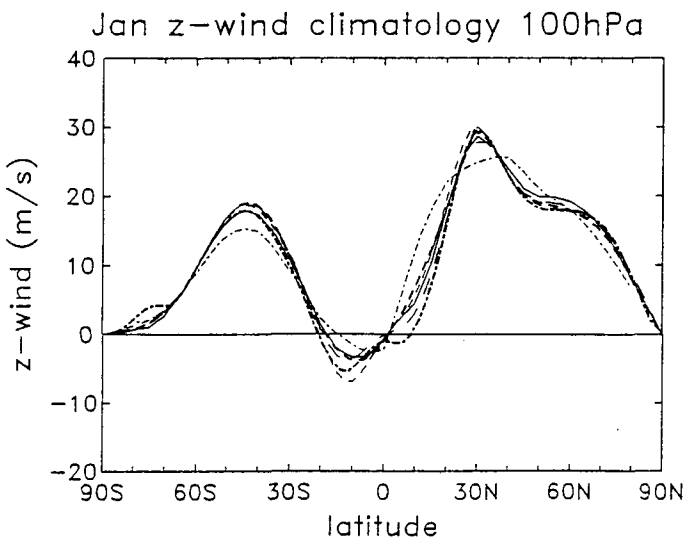
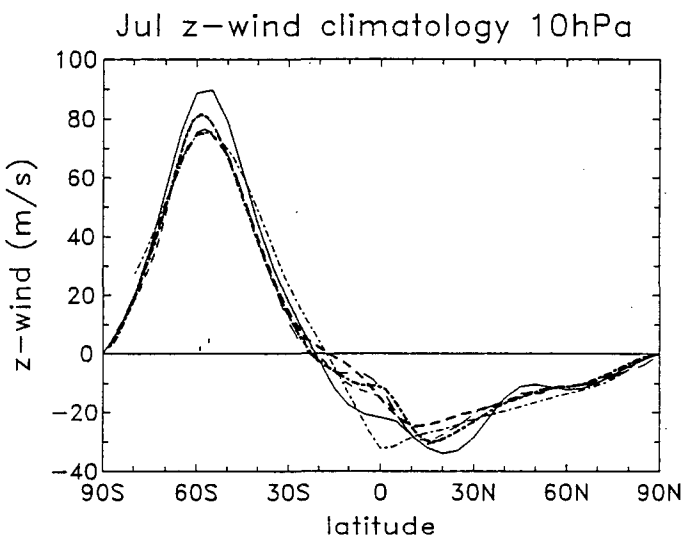
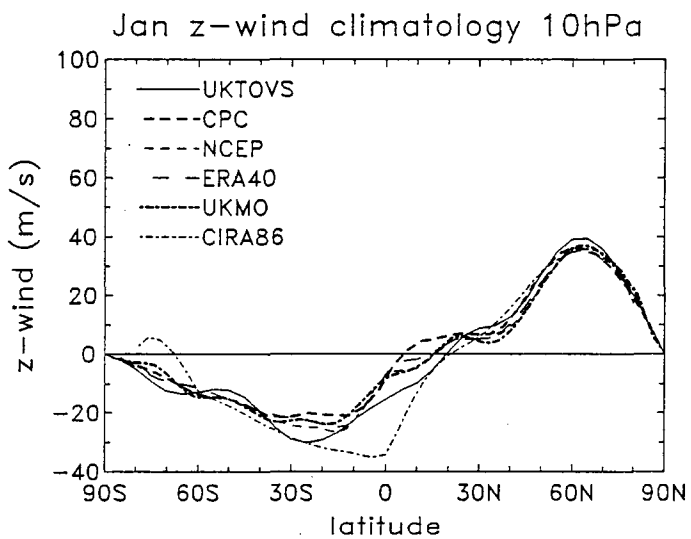
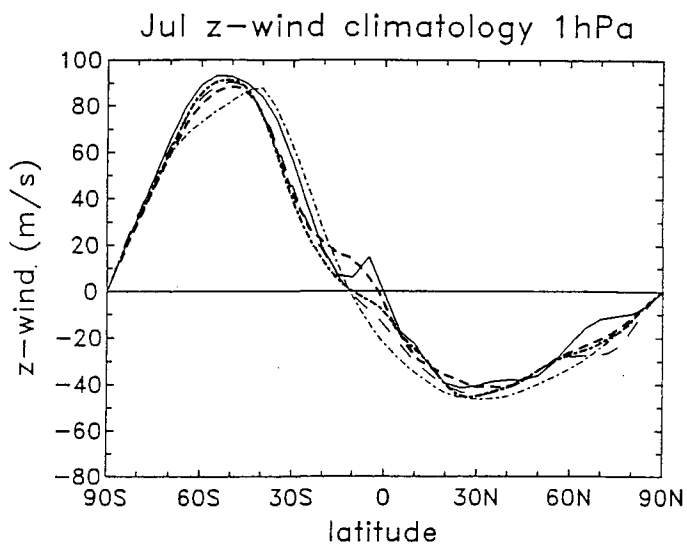
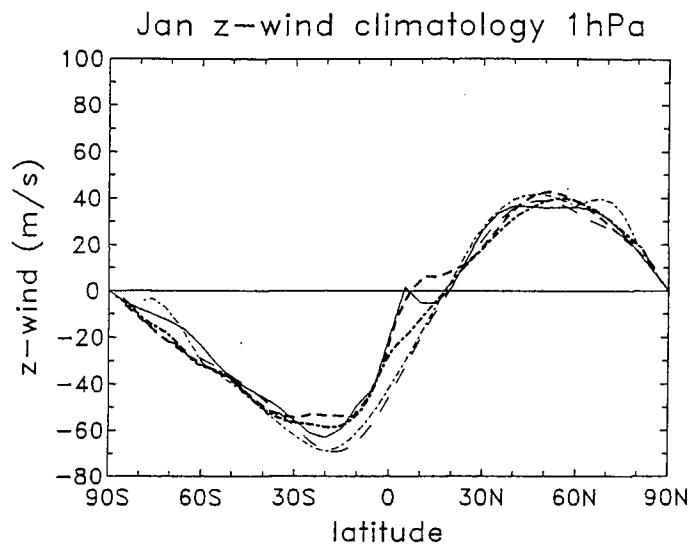


Fig. 35

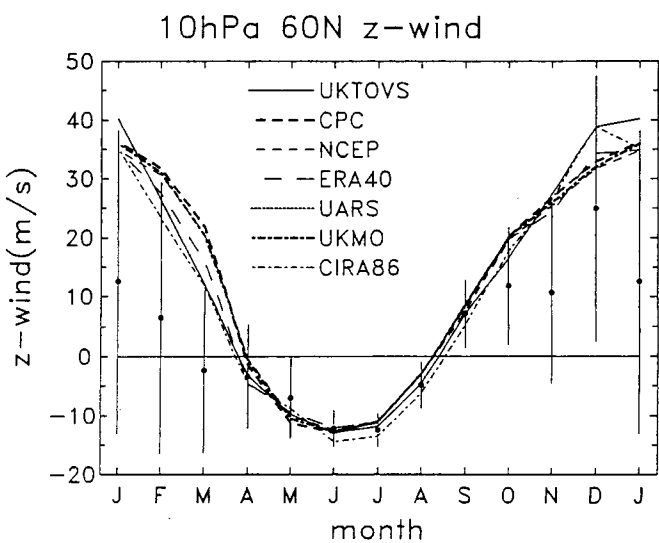
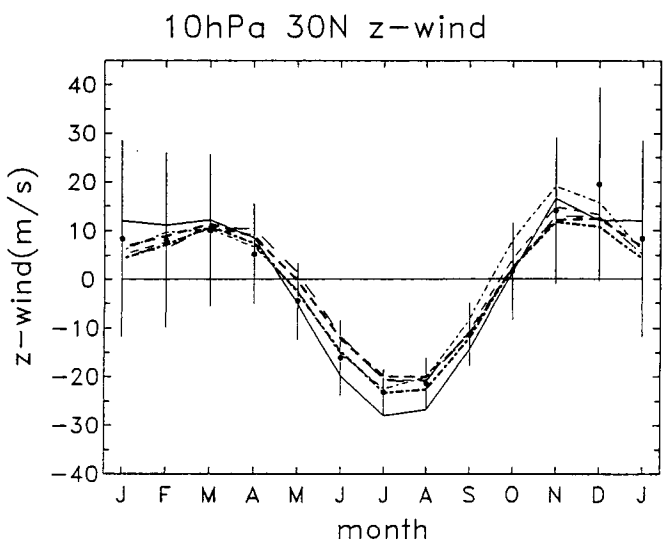
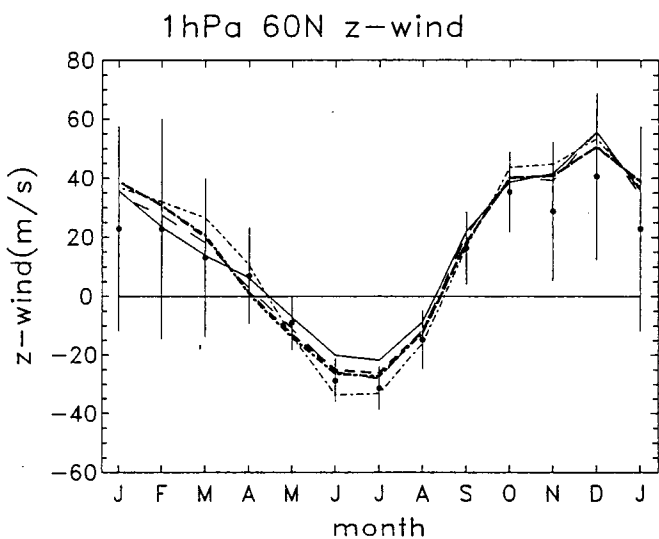
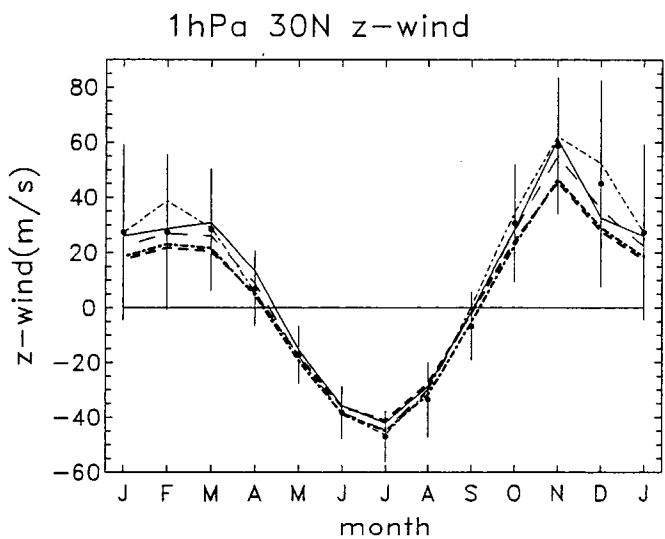
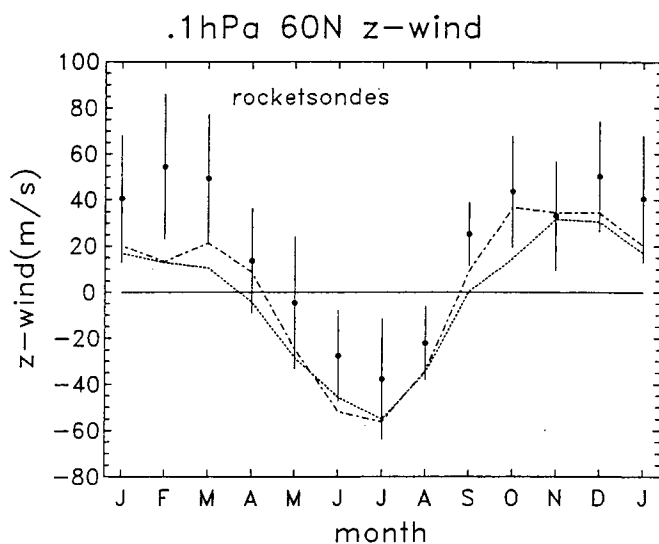
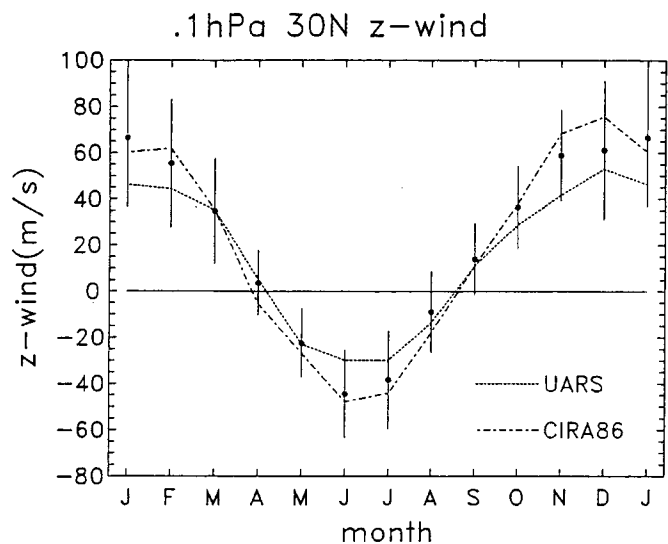


Fig. 36

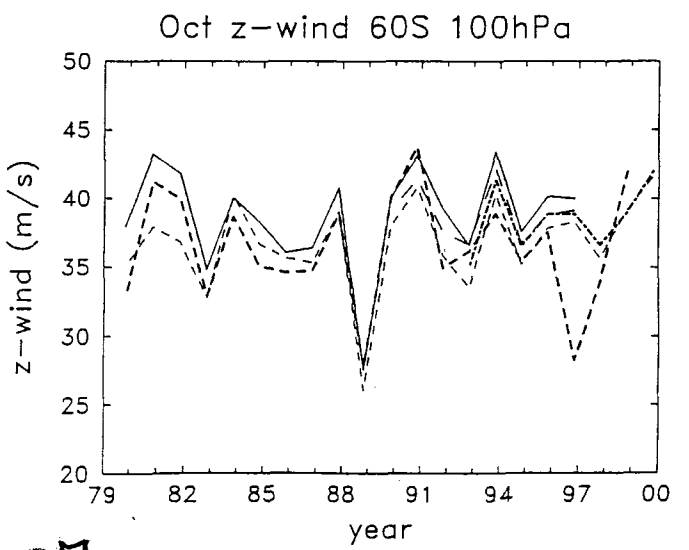
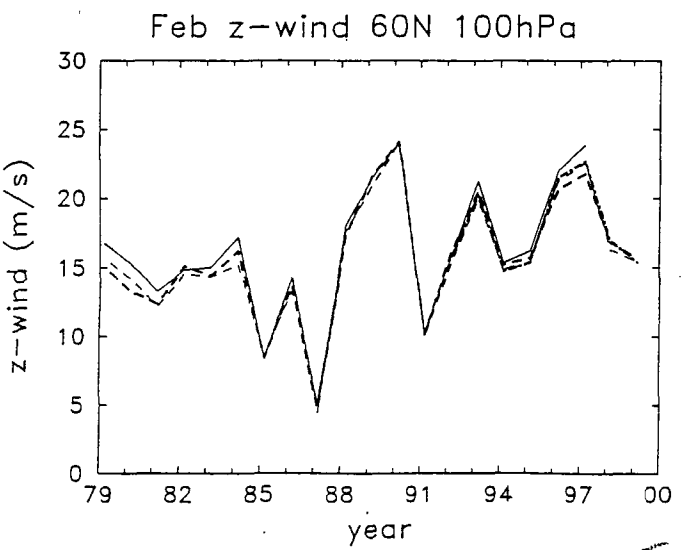
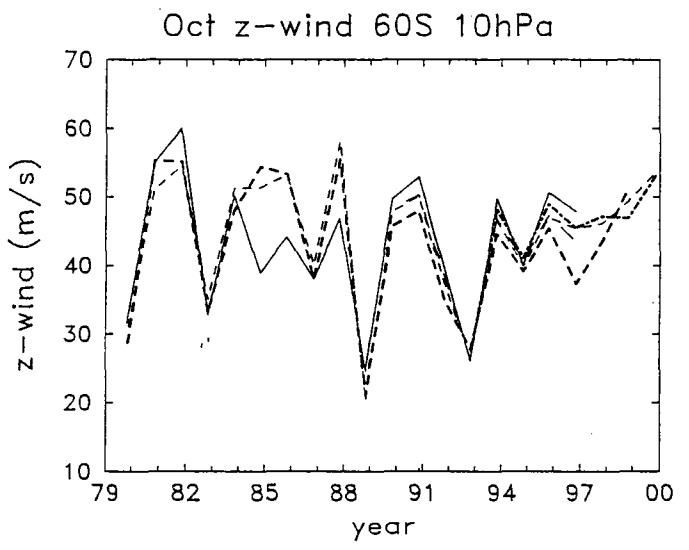
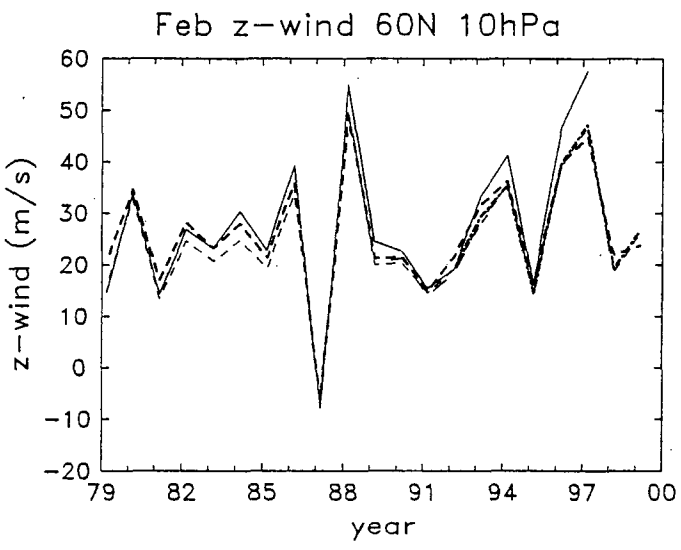
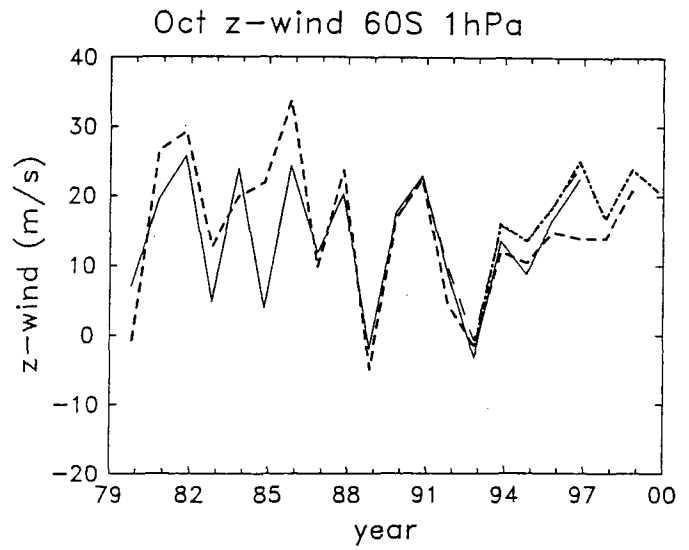
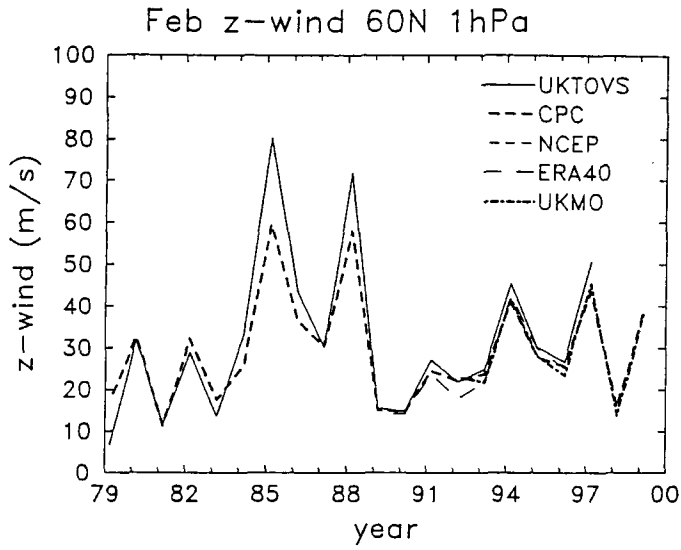


Fig. 37

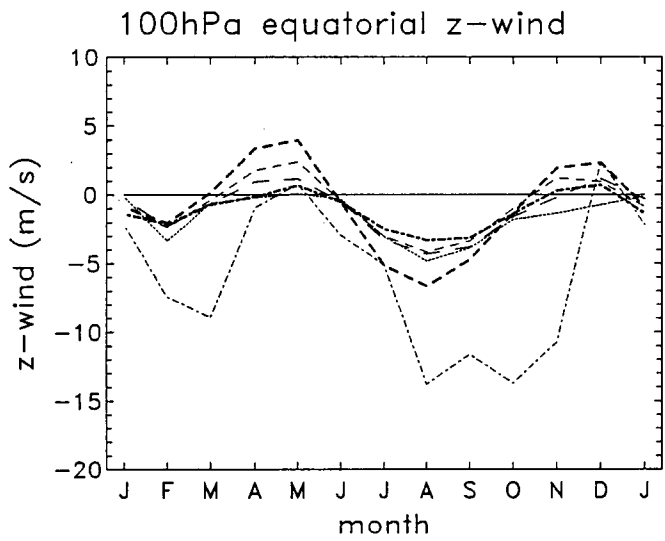
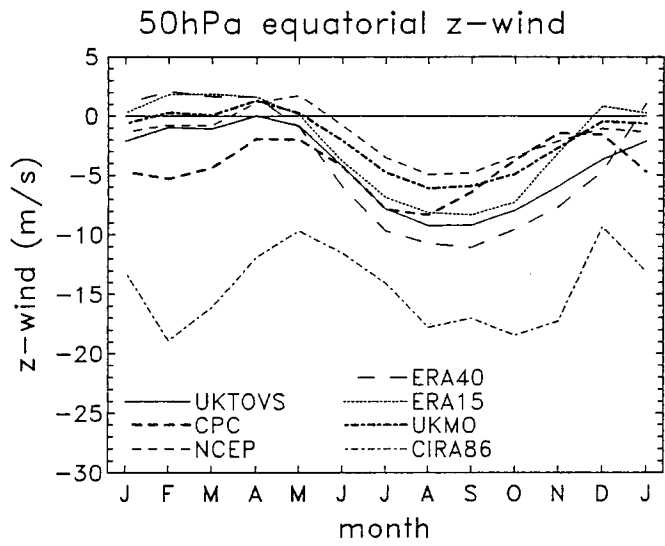


Fig. 38

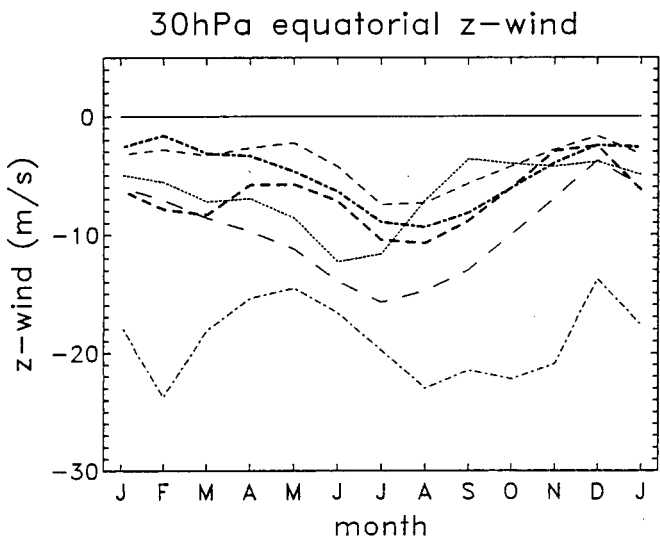
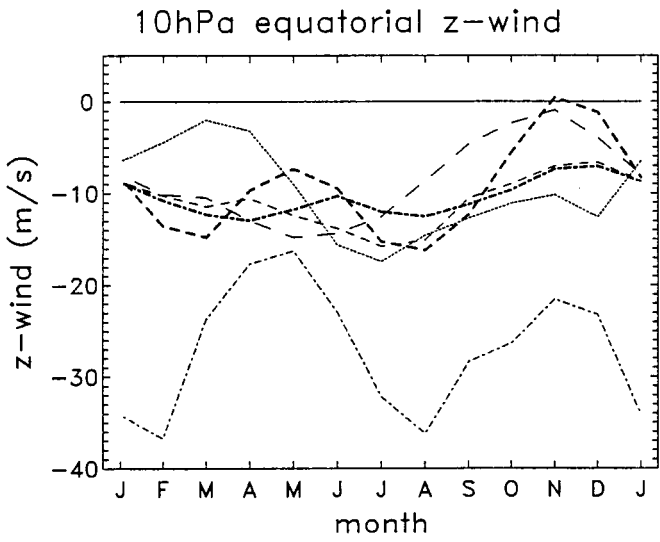
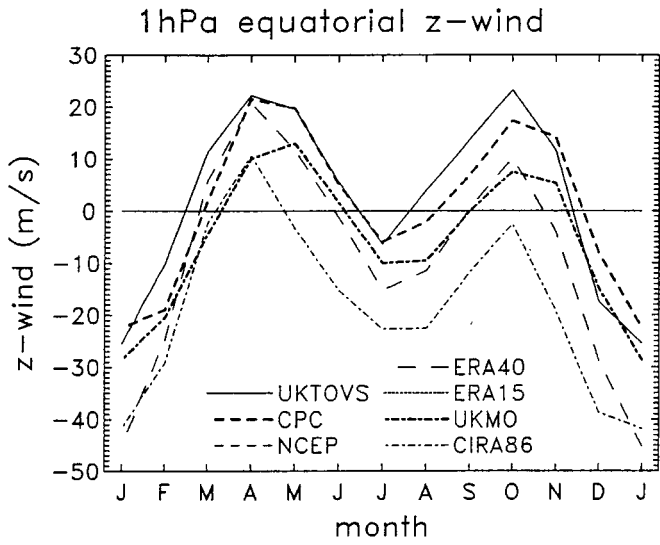


Fig. 39

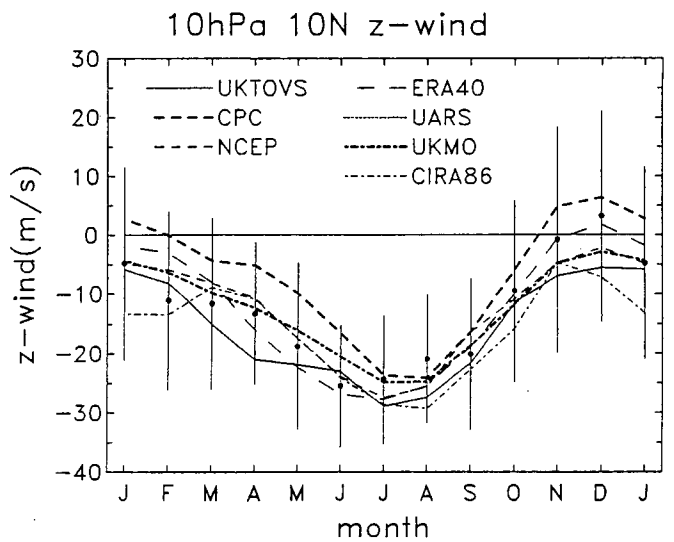
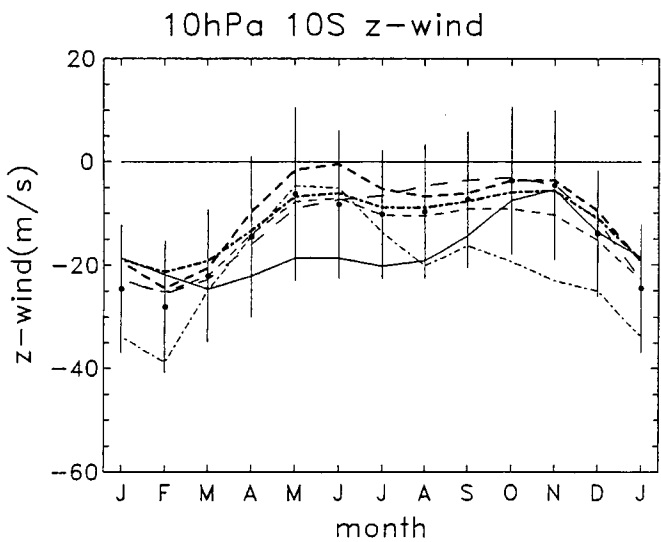
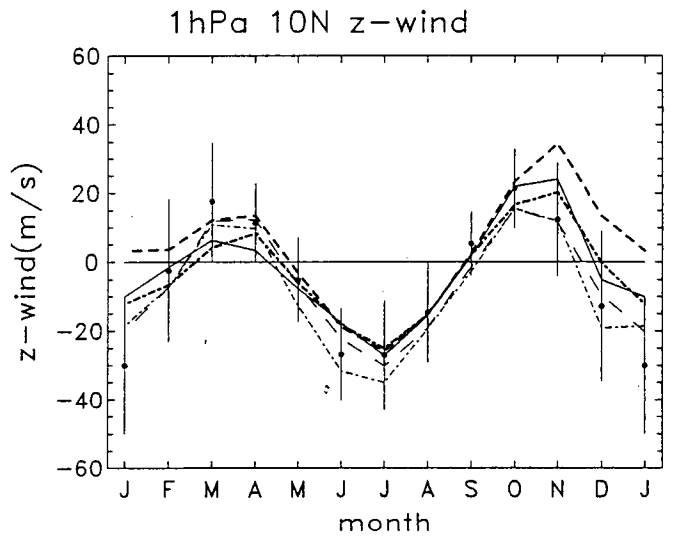
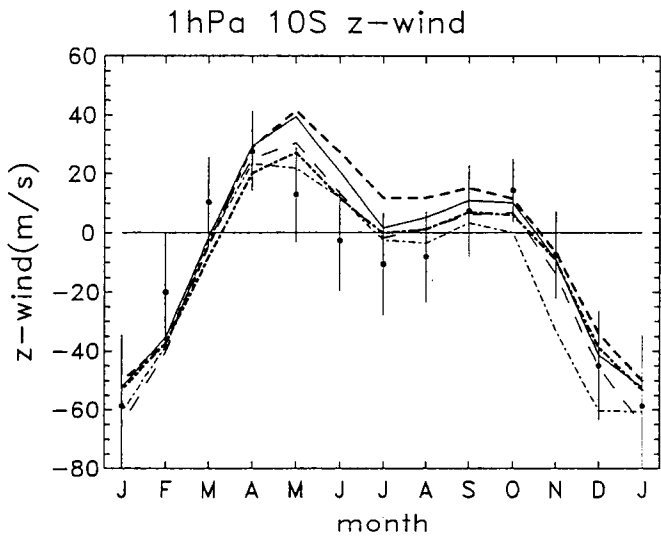
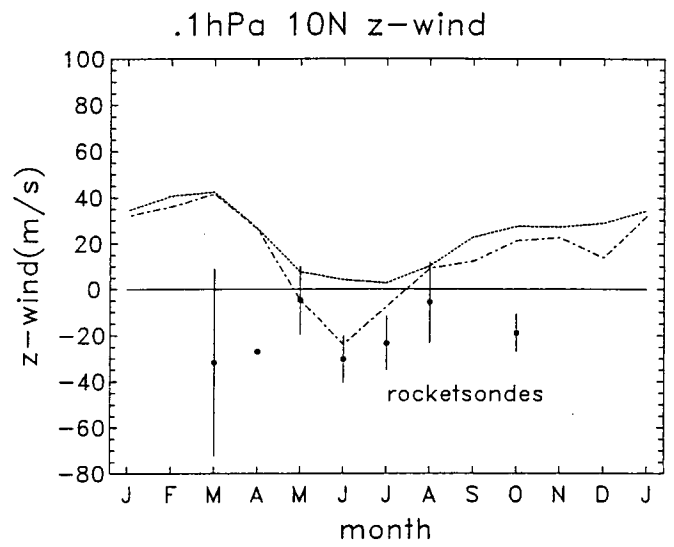
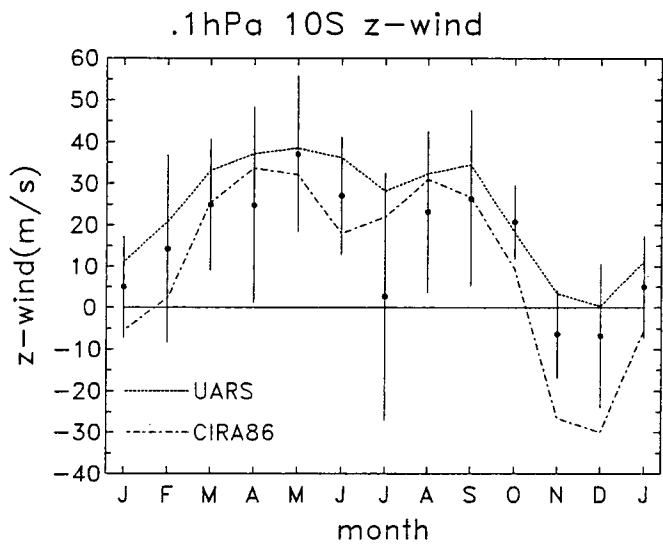


Fig. 40

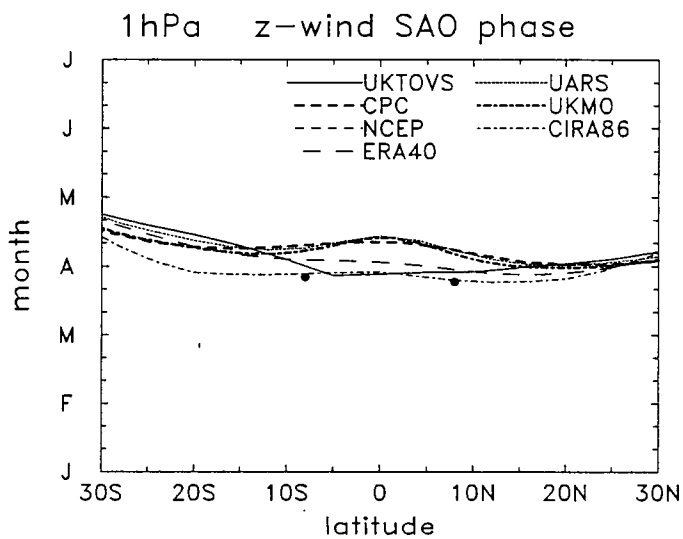
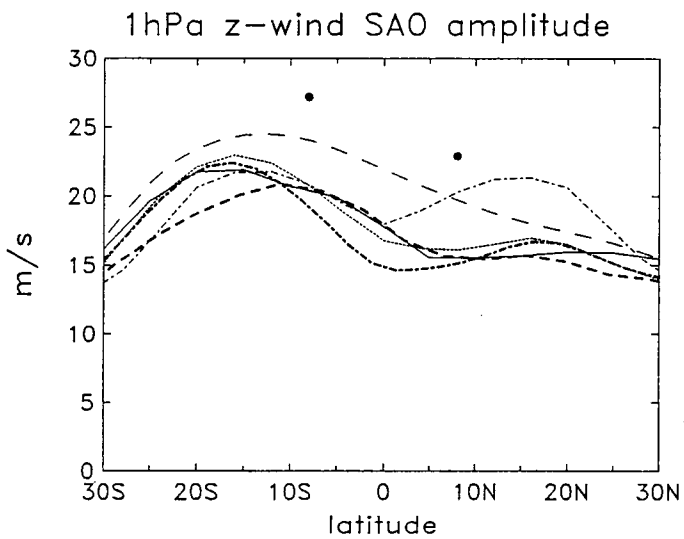
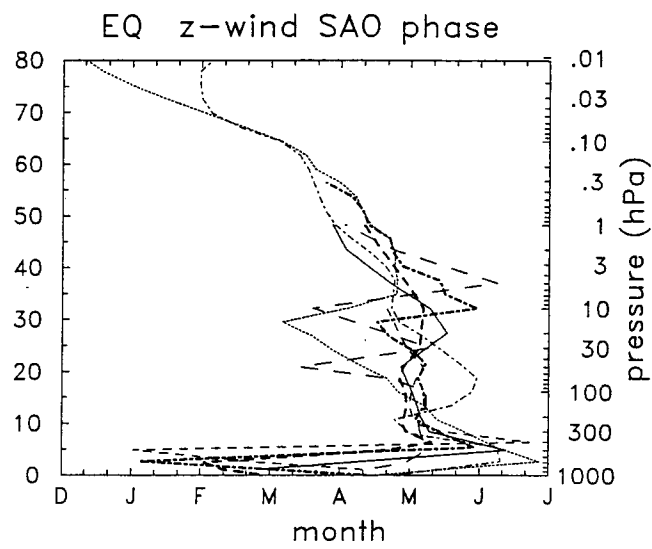
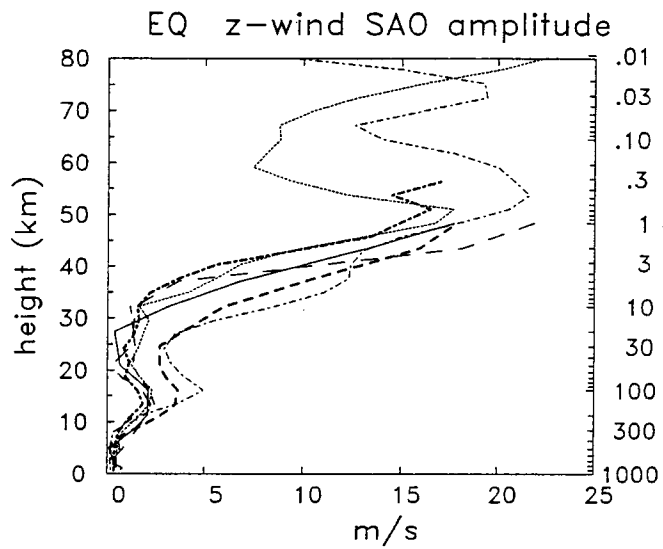
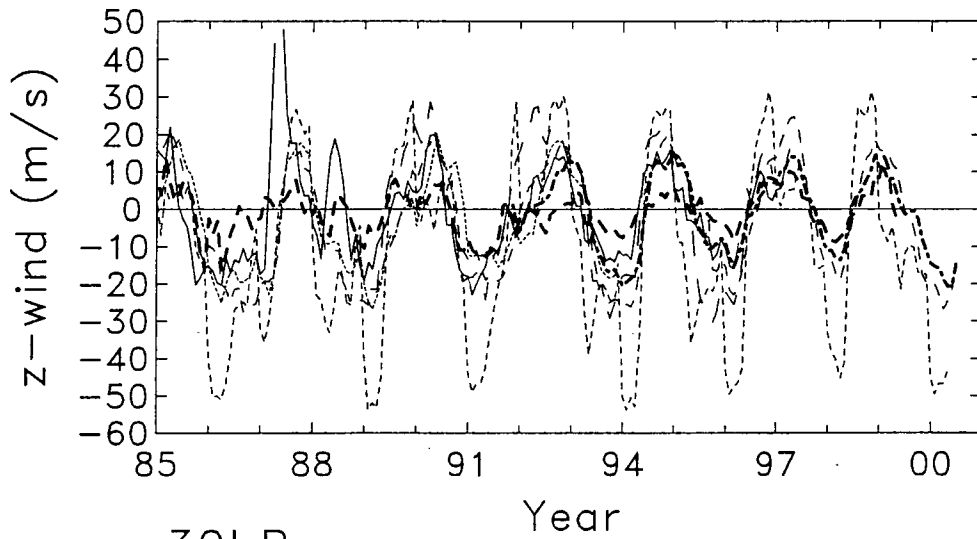
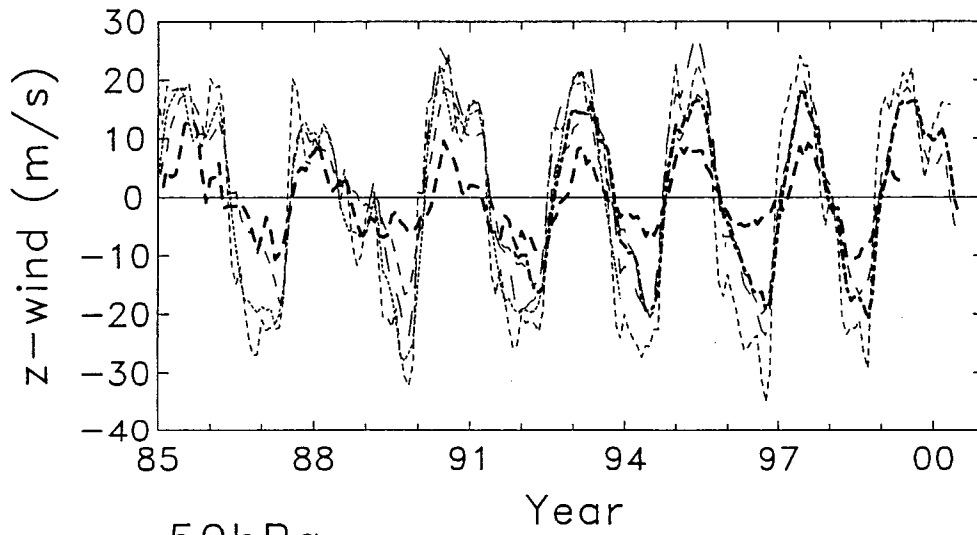


Fig. 41

10hPa z-wind anomalies equator



30hPa



50hPa

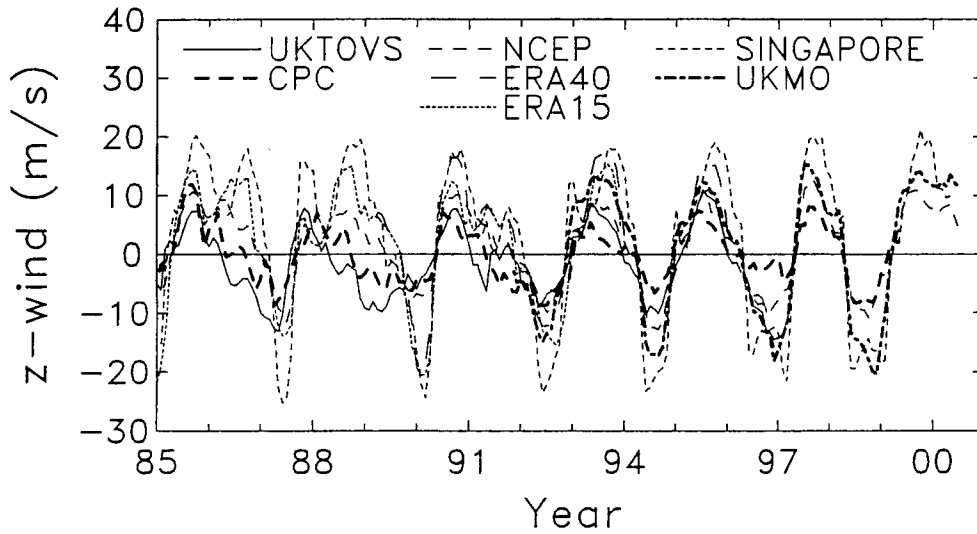


Fig. 42

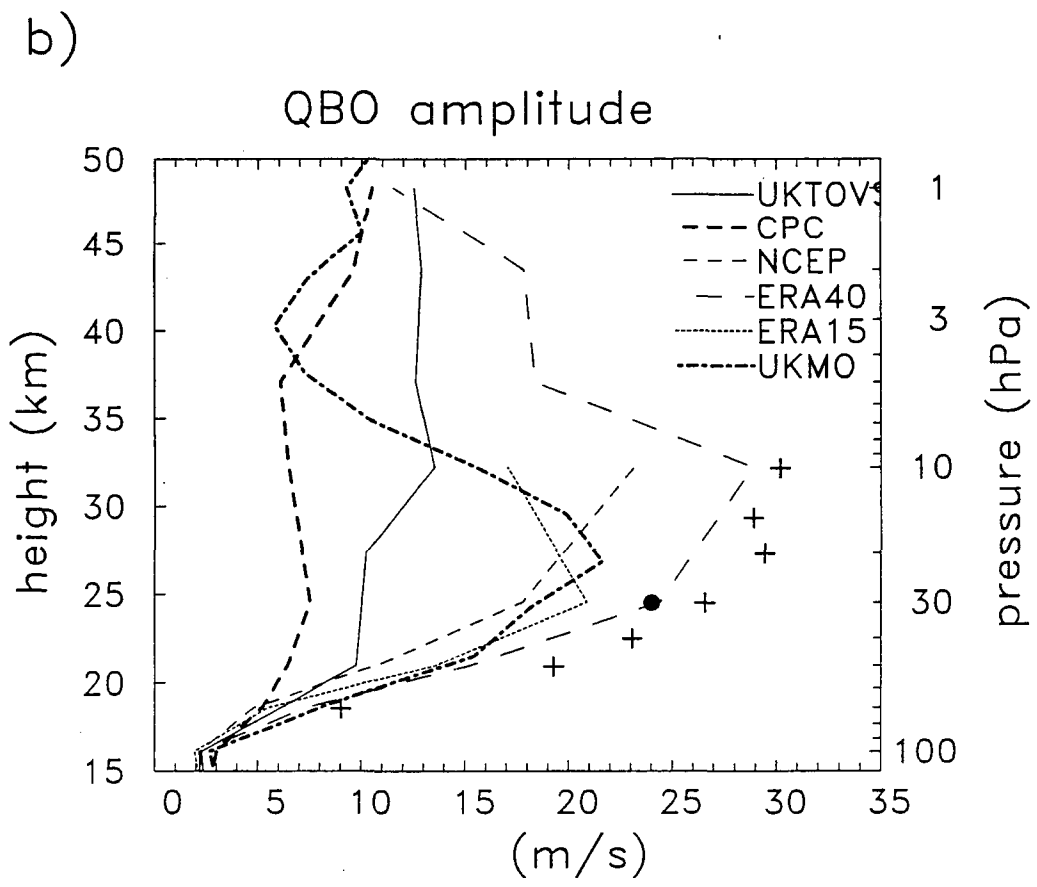
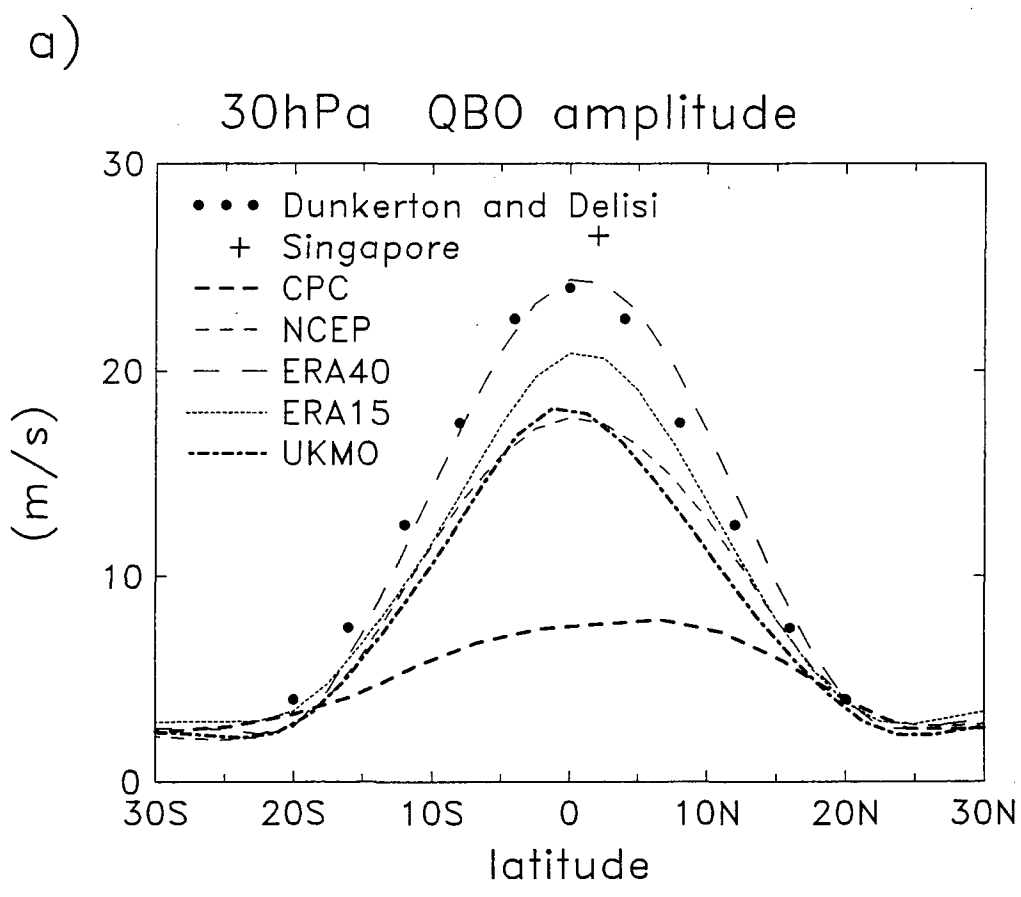


Fig. 43

1hPa z-wind anomalies equator

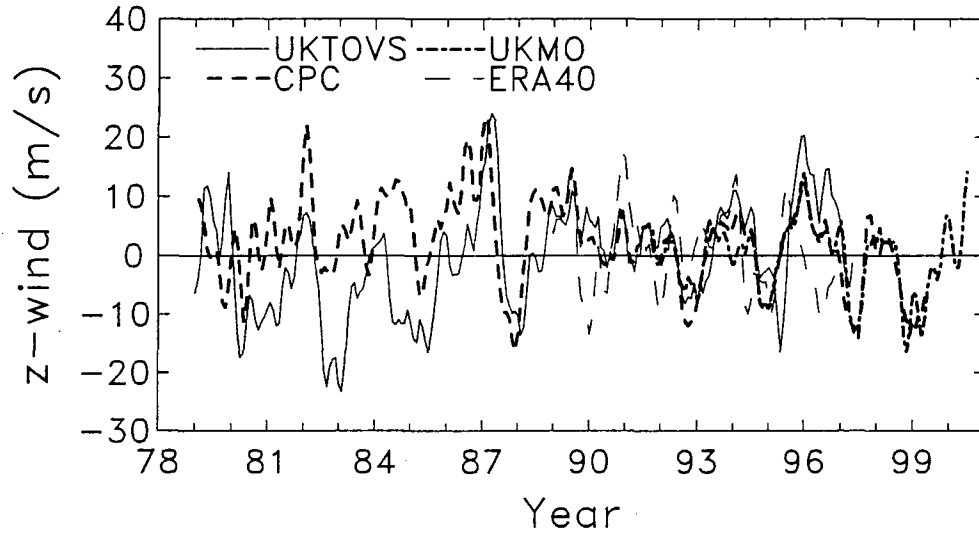


Fig. 44

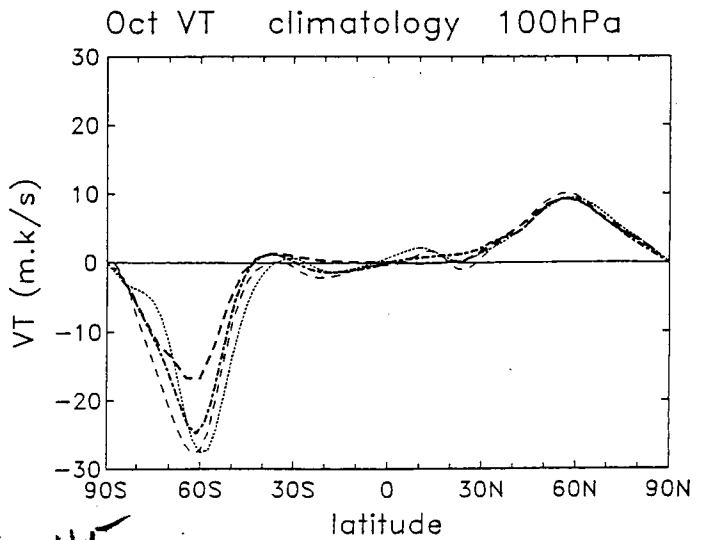
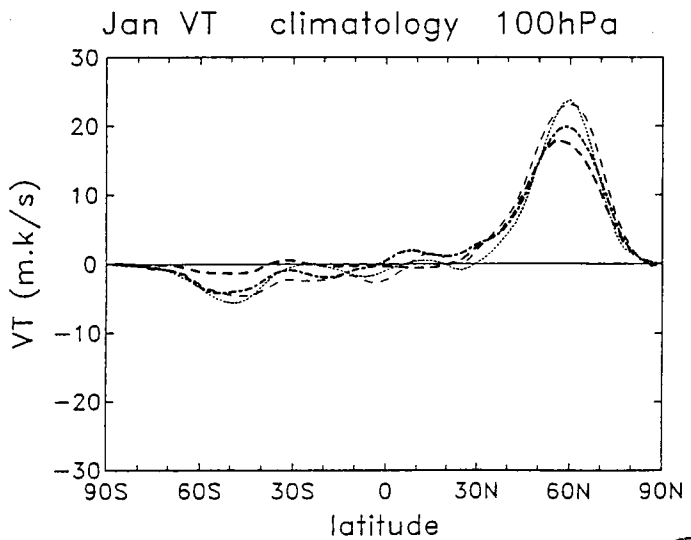
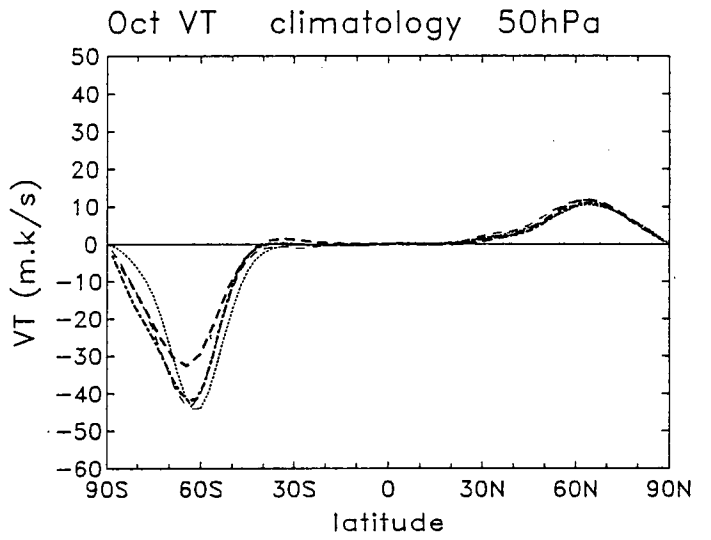
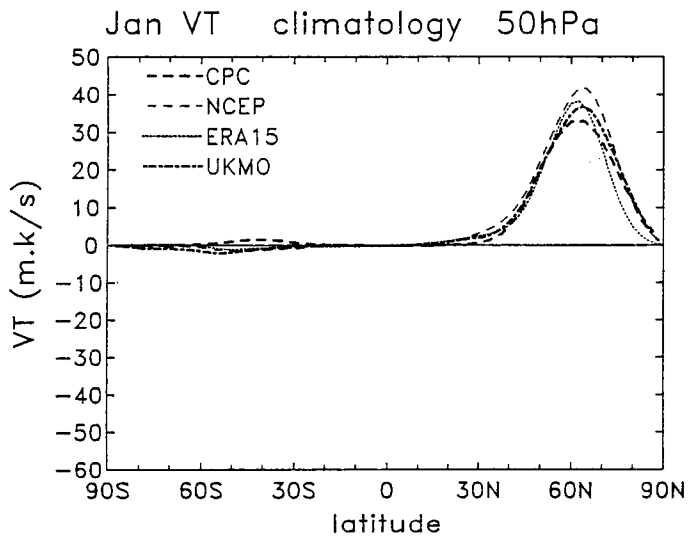
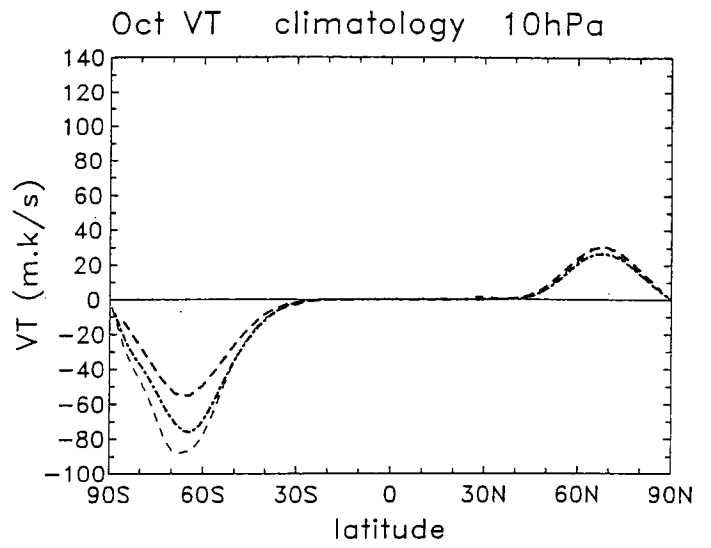
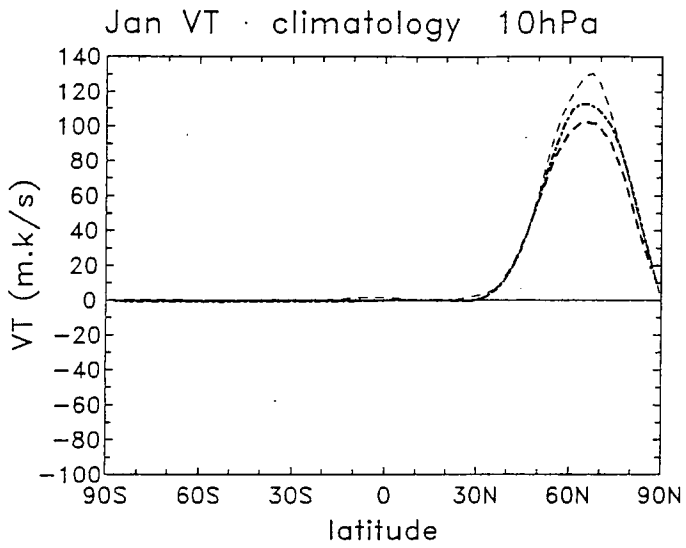


Fig. 45

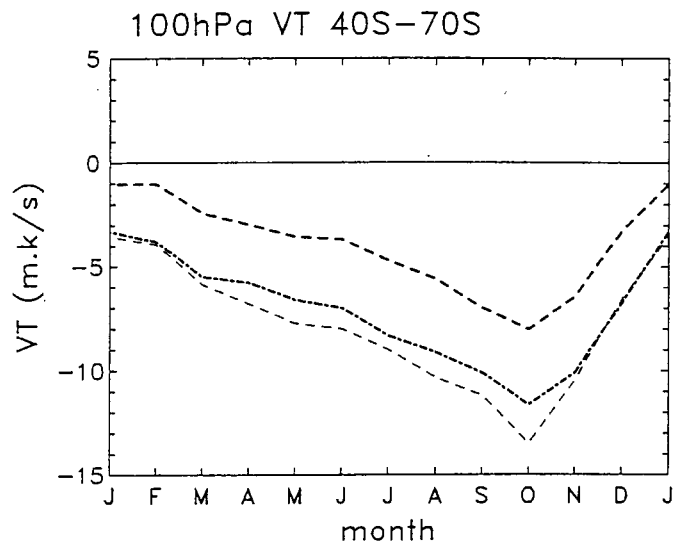
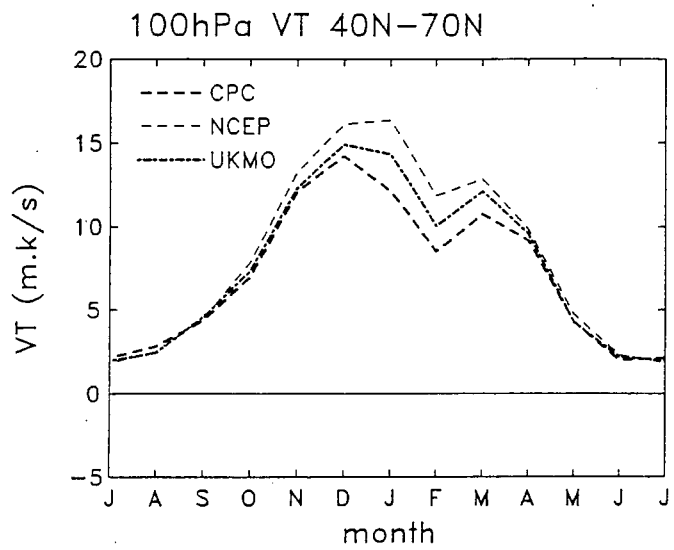


Fig. 46

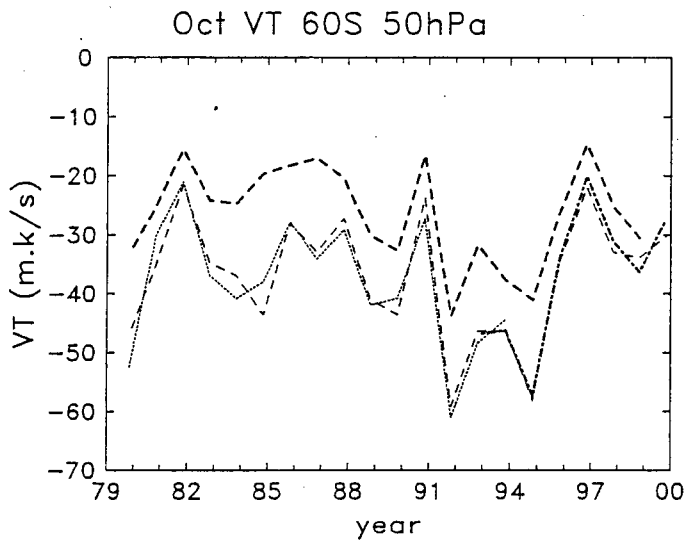
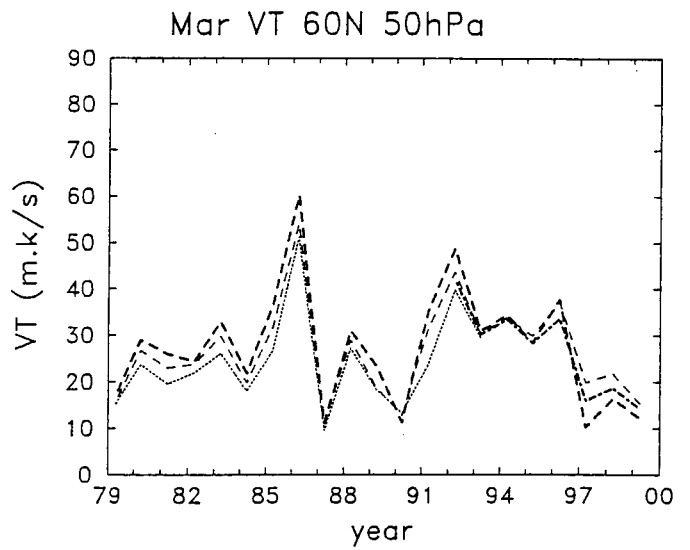
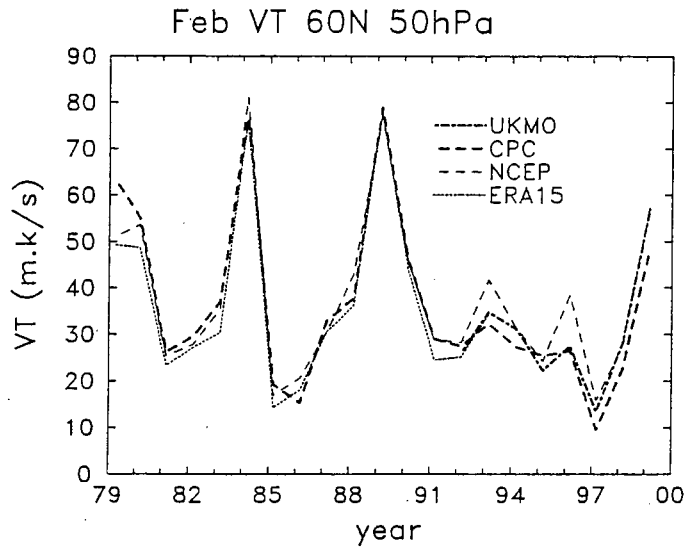


Fig. 47

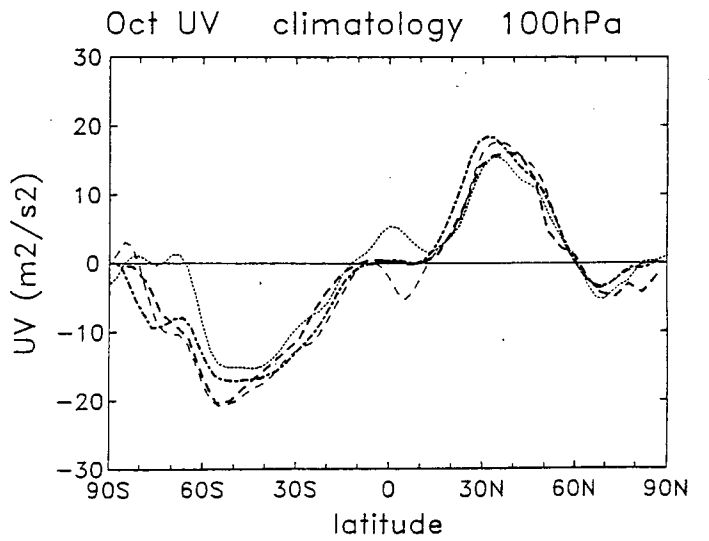
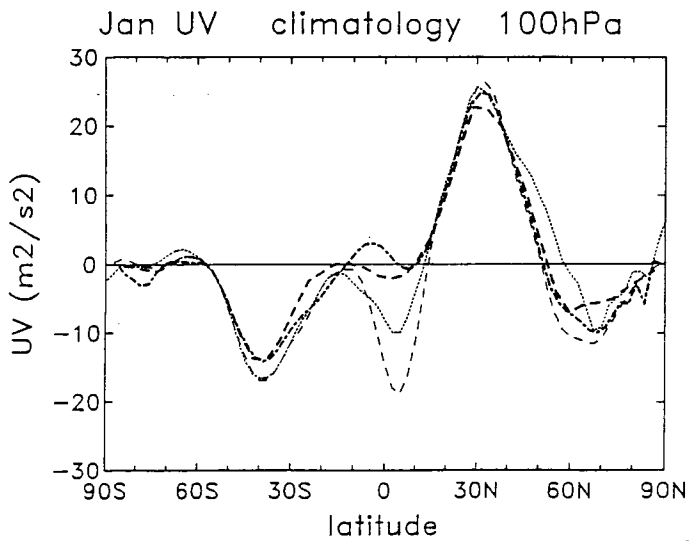
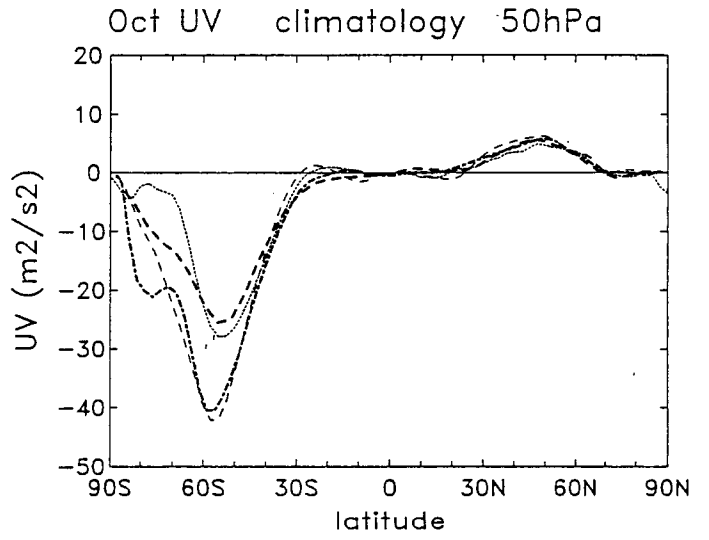
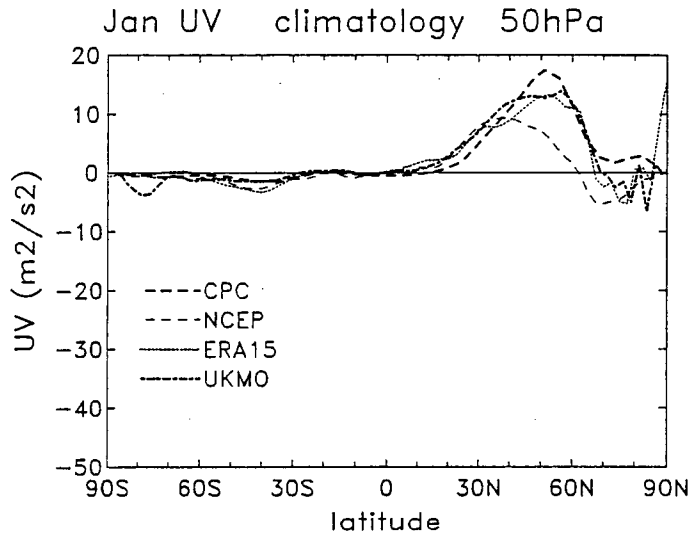
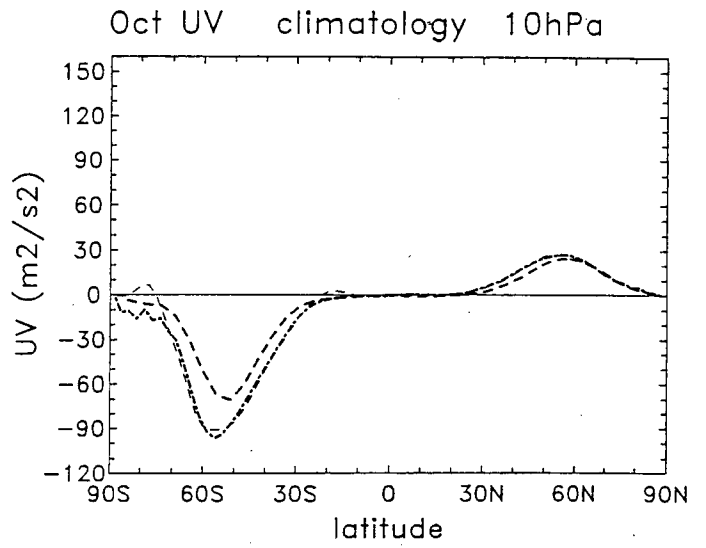
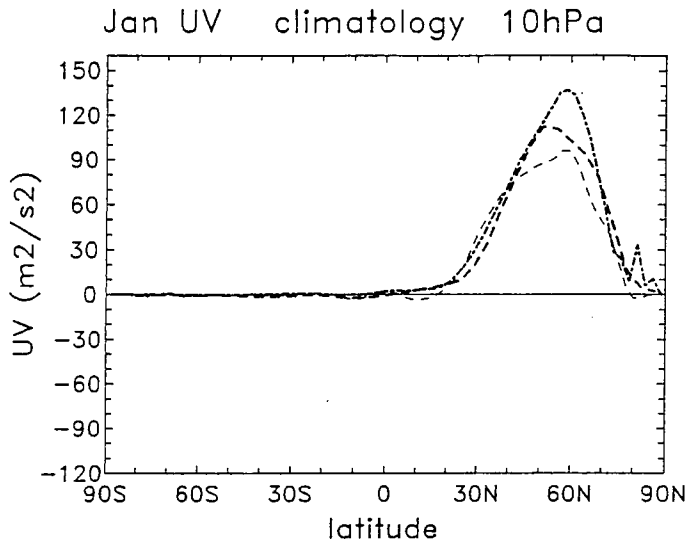
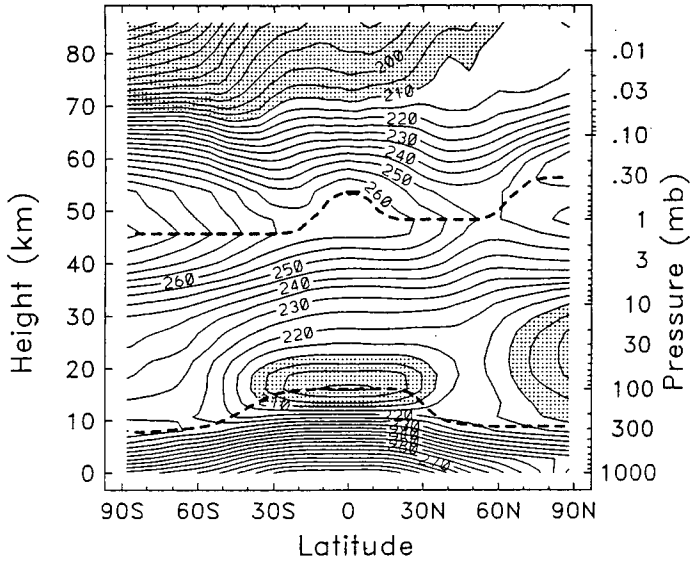
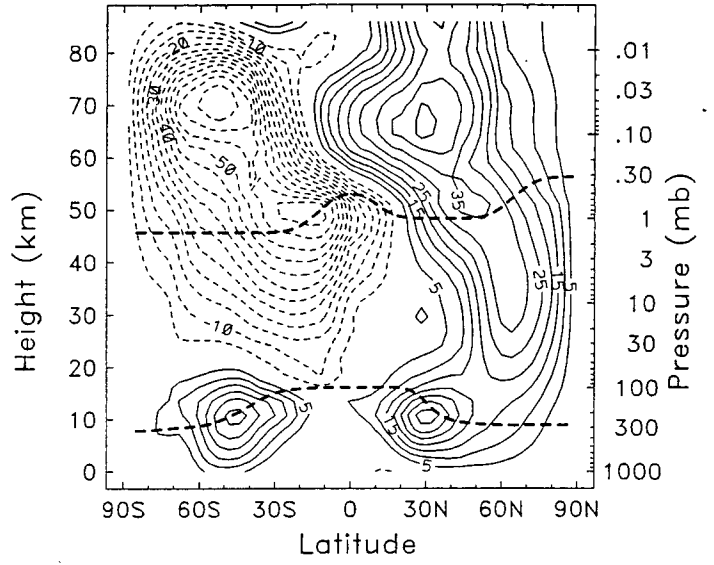


Fig. 48

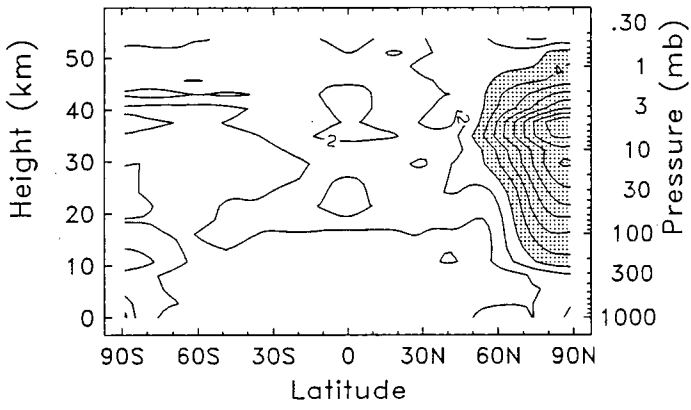
January temperature



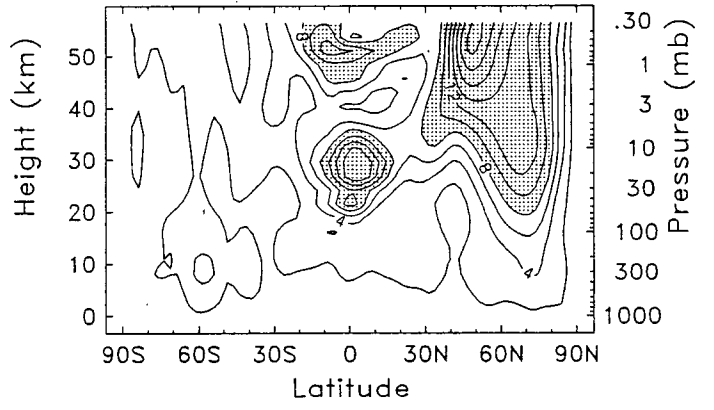
January zonal wind



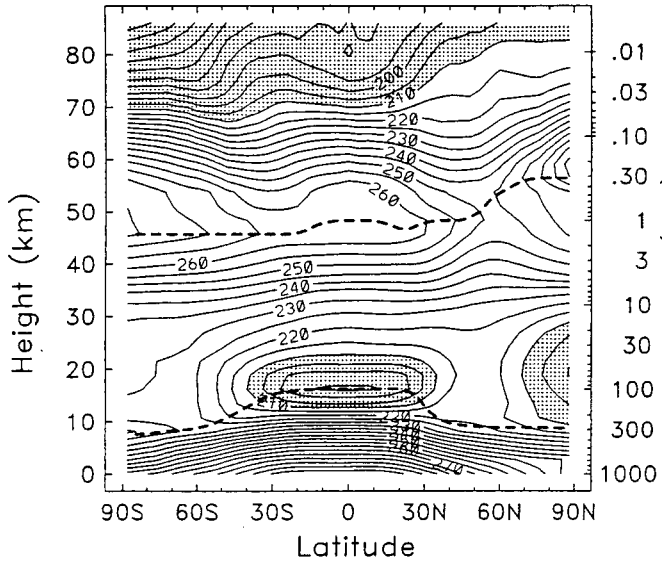
January temp int var



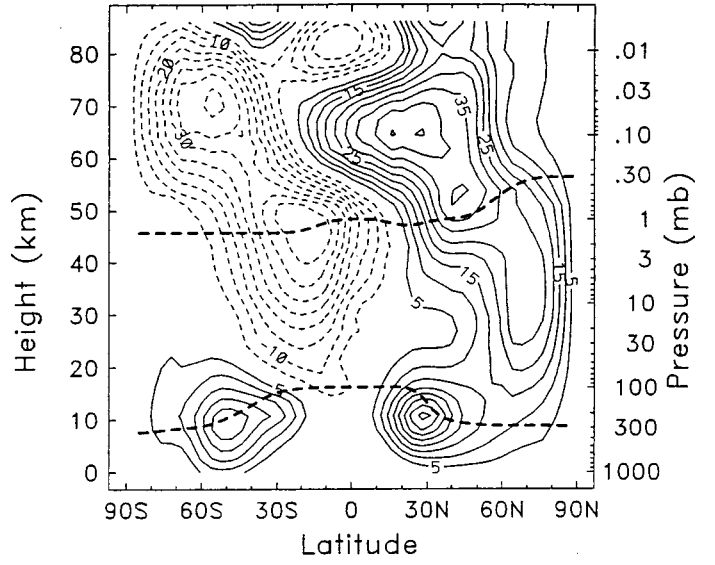
January zonal wind int var



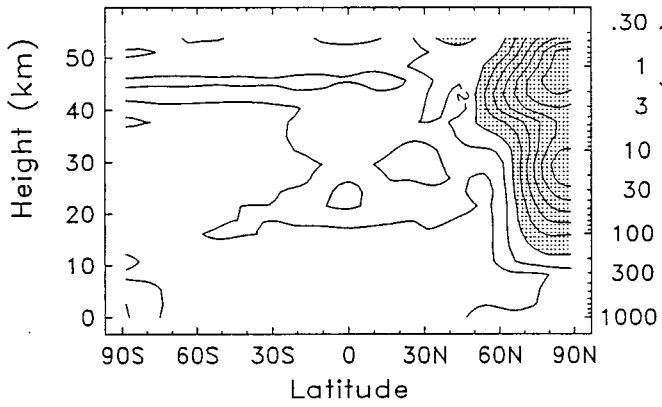
February temperature



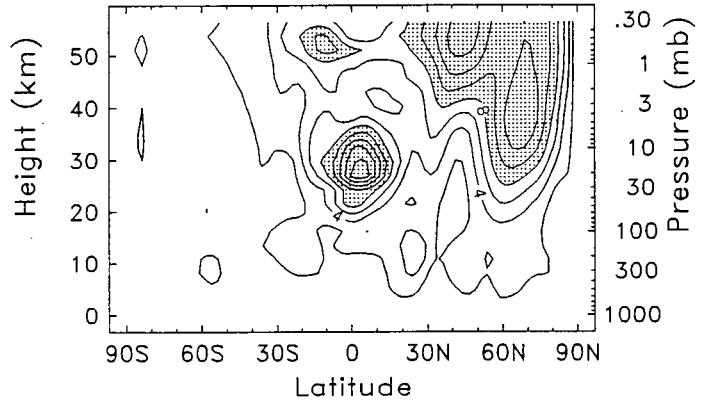
February zonal wind



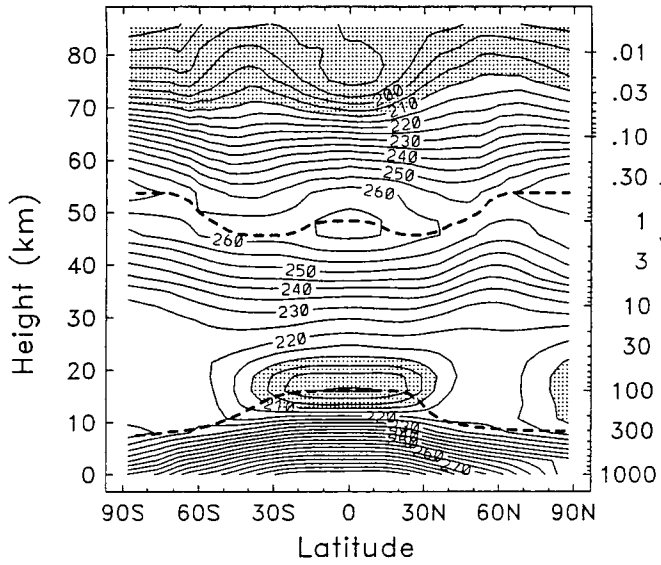
February temp int var



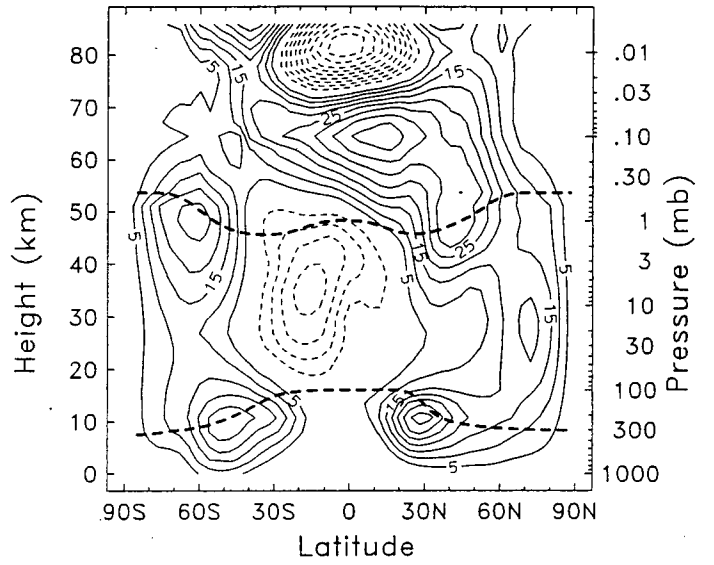
February zonal wind int var



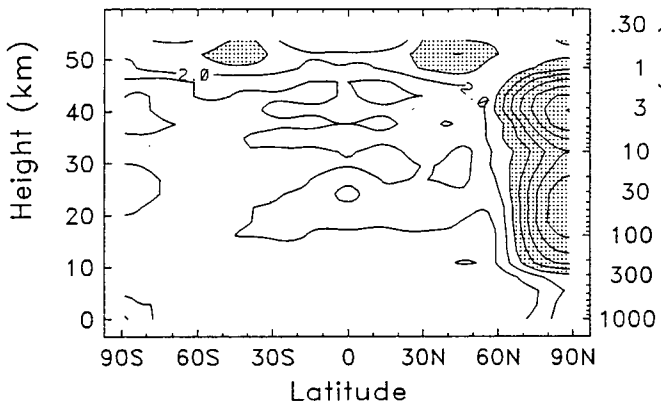
March temperature



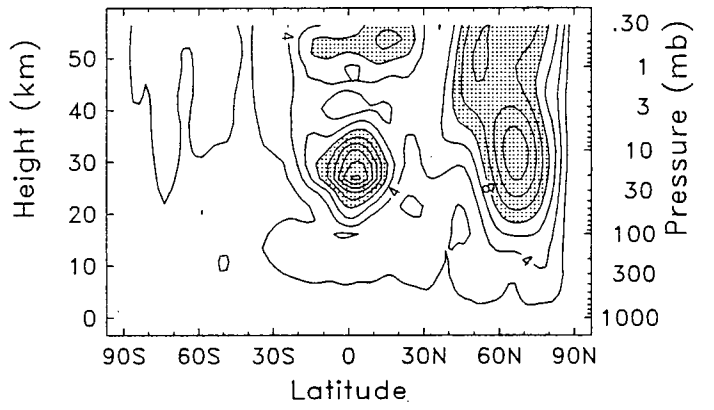
March zonal wind



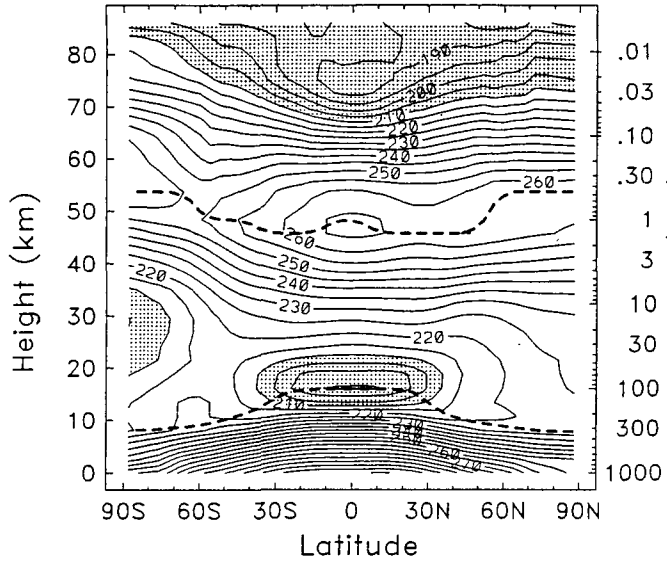
March temp int var



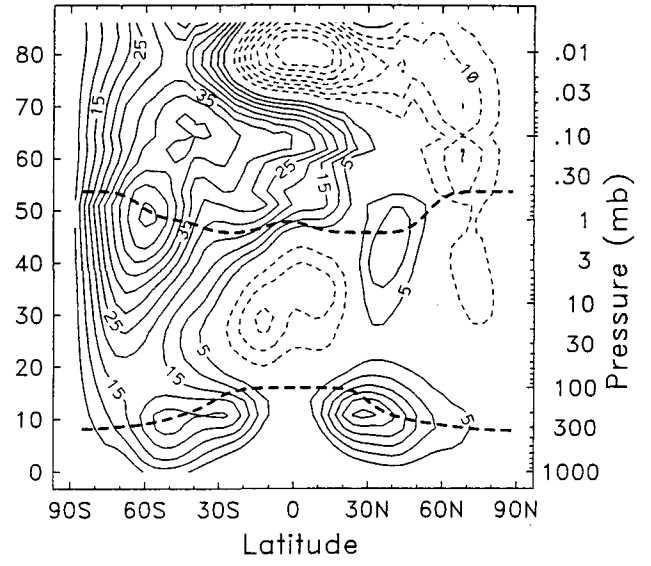
March zonal wind int var



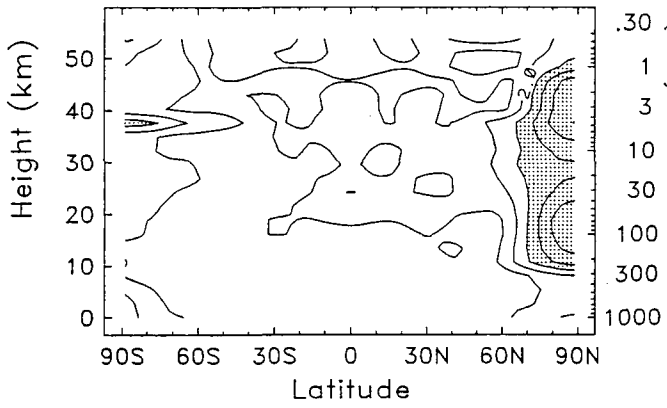
April temperature



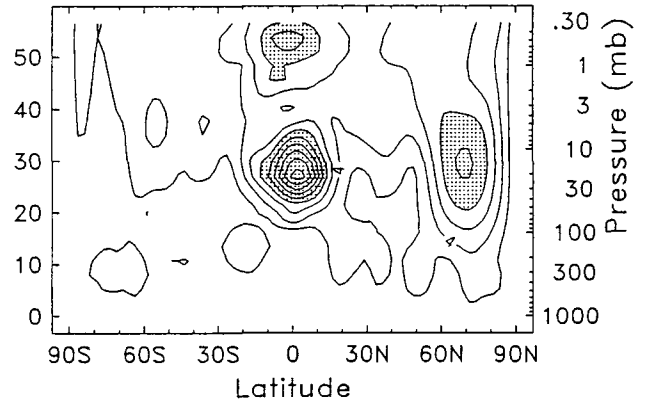
April zonal wind



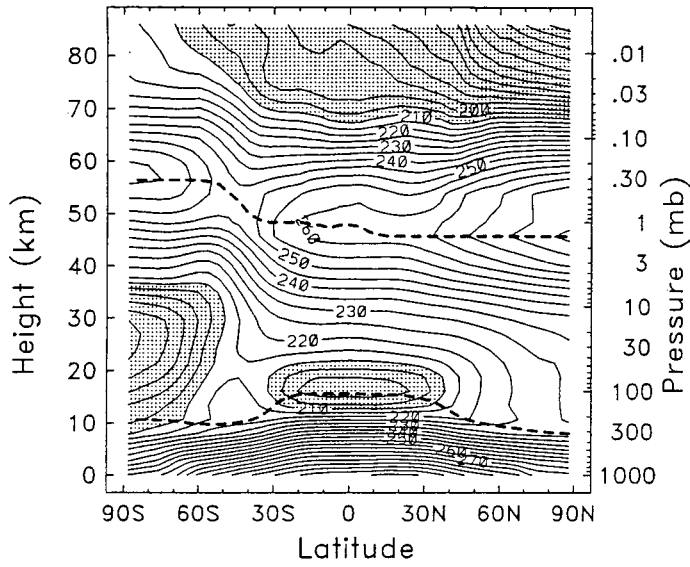
April temp int var



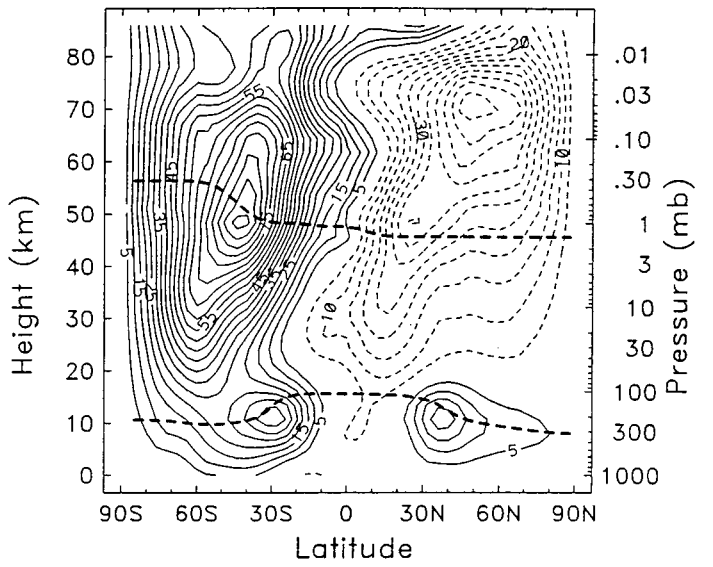
April zonal wind int var



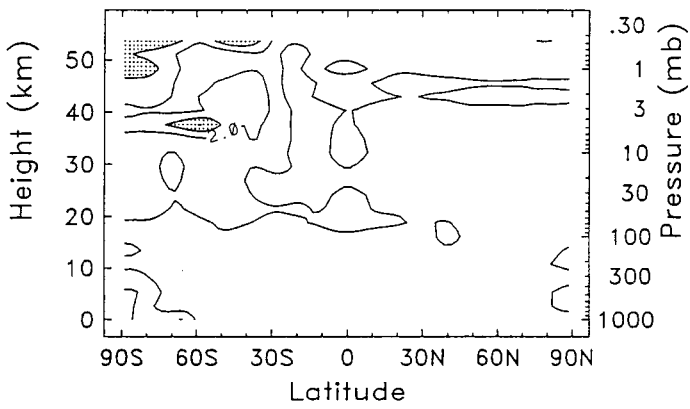
June temperature



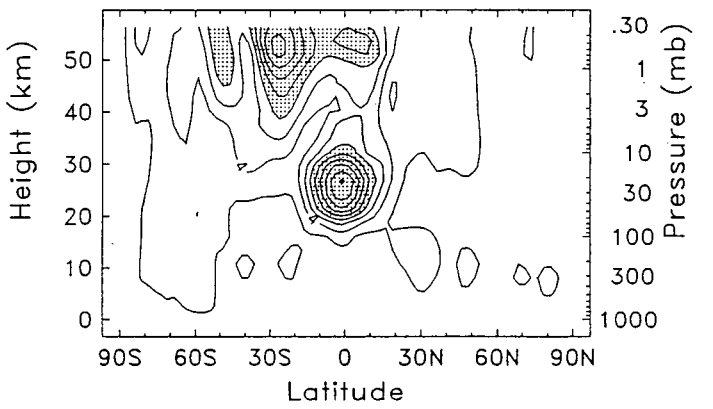
June zonal wind



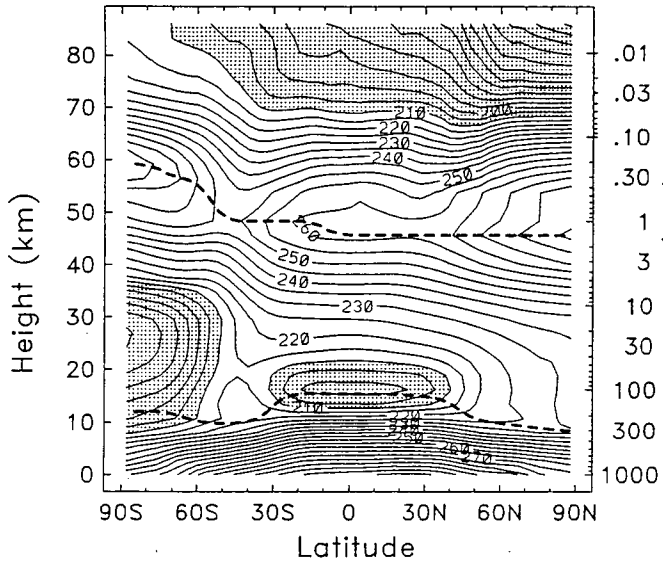
June temp int var



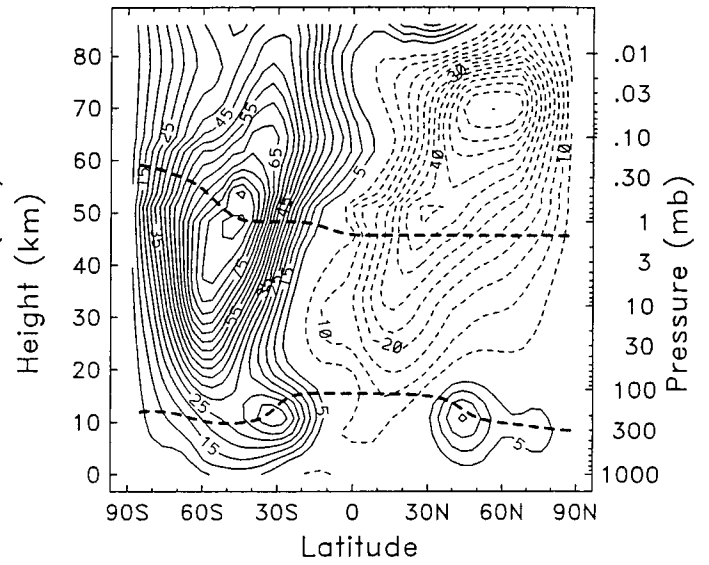
June zonal wind int var



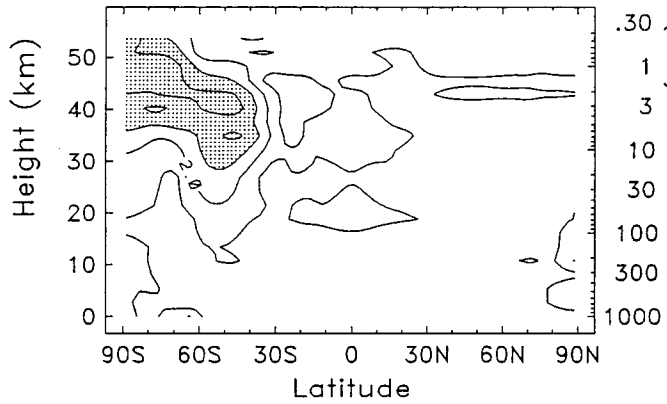
July temperature



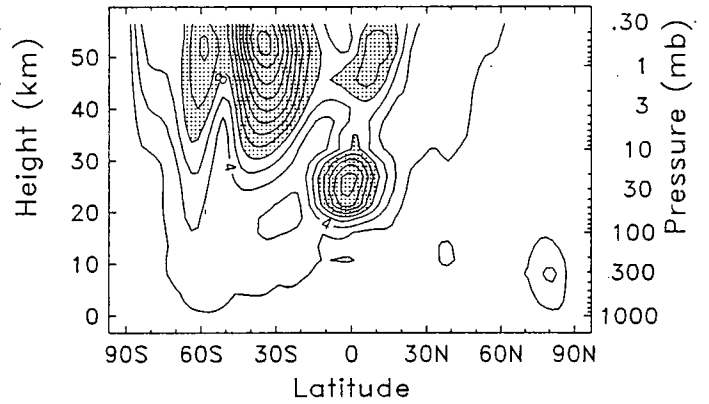
July zonal wind



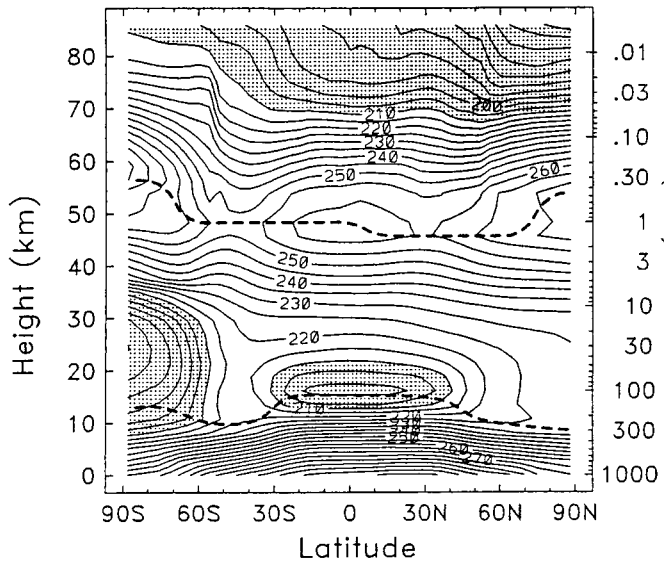
July temp int var



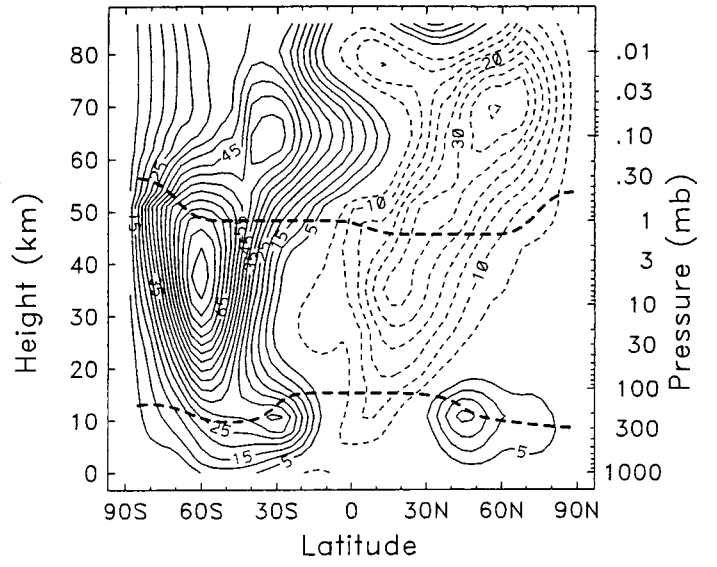
July zonal wind int var



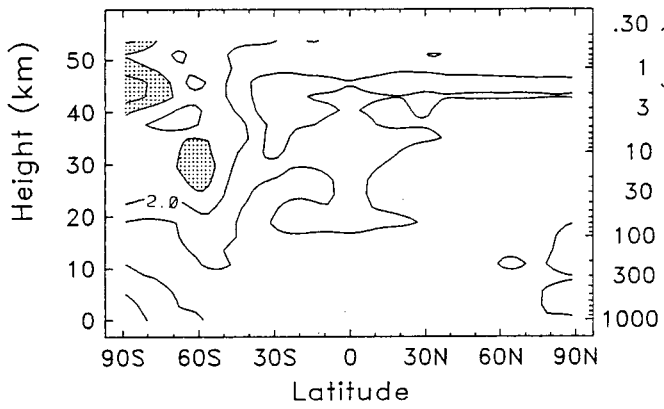
August temperature



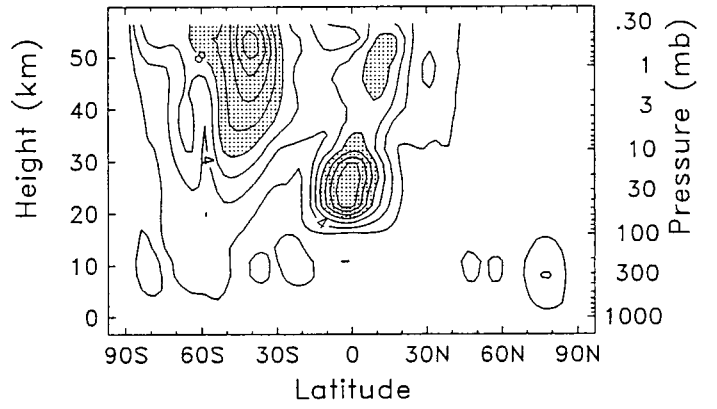
August zonal wind



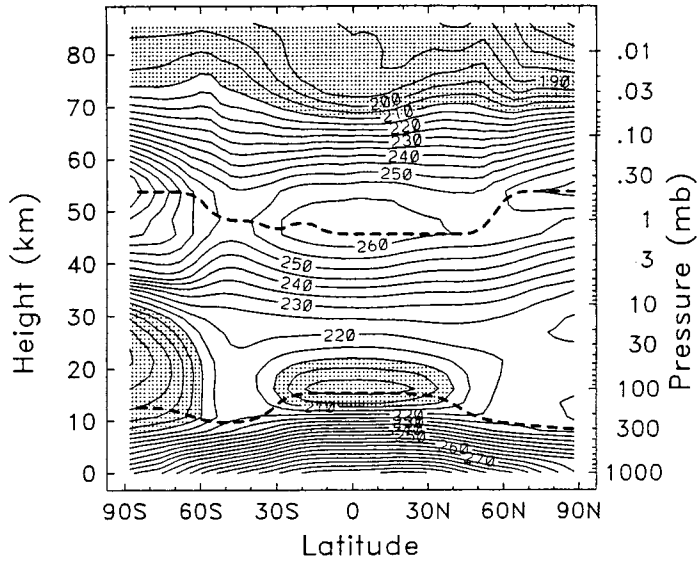
August temp int var



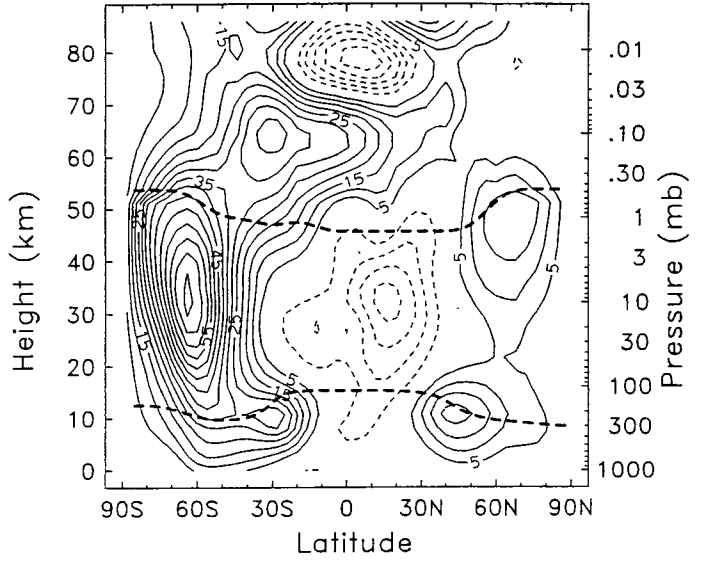
August zonal wind int var



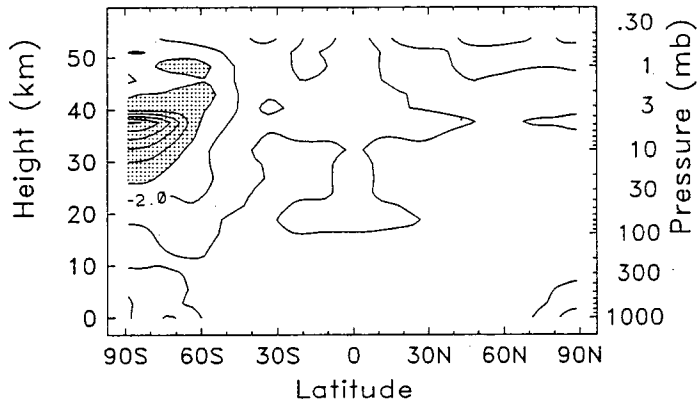
September temperature



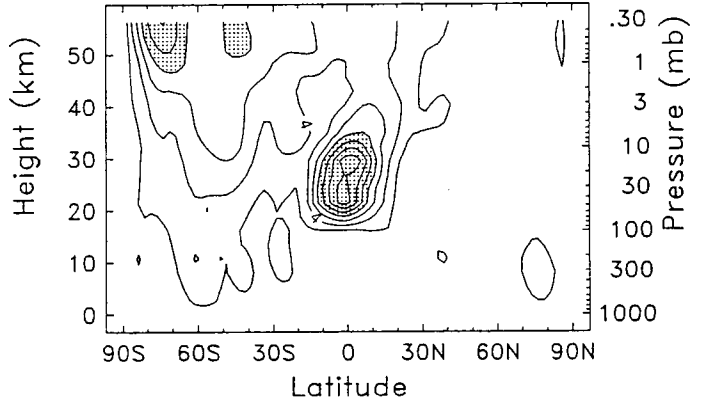
September zonal wind



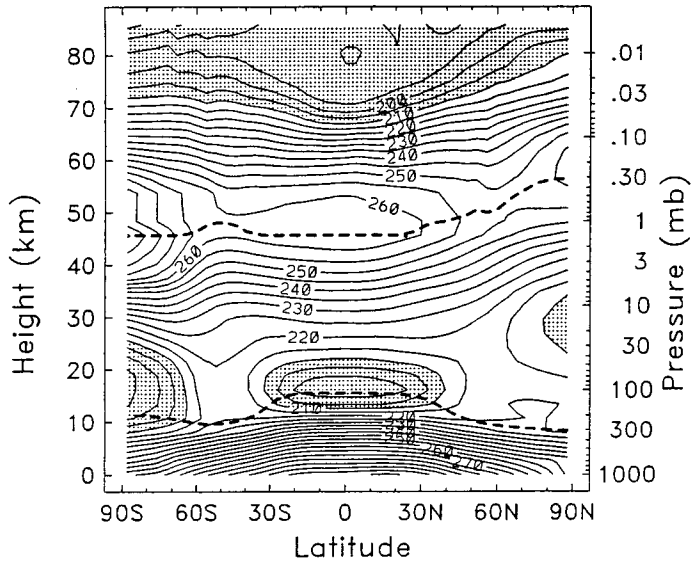
September temp int var



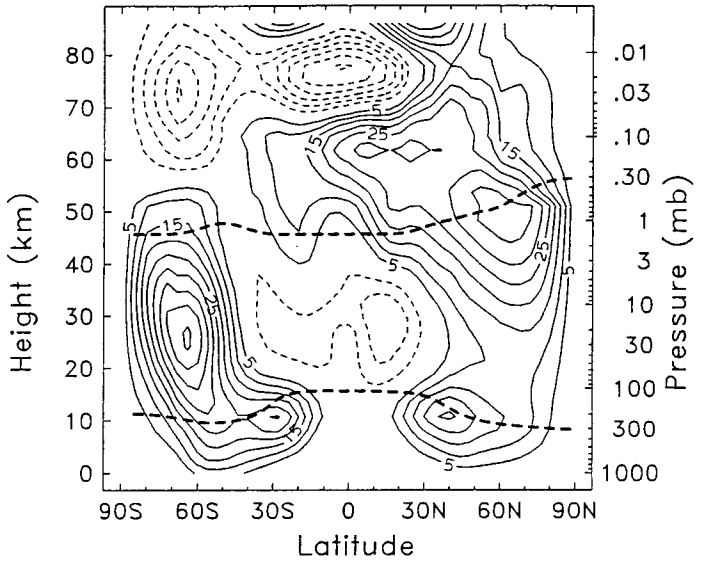
September zonal wind int var



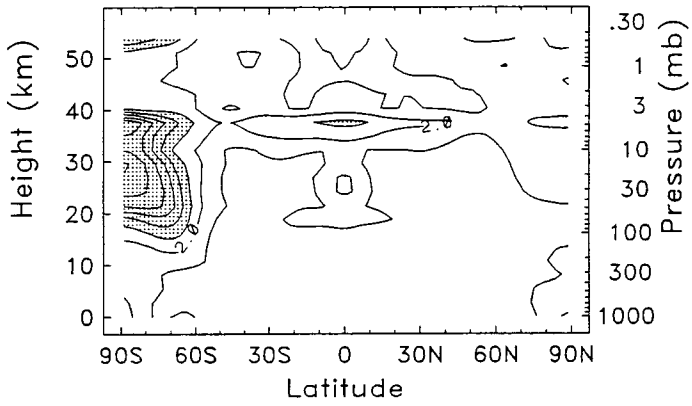
October temperature



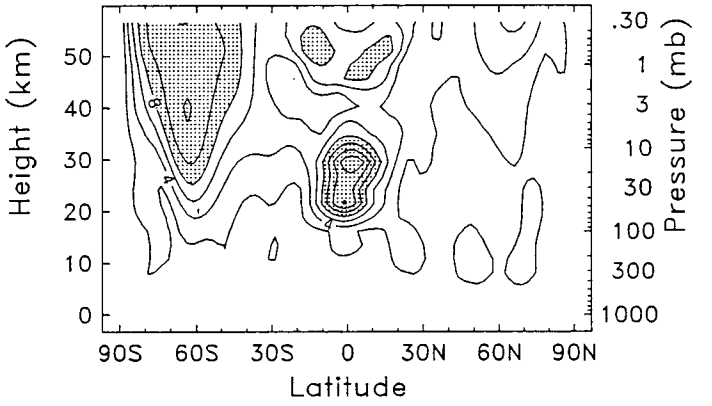
October zonal wind



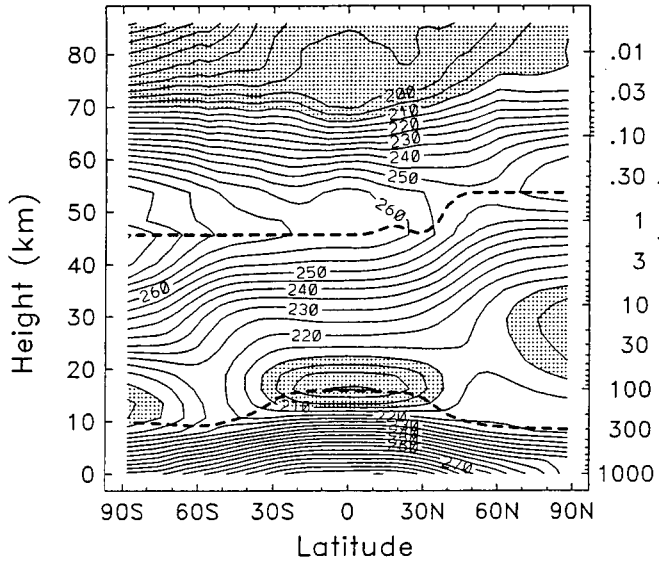
October temp int var



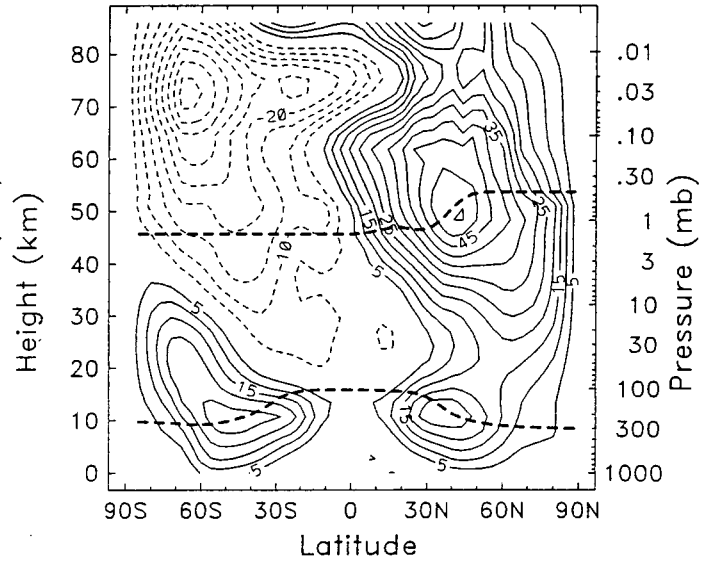
October zonal wind int var



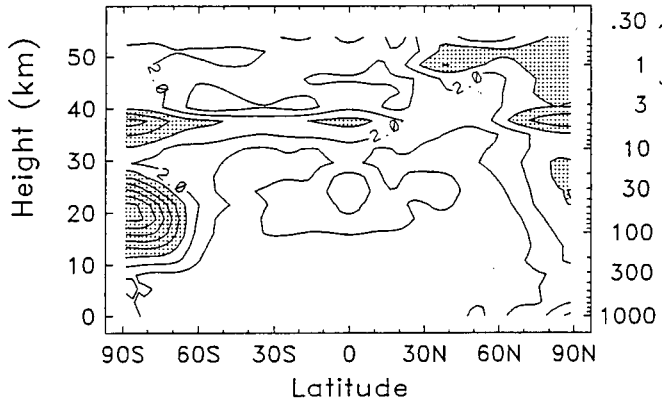
November temperature



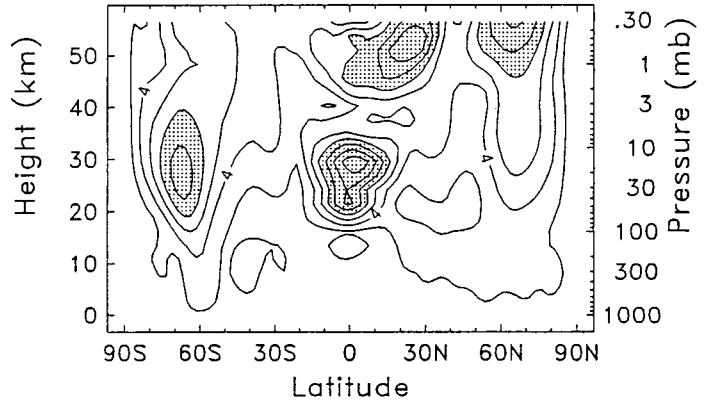
November zonal wind



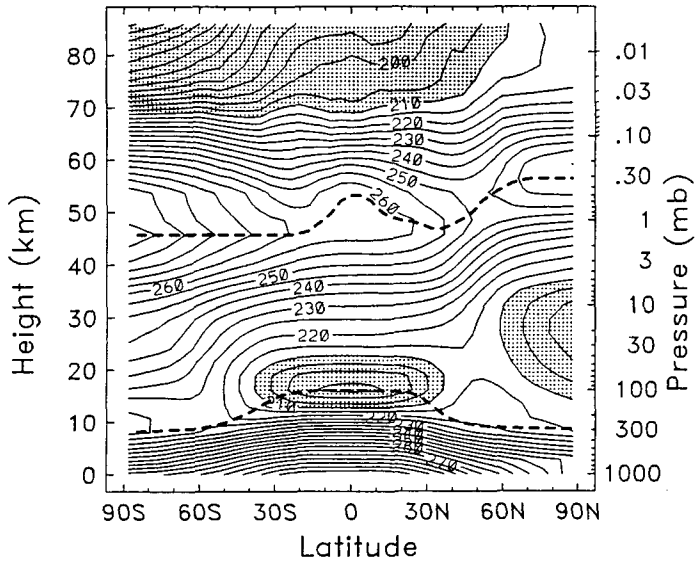
November temp int var



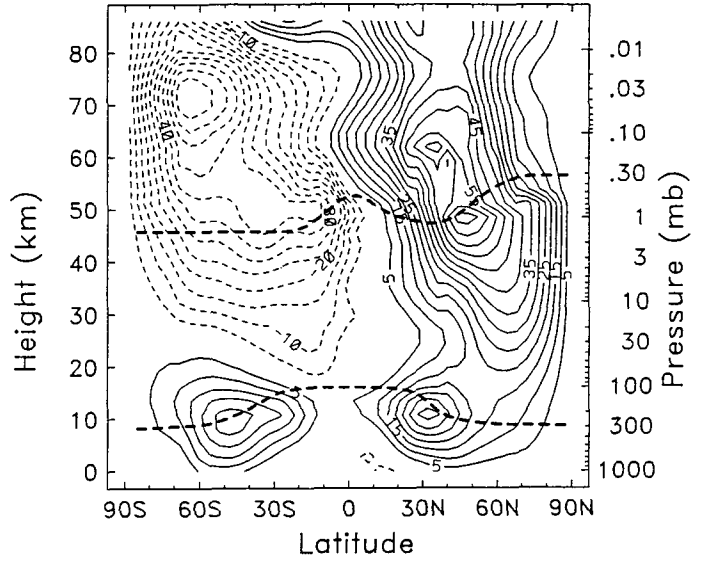
November zonal wind int var



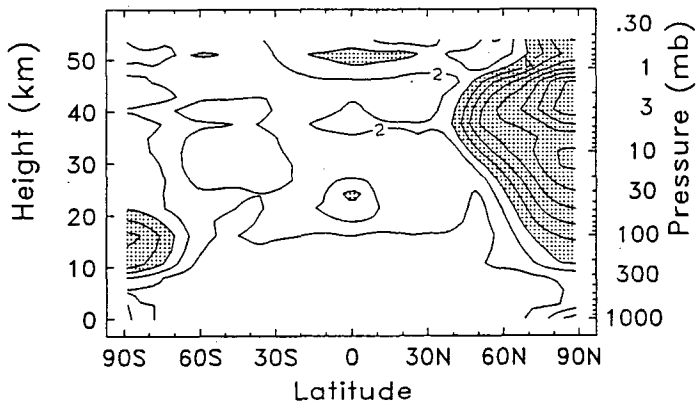
December temperature



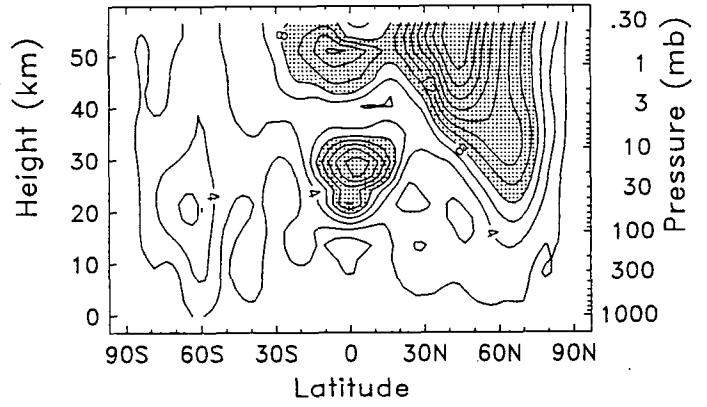
December zonal wind



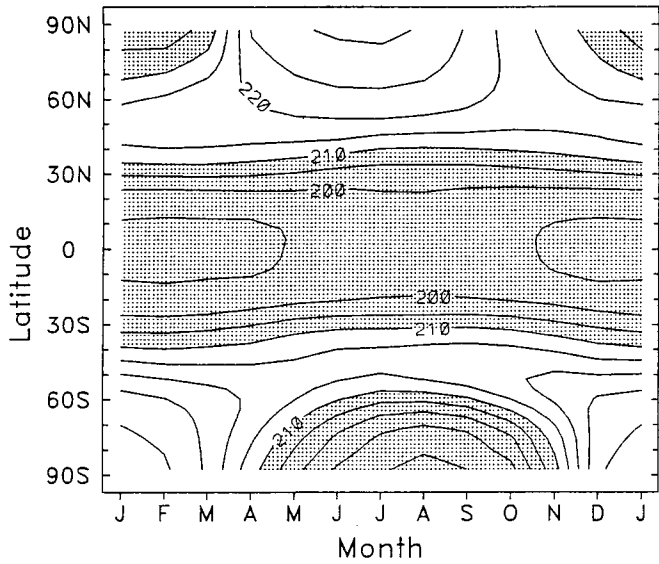
December temp int var



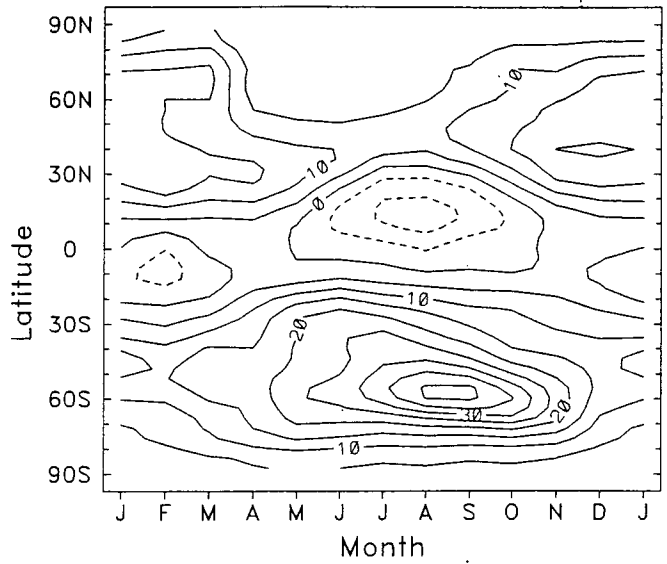
December zonal wind int var



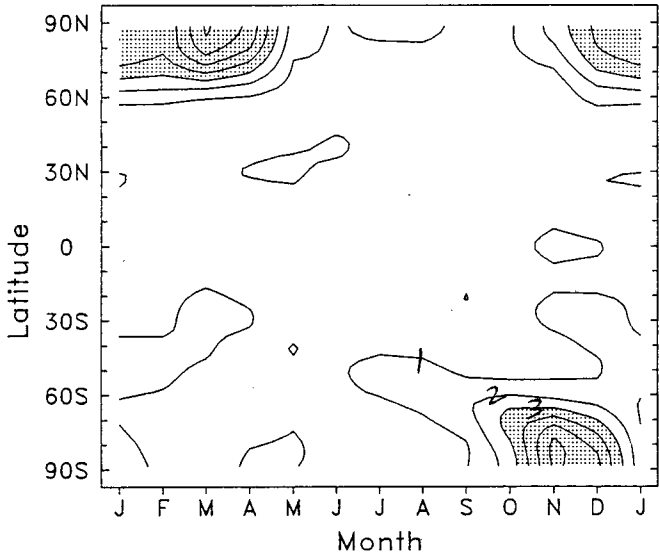
Temperature 100hPa



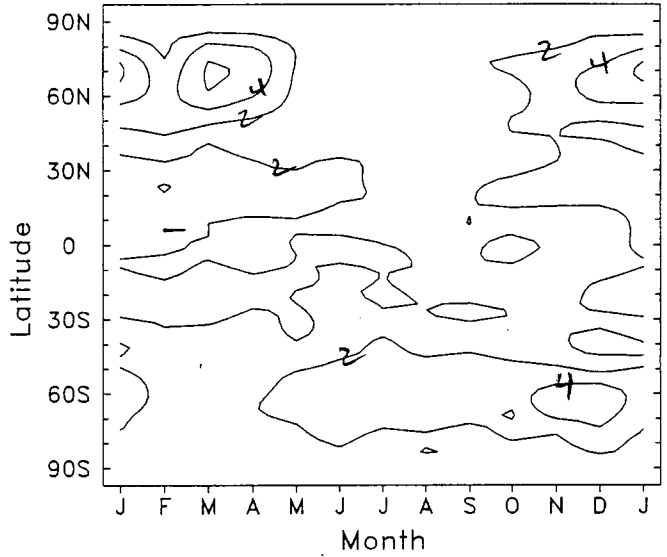
Zonal wind 100hPa



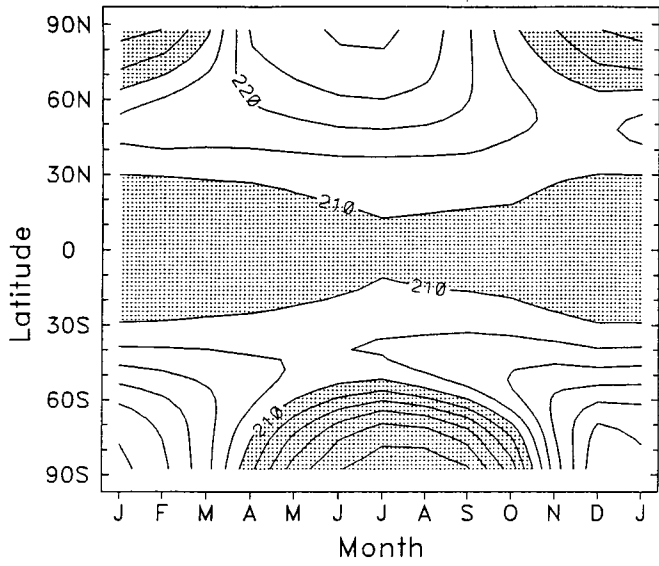
Temperature int var 100hPa



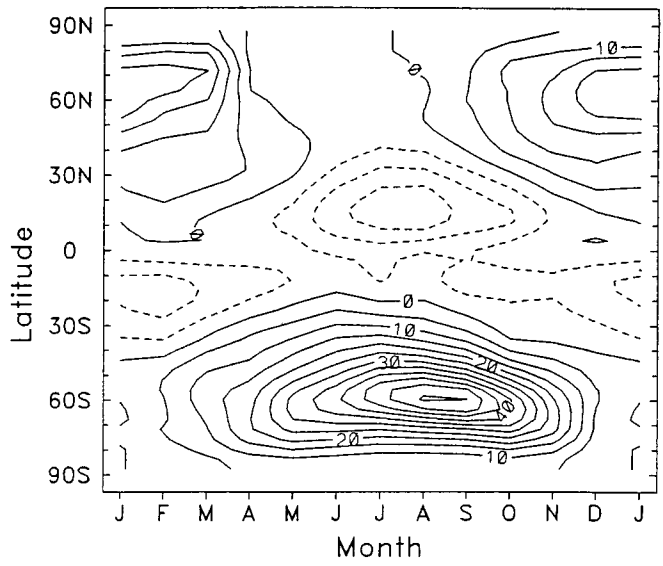
Zonal wind int var 100hPa



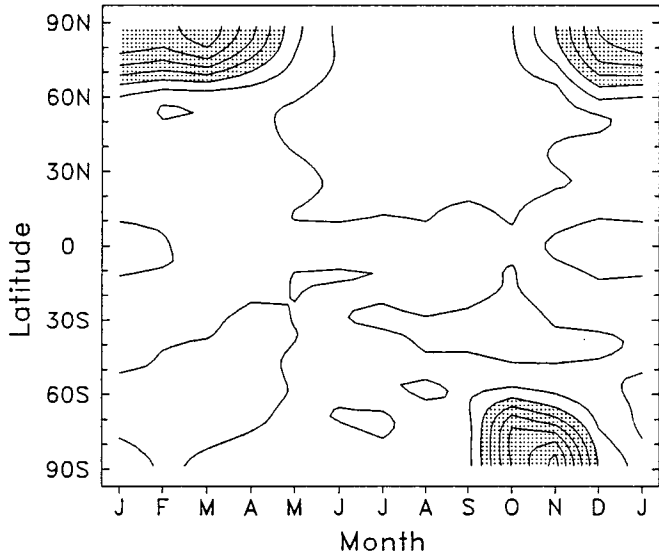
Temperature 46hPa



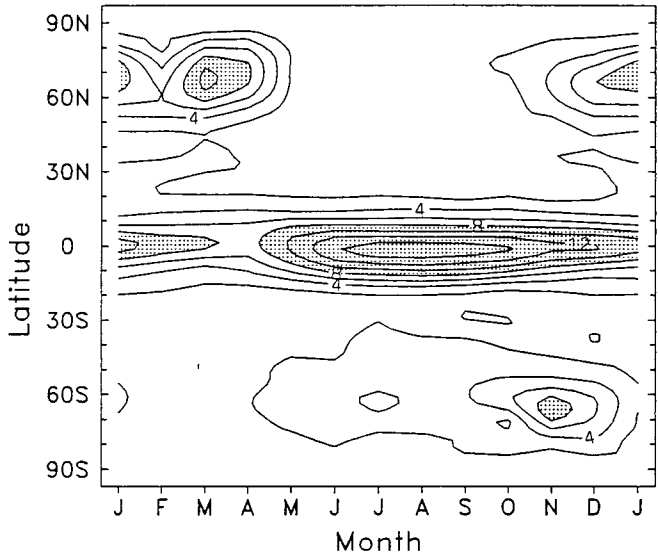
Zonal wind 46hPa



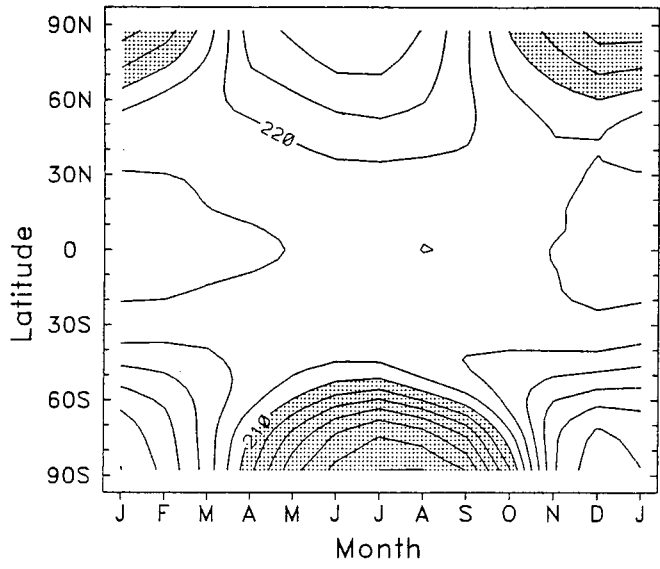
Temperature int var 46hPa



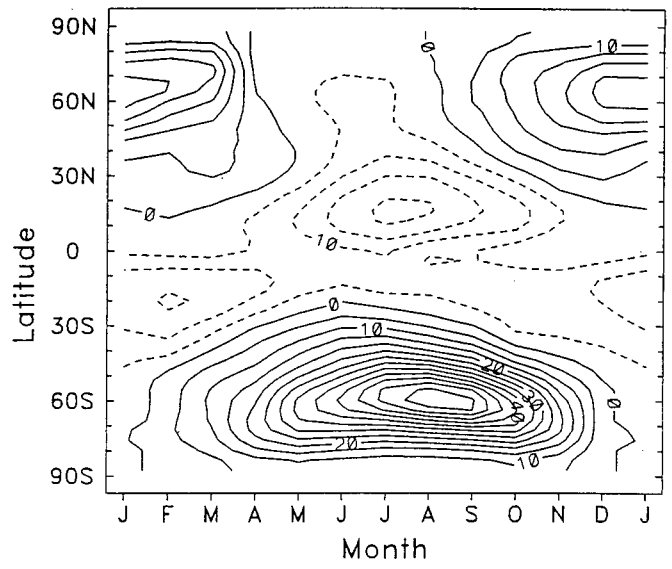
Zonal wind int var 46hPa



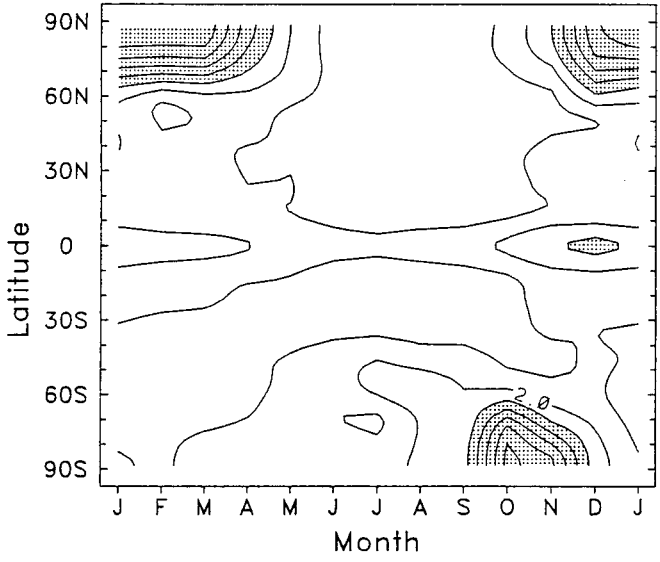
Temperature 31hPa



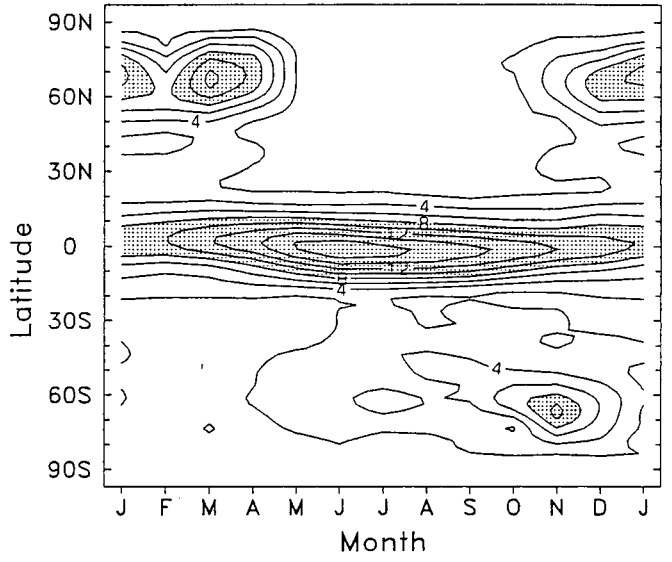
Zonal wind 31hPa



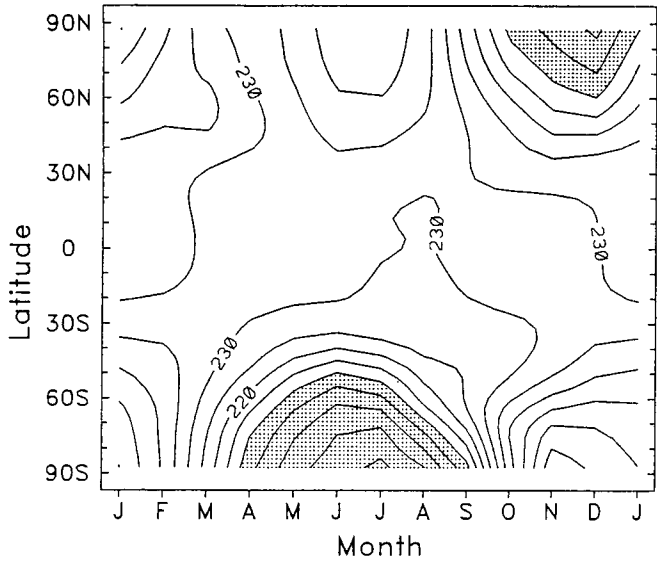
Temperature int var 31hPa



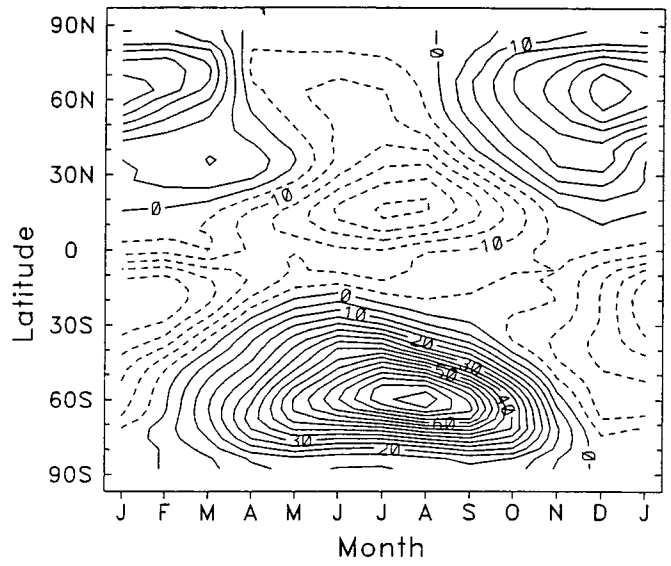
Zonal wind int var 31hPa



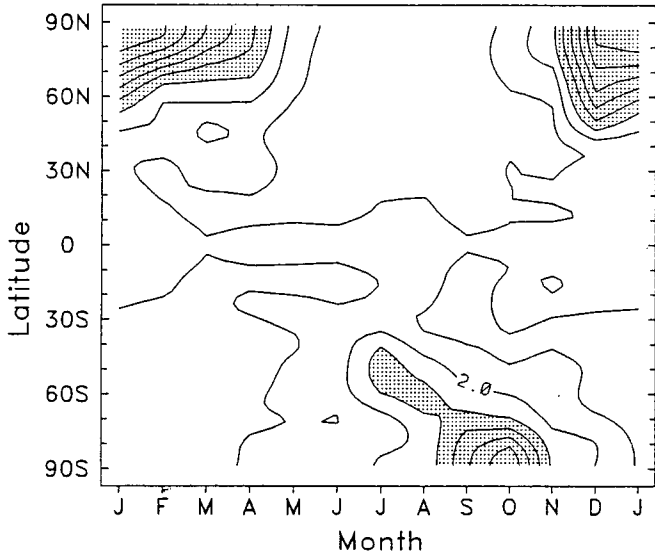
Temperature 10hPa



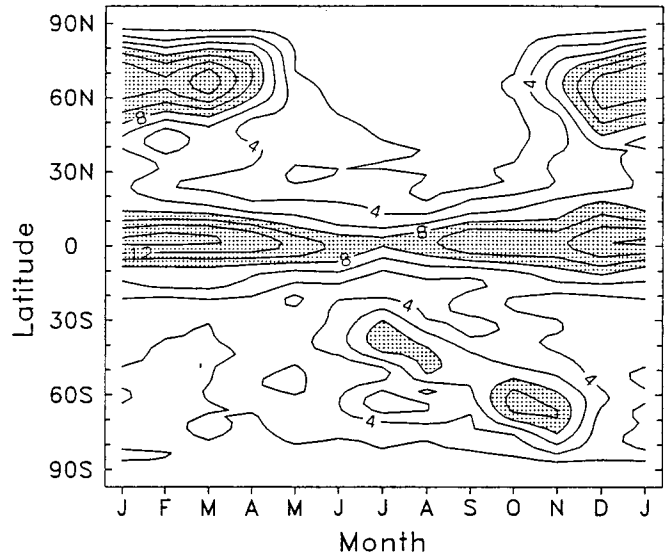
Zonal wind 10hPa



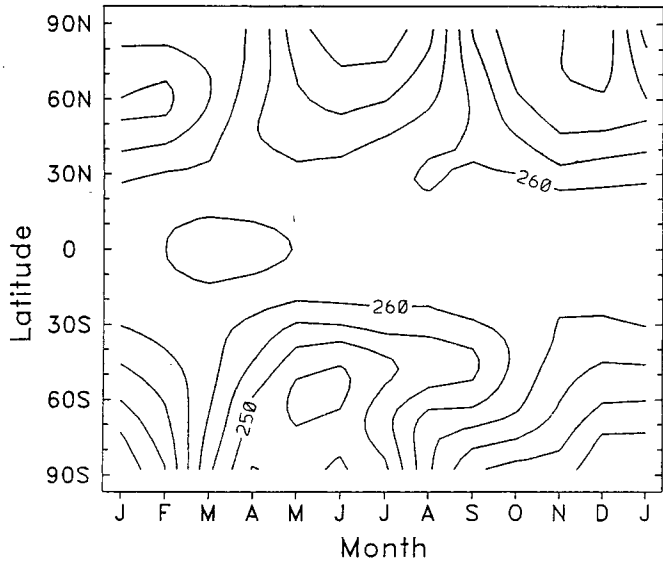
Temperature int var 10hPa



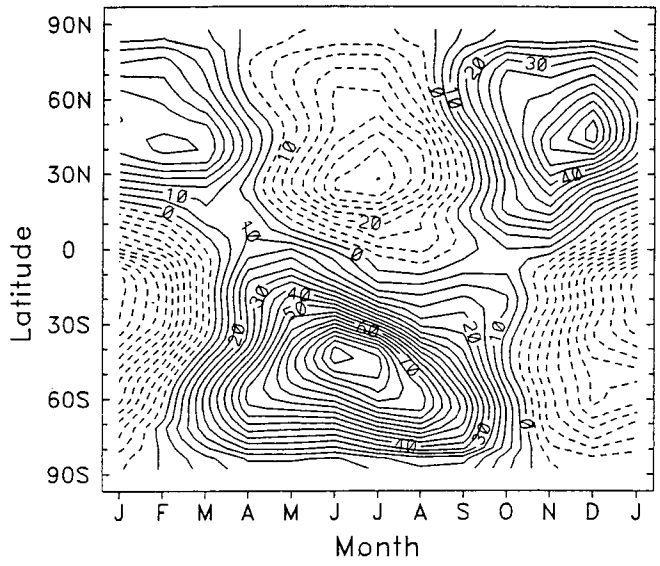
Zonal wind int var 10hPa



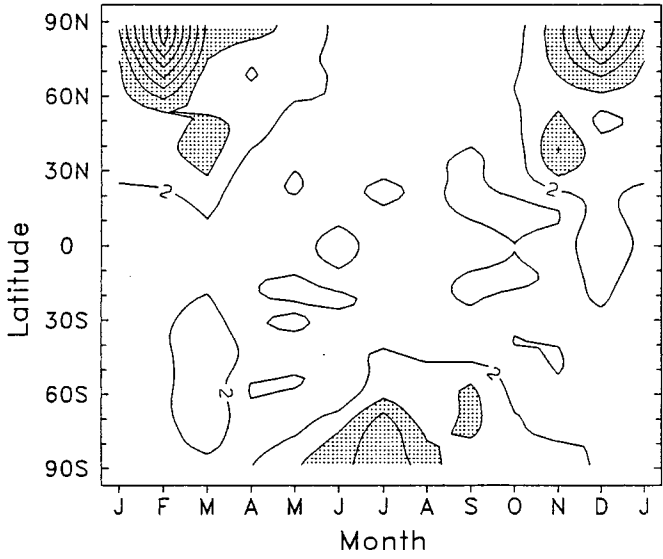
Temperature 1hPa



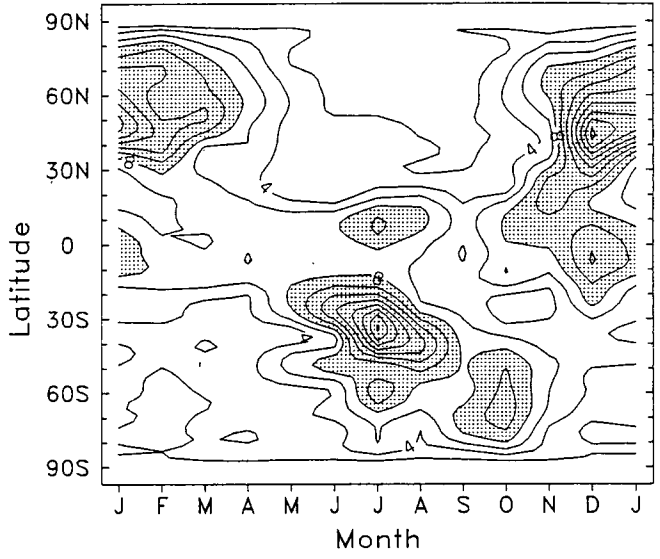
Zonal wind 1hPa



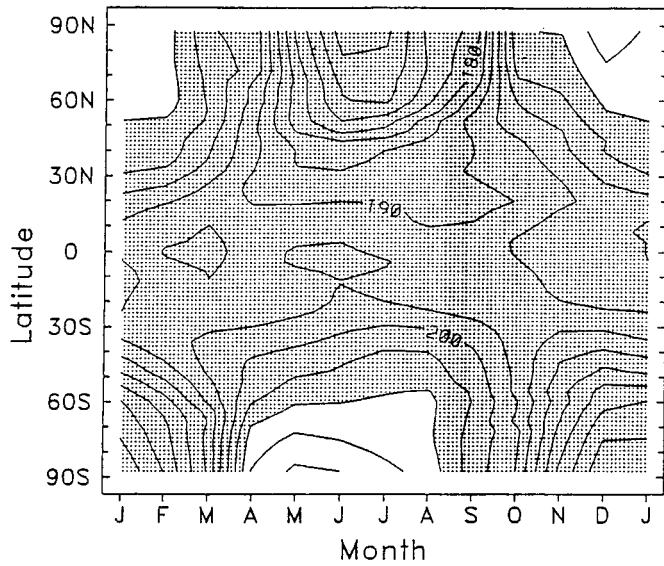
Temperature int var 1hPa



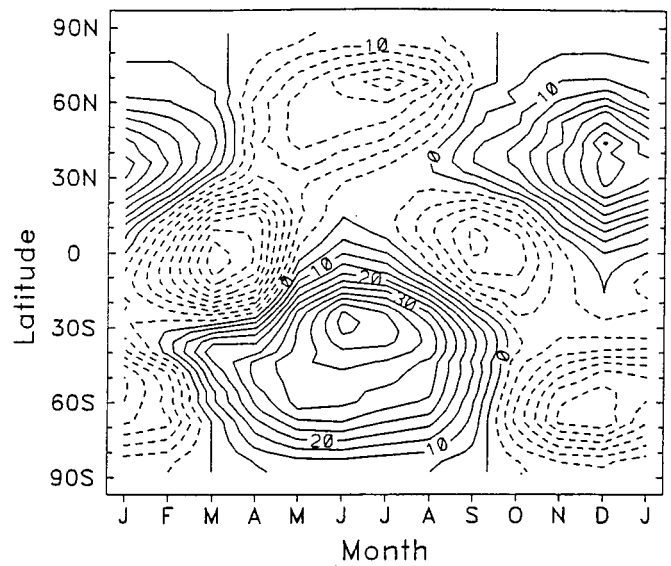
Zonal wind int var 1hPa



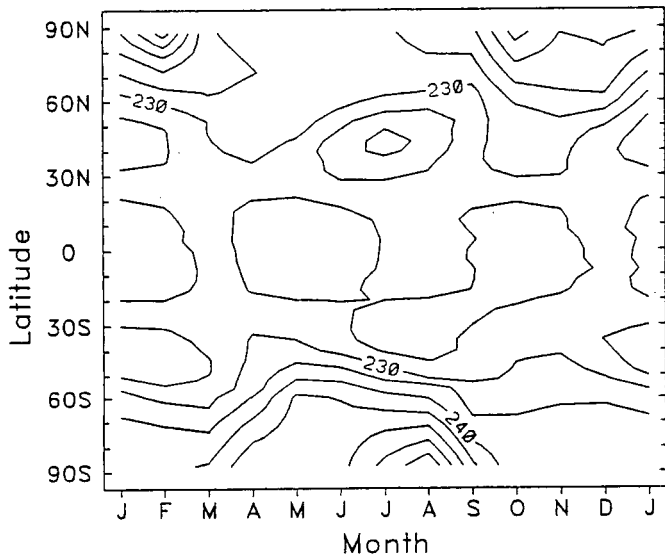
Temperature .01hPa



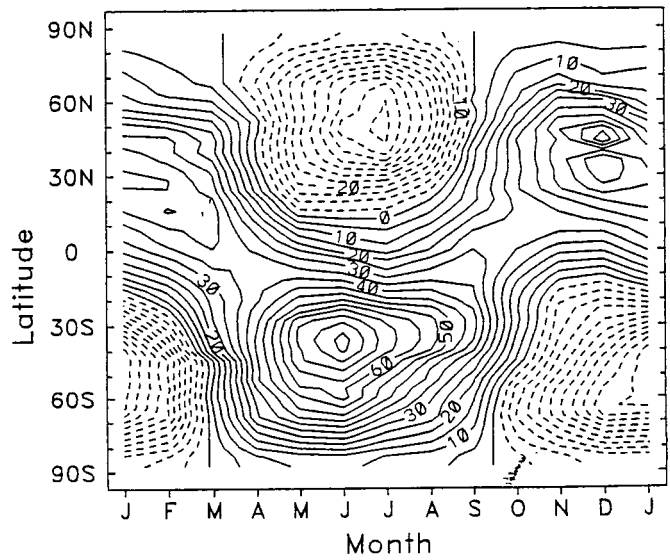
Zonal wind .01hPa



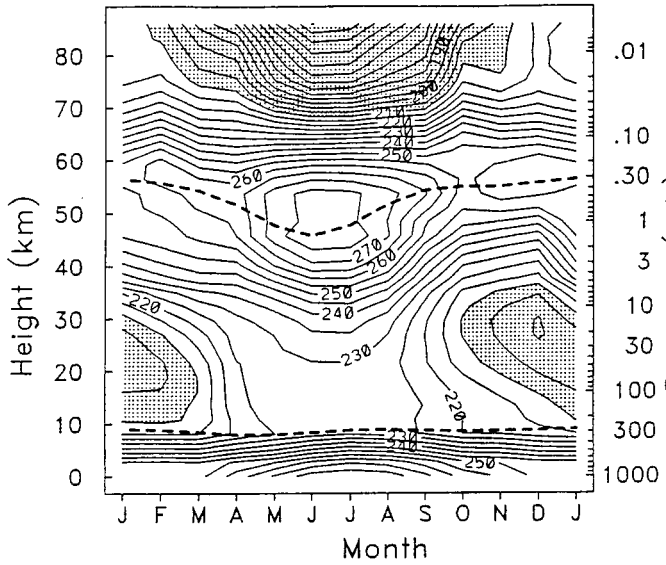
Temperature .10hPa



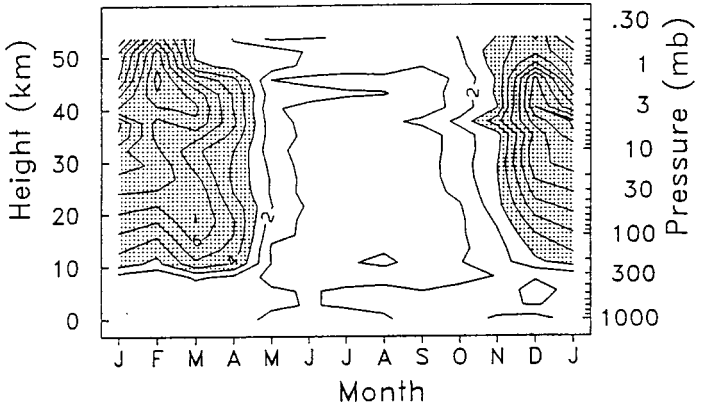
Zonal wind .10hPa



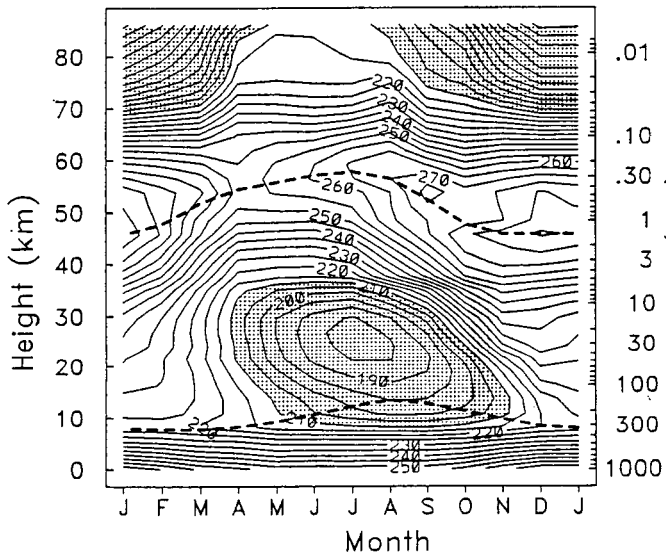
Temperature 80N



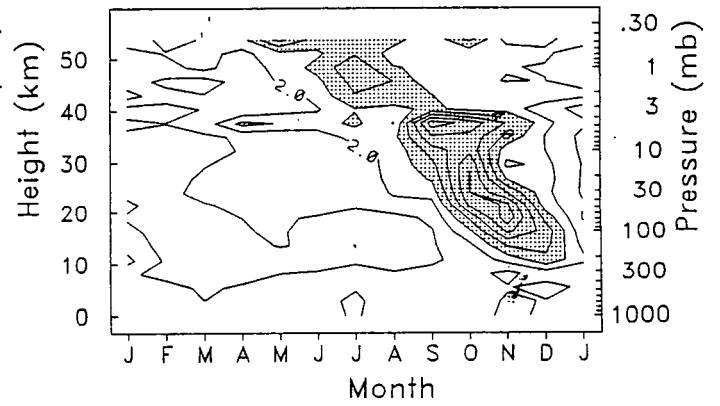
Temperature int var 80N



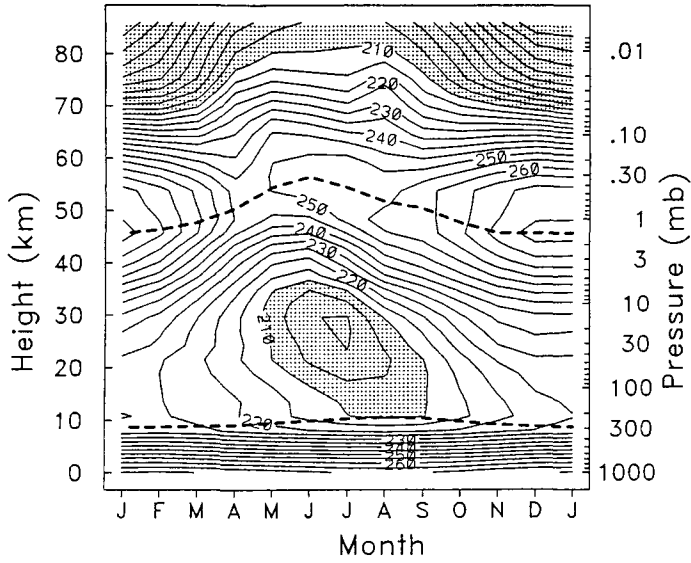
Temperature 80S



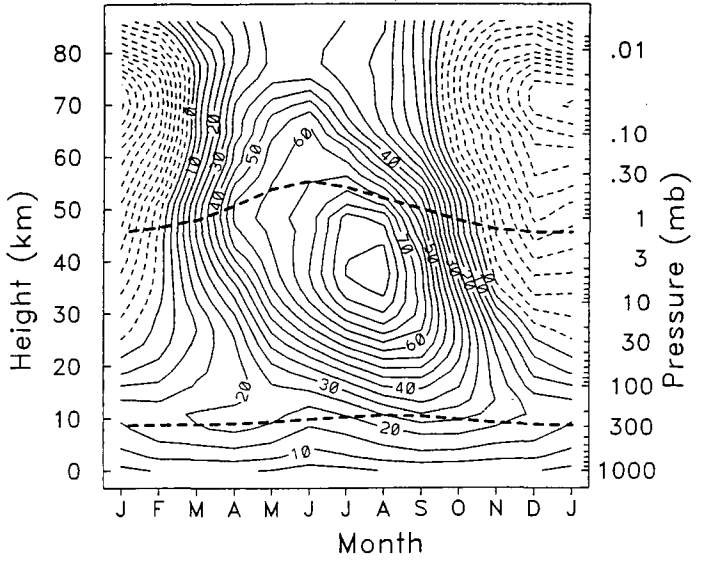
Temperature int var 80S



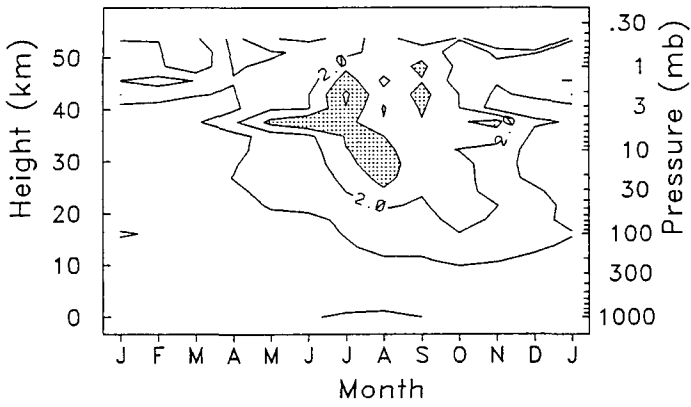
Temperature 60S



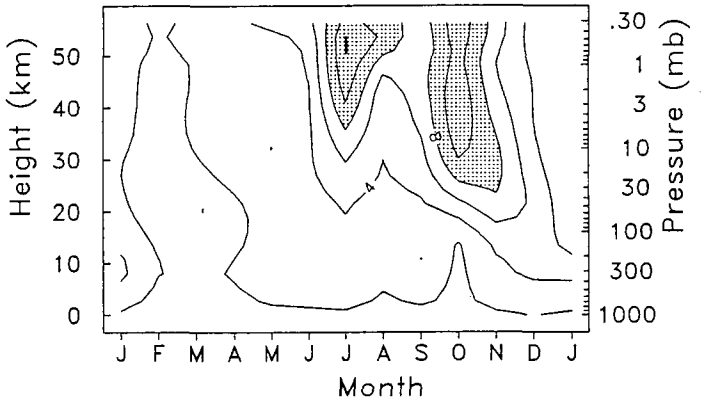
Zonal wind 60S



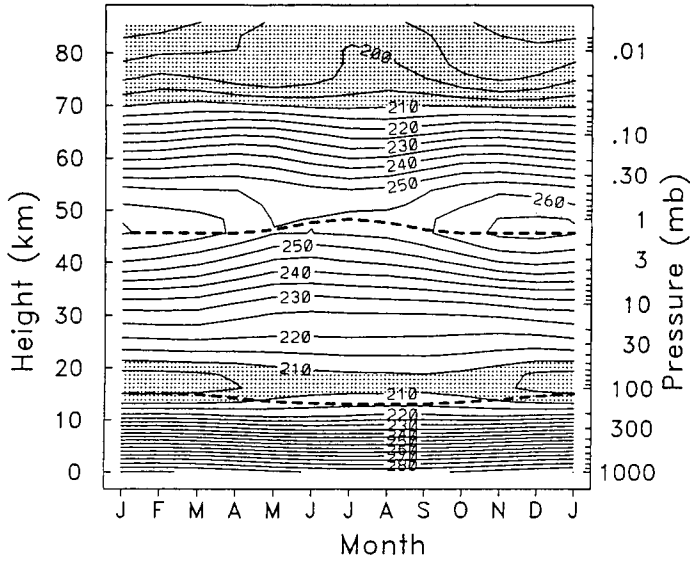
Temperature int var 60S



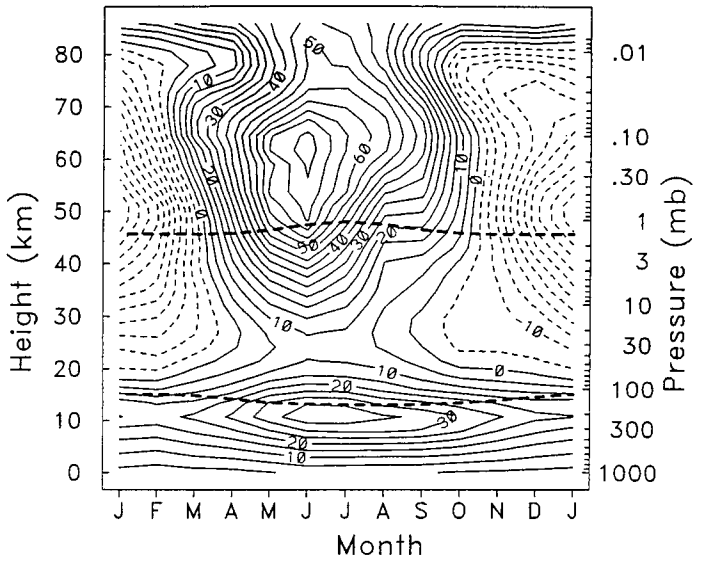
Zonal wind int var 60S



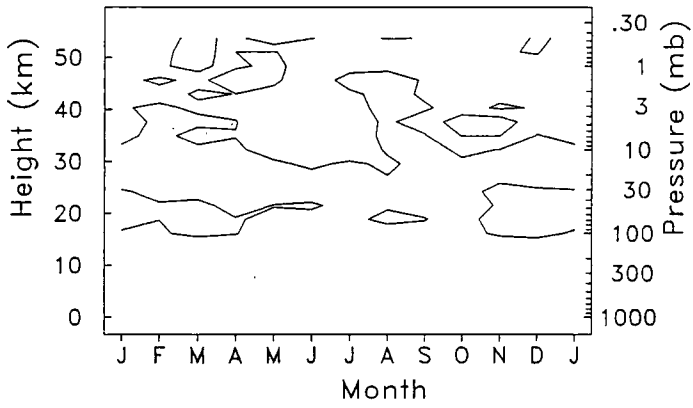
Temperature 30S



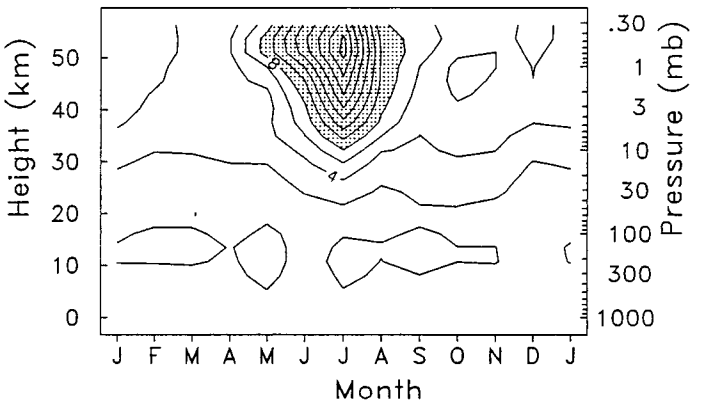
Zonal wind 30S



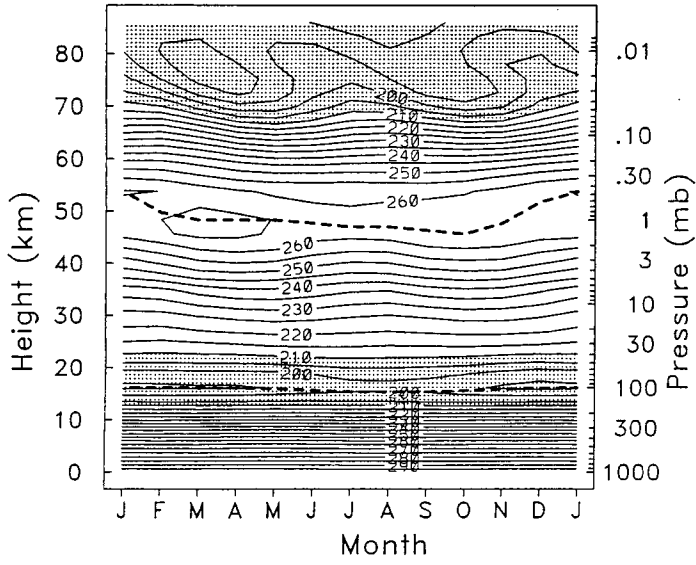
Temperature int var 30S



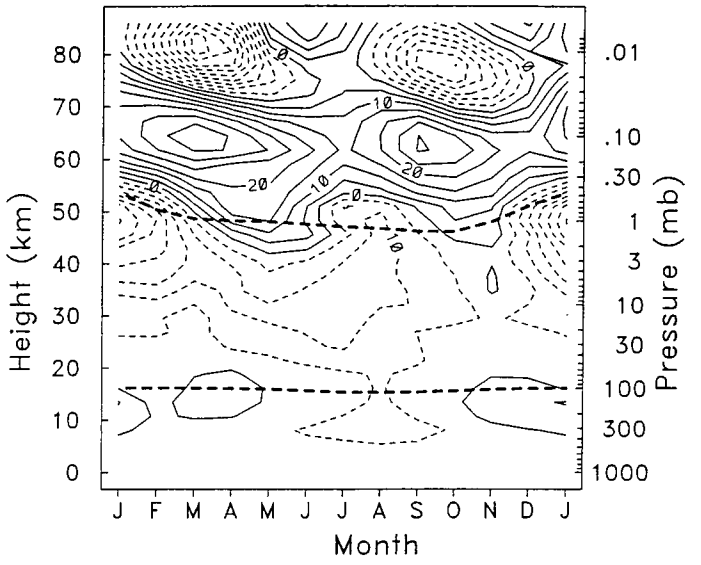
Zonal wind int var 30S



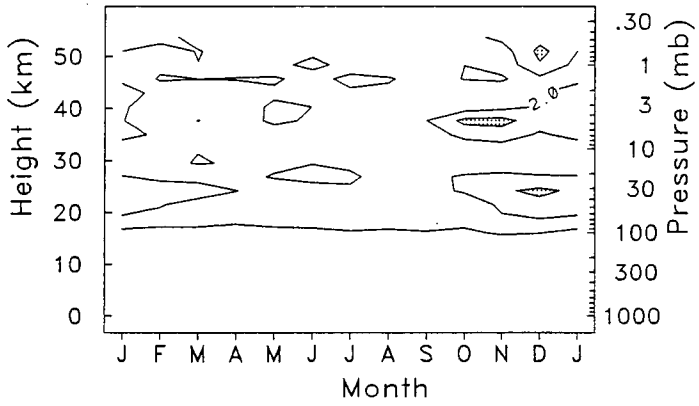
Temperature EQ



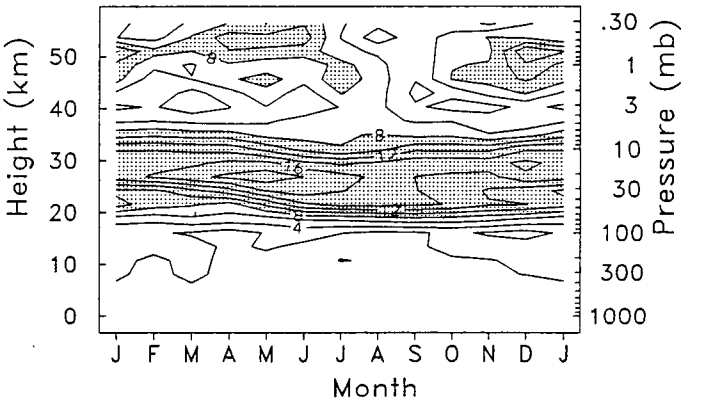
Zonal wind EQ



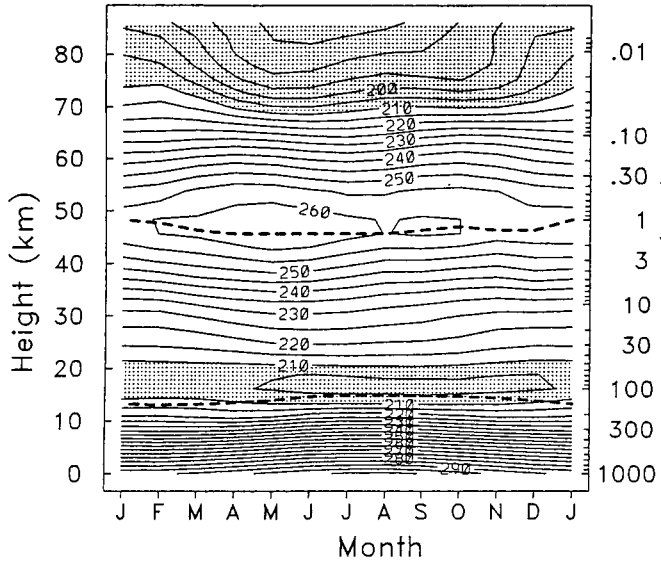
Temperature int var EQ



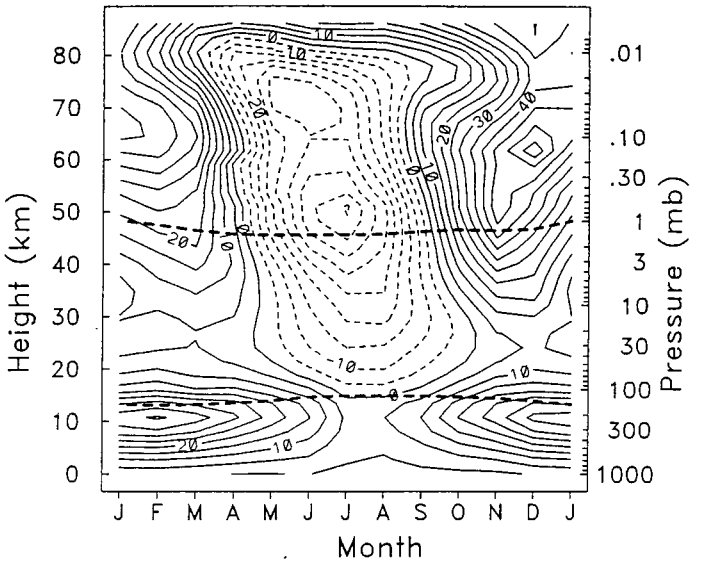
Zonal wind int var EQ



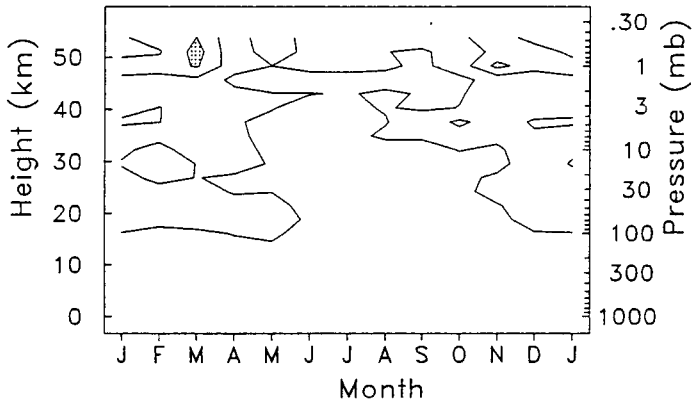
Temperature 30N



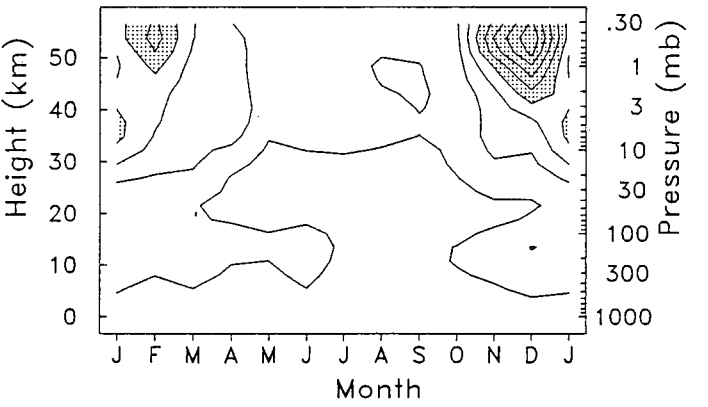
Zonal wind 30N



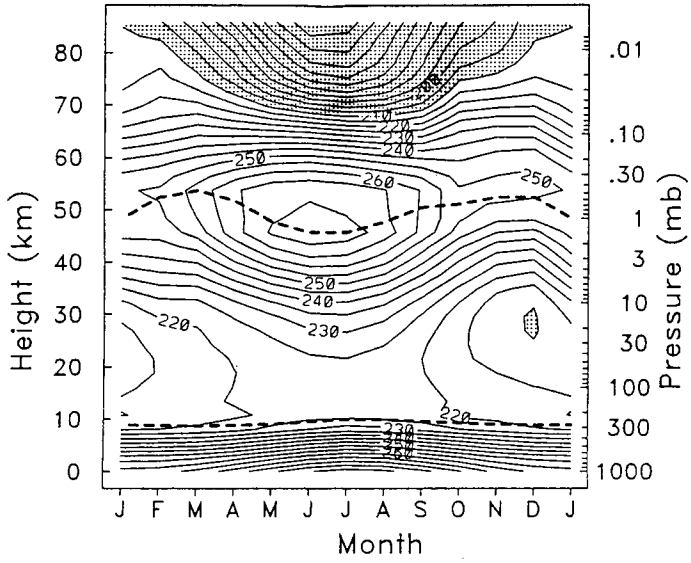
Temperature int var 30N



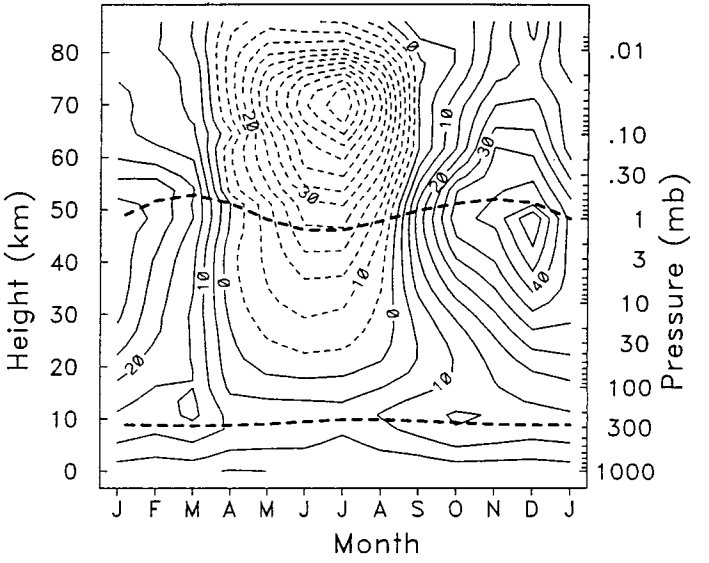
Zonal wind int var 30N



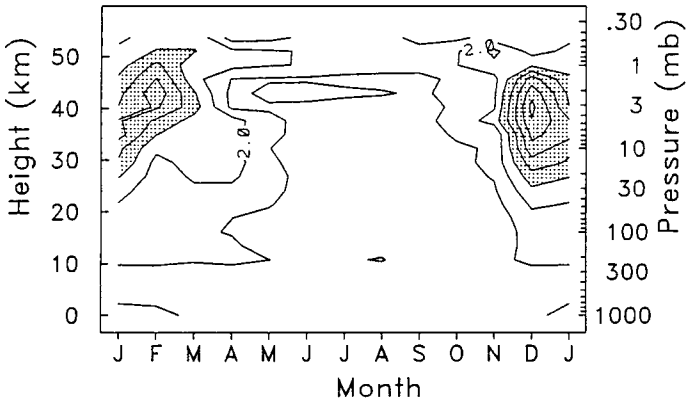
Temperature 60N



Zonal wind 60N



Temperature int var 60N



Zonal wind int var 60N

